PREPARATION AND CHARACTERIZATION OF InGaPAs ALLOYS

Sho SHIRAKATA

February, 1987

Osaka University
Faculty of Engineering Science
Toyonaka, Osaka

PREPARATION AND CHARACTERIZATION OF InGaPAs ALLOYS

Sho SHIRAKATA

Department of Electrical Engineering

Faculty of Engineering Science

Osaka University, Toyonaka, Osaka

February, 1987

ABSTRACT

A series of experimental investigations has been carried out on the crystal growth and optical characterization of the InGaPAs alloy semiconductor. These InGaPAs alloy semiconductors were grown on GaAs substrate by liquid phase epitaxy (LPE) using the two-phase melt method with excess GaP. The relationship between liquid and solid compositions has been made clear by comparing the experimental results with the calculated phase diagram over the wide composition range including the immiscibility region. The LPE growth in the immiscibilty region has been found to be possible due to the elastic energy from the substrate, however, sensitive to the initial supercooling and growth time.

The photoluminescence (PL) and electroreflectance (ER) spectra have been investigated for InGaPAs/GaAs LPE layers. Lattice-mismatch dependences of near-band edge PL and ER spectra have shown that good

quality $In_{1-x}Ga_xP_{0.96}As_{0.04}$ LPE layers can be grown under the lattice-matching condition at growth temperature. The crystal quality of InGaPAs LPE layers grown inside the immiscibility region has been investigated. The analyses of the ER and PL spectra in such a region have shown that both the extraordinarily broadened near-band edge and low-energy PL bands are not due to the spinodal decomposition but the incorporation of lattice defects during the growth by immiscibility which is closely related to the strain energy induced by the lattice mismatch.

A new technique has been developed for characterization of the interface stress at InGaPAs/GaAs heterostructure using the Cr-related PL line in GaAs:Cr at 0.839 eV. The magnitude of the interface stress at InGaPAs/GaAs has been obtained by the analysis of the Cr-related PL line, the result being compared with the calculated values. The detection limit of this method has been estimated to be $\sim$0.4 MPa. Furthermore, this method has been also successfully applied to other AlGaAs/GaAs and ZnSe/GaAs heterostructures.

The 3d-transition metal-related luminescence in InGaP and GaAsP alloys has been investigated with emphasis on the local structure of these alloy semiconductors. Measurements and analyses of the Co-related PL spectra have shown that they are composed of several PL bands reflecting the local arrangement of the constituent atoms around the Co luminescent center. The local lattice constant and disordering of atoms have been well characterized from the Co-related luminescence, the results showing that the Co center is a good probe for a study of the local structure of alloy semiconductors.

ACKNOWLEDGEMENT

The author would like to express his sincere thanks to Professor Y. Hamakawa for his useful advice and critical reading of this thesis. The author wishes to make his deep acknowledgement to Professors S. Namba, T. Sueta and S. Yamamoto for their kind guidance in the course of this study at Osaka University.

This work has been done at Semiconductor Laboratory, Faculty of Engineering Science, Osaka University, Toyonaka, Osaka under the direction of Professors Y. Hamakawa and T. Nishino. In particular, the author is much indebted to Professor Y. Hamakawa for his valuable and kind teaching, advice and encouragement throughout the course of this work. The author also wants to express his greatest thanks to Professor T. Nishino for his constant teaching, advice and encouragements throughout the course of this study and for critical reading of this thesis. The author wishes to give his great appreciation to Professor T. Kariya of Kochi University for his useful advice, discussion and measurements, and Professors T. Irie and S. Endo of Science University of Tokyo and Professor J. Nakai, Dr. T. Shirakawa and Dr. A. Moritani of Osaka university and Professor S. Isomura of Ehime University for their encouragements.

The author wishes to thank Dr T. Kato and Professor T. Ishida of Yamanashi University for supplying InGaP bulk crystals. The author wants to express his thanks to Professor S. Fujita of Kyoto University for his supply of ZnSe/GaAs samples and useful discussion.

The author is much indebted to Professor M. Okuyama, Dr. H. Takakura, Dr. H. Okamoto and Mr. C. Sada for their useful advices and discussion throughout of this study. Useful and enjoyable discussions with his colleagues, especially, Dr. Y. Fujiwara, Mr. H. Kida, Mr. D. Kruangam and Mr. K. Inoue are much appreciated by the author.

The author wishes to express his gratitude to his co-workers, Mr. T. Yagi, Mr. K. Takemura, Mr. M. Kondo, Mr. A. Tsushi, Mr.T. Hakugin, Mr. Y. Kita, Mr. Y. Inoue, Mr. Y. Tonami and Mr. H. Suzawa for their skillful technical help on this thesis work.

Finally, the author would like to thank his parents and some friends for their encouragements and supports.

TABLE OF CONTENTS

1. INTRODUCTION

1-1. Historical background

The III-V compound semiconductor family contains a large number of compounds according to the combination of group III elements, Al, Ga and In, and group V elements, P, As and Sb. Because of various interesting material properties, unique for each compound, they are widely used as materials for optoelectronic and high-speed devices. One of the most important development of III-V semiconductors in 1970's is the fabrication of heterostructures using the solid solution of III-V compounds, so called "III-V alloy semiconductor", along with the epitaxial growth technology. The success in room-temperature CW operation of semiconductor laser diodes employing AlGaAs/GaAs double heterostructure has shown us the usefulness of III-V alloy semiconductors.[1] Alloy semiconductors have characteristic properties that the band-gap can be changed according to the alloy composition desired for target device. However, in most of ternary alloy systems, the lattice constant changes with the alloy composition, which is called Vegard's law, and therefore one cannot choose the energy gap and lattice constant to a desired value simultaneously. In 1973, the appearance of quaternary alloys has overcome this problem, since the energy gap and lattice constant can be varied independently.[2] This was first demonstrated for the InGaPAs quaternary alloy lattice-matched to InP substrate, and a semiconductor laser diode emitting a 1.55 μm light has been realized[3] for optical communication using a quartz fiber. Along with the recent development of epitaxial growth technologies such as liquid phase epitaxy (LPE), organometalic

vapor phase epitaxy (OMVPE) and molecular beam epitaxy (MBE), III-V alloy semiconductors have come to be used widely for the fabrication of devices using the heterostructure, and gained a position indispensable for semiconductor devices.

The InGaPAs alloy semiconductor is the most intensively investigated quaternary alloy system.[4] Figure 1-1 shows the relationship between the band-gap energy and lattice constant of the InGaPAs alloy system. As can be seen in the figure, the band-gap energy and lattice constant of the InGaPAs quaternary alloy can be chosen at any value within a two dimensional area of the closed loop with those of four binary compounds InAs, GaAs, GaP and GaP in its corners. It is noted that the energy gap of InGaPAs alloy can be changed under the lattice-matching condition to a desired substrate. So far, the investigations of InGaPAs alloys have been focused on the composition lattice-matched to InP substrate because the energy gap can be chosen suitable for the fabrication of light emitting devices[3] and photodetectors[5] for the use of the lowest loss wavelength of a quartz optical fiber.[6] In 1980's, due to the requirement of the light source for laser printer, compact disk player, plastic optical fiber and optical information processor, researches and developments for visible-light semiconducting laser diodes become active. The InGaPAs alloys lattice-matched to GaAs substrate are promising materials for such visible-light laser diodes since the band-gap is direct-transition type over the whole composition range and can be chosen from 1.43 to 1.9eV.[7] The room-temperature CW operation of a visible-light laser diode at 720 nm has been realized.[8,9] However, the operating life time of these visible-light laser diodes was short

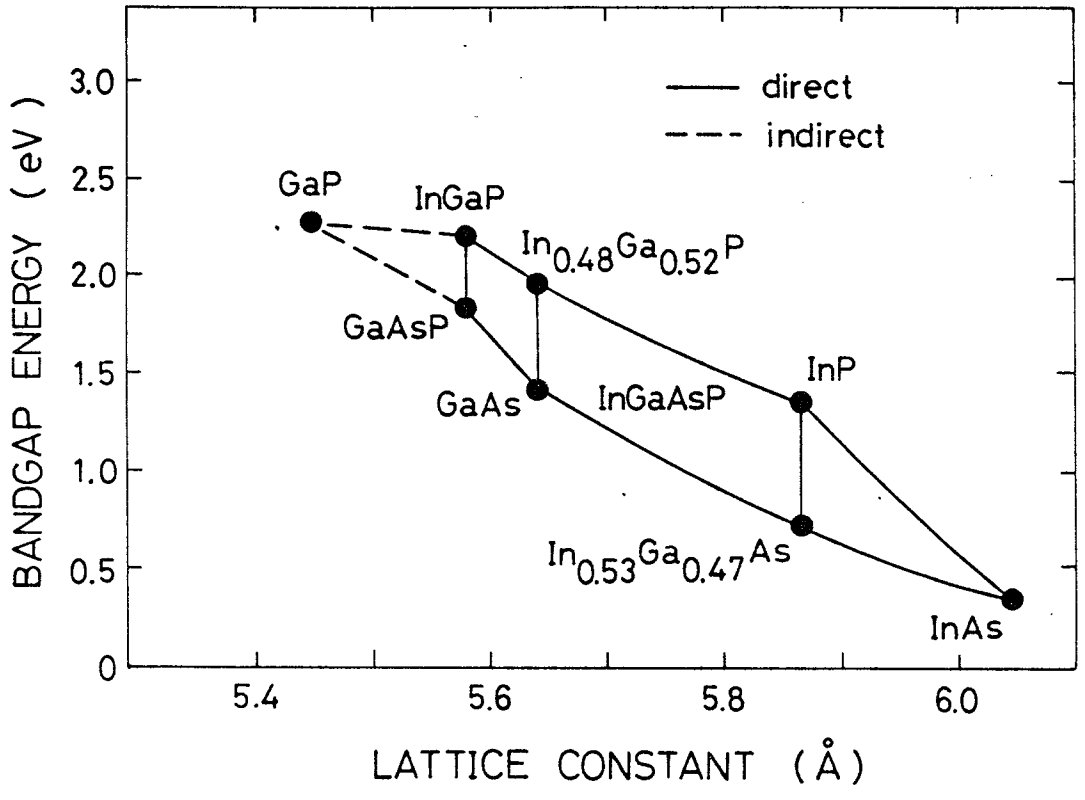

Fig. 1-1 Relationship between band-gap energy and lattice constant of InGaPAs alloys. The lattice-matching composition to GaAs is shown by the vertical line between $In_{0.48}Ga_{0.52}P$ and GaAs.

and degraded rapidly.[10] It seems that there remain a lot of problems in this alloy system.

1-2. Purpose of this work

In view of the technological application of this alloy system to optoelectronic devices such as visible-light semiconductor laser diode, various kinds of properties of InGaPAs alloys should be characterized in connection with the crystal growth. Furthermore, the heterointerface and microscopic structures should be clarified together with the development of characterization techniques.

The epitaxial growth of InGaPAs alloys on GaAs substrate has been mainly performed by LPE.[11-16] Suzuki et al.[11] and Mukai et al.[12,13] have reported low reproducibility of the LPE growth. Hiramatsu et al. have reported that the morphology of grown layers depends critically on the crystal growth condition.[16] These results show that the LPE growth of InGaPAs on GaAs is difficult compared with that on InP. On the other hand, de Cremoux has predicted the existence of the miscibility gap in the InGaPAs alloy system which is a serious problem for both the crystal growth and crystal quality.[17] The existence of the miscibility gap has been found in the LPE growth of InGaPAs on InP by Quillec el al.[18] and Takahei et al.[19], and in the LPE growth of InGaPAs on GaAs by Mukai et al.[20] However, very few has been understood on the effects of this immiscibility.

Another important problem is stress at heterointerface which plays an important role in the characteristics and performance of most devices. However, there is no effective characterization technique for the heterostructure practically employed as devices.

As to microscopic structures of alloy semiconductors, the lattice constant of alloy semiconductors, in the earlier stage, has been treated by the virtual crystal approximation (VCA). Mikkelesen et al, have shown from an Extended x-ray Absorption Fine Structure study that the bonding length is different from that predicted from VCA.[21] Recently, theoretical approaches have been done for obtaining a picture of the microscopic structure.[22] However, the microstructure of alloy semiconductors has not yet been made clear.

The purpose of this work is to carry out a systematic investigation for the InGaPAs alloy system with stress on the crystal-growth and the characterization of the crystal quality, the heterointerface and microstructure of alloys, and to establish the back bone about physics of this important quaternary alloy system.

In Chapter 2, the author describes the LPE growth of InGaPAs on GaAs substrate, and makes clear the crystal growth condition such as liquid and solid composition.[23,24] Great effort has been paid to the effects of immiscibility on LPE growth conditions.[25] Also the solution growth of bulk InGaP alloys is briefly described.

In Chapter 3, the author discusses the photoluminescence (PL) and electroreflectance (ER) characterization of LPE InGaPAs layers.[26] The crystal quality of this InGaPAs LPE layer is discussed in terms of lattice mismatch. The effects of immiscibility on InGaPAs LPE layers are examined comparing PL spectra with ER spectra, and the crystal quality under the influence of immiscibility is discussed in terms of phase separation, defect level and strain energy due to lattice mismatch.[25,26]

Chapter 4 deals with the 3d-transition metal related luminescence in III-V compounds and alloys. The Cr-related luminescence in GaAs is briefly described as the introduction of Chapter 5, and the effect of stress on the Cr energy level in GaAs is described. As the introduction of Chapter 6, various 3d-transition metal related luminescences in GaP, AlGaAs and GaAsP are discussed.

In Chapter 5, the author describes a new high-sensitive technique for the characterization of stress at InGaPAs/GaAs heterointerface using the Cr-related PL line at 0.839 eV in GaAs.[27,28] The systematic measurements on the Cr-related PL spectra from InGaPAs/GaAs:Cr have been carried out, and the effects of interface stress on this PL line are discussed. The magnitude of the interface stress has been obtained and compared with the calculated values. Furthermore, this technique has been successfully applied for the heterointerface of AlGaAs/GaAs:Cr and ZnSe/GaAs:Cr.[29]

In Chapter 6, the author describes the characterization of the local structures of InGaP and GaAsP alloys using the 3d-transition metal-related PL spectra.[30] Firstly, a series of transition metal-related PL spectra in InGaP has been measured and examined. Secondly, the Co-related PL measurements in InGaP and GaAsP alloys have been carried out. The Co-related luminescence has been discussed in connection with the local arrangement of atoms around the Co center and shown that the transition-metal impurity is a good probe to investigate the local structure of alloy semiconductors.

Finally, some conclusions obtained in this thesis work are summarized in the final Chapter 7.

REFERENCES

1) M. B. Panish, I. Hayashi and S. Sumski: Appl. Phys. Lett. 16 (1970) 326.

2) G. A. Antypas and R. L. Moon: J. Electrochem. Soc. 120 (1973) 1574.

3) J. J. Hsieh: Appl. Phys. Lett. 28 (1976) 283.

4) T. P. Pearsell ed. GaInAsP Alloy Semiconductors (Wiley, New York, 1982)

5) M. Feng, D. J. Oberstar, T. M. Windhorm, L. W. Cook, G. E. Stillmann and G. B. Streetman: Appl. Phys. Lett. 34 (1979) 591.

6) M. Horiguchi and H. Osanai: Electron. Lett. 12 (1976) 310.

7) R. L. Moon, G. A. Antypas and J. W. James: J. Electronic Materials 3 (1974) 635.

8) K. Wakao, H. Nishi, T. Kusunoki, S. Isozumi and S. Osaka: Appl. Phys. Lett. 44 (1984) 1035.

9) S. Kaneiwa, H. Takiguchi, T. Hayakawa, S. Yamamoto, H. Hayashi, S. Yano and T. Hijikata: Appl. Phys. Lett. 46 (1985) 455.

10) O. Ueda, K. Wakao, A. Yamaguchi, S. Komiya, S. Isozumi, H. Nishi and I. Umebu: Appl. Phys. Lett. 44 (1984) 861.

11) A. Suzuki, H. Kyuragi, S. Matsumura and H. Matsunami: Jpn. J. Appl. Phys. 19 (1980) L207.

12) S. Mukai, M. Matsuzaki and J. Shimada: Jpn. J. Appl. Phys. 19 (1980) L505.

13) S. Mukai, M. Matsuzaki and J. Shimada: Jpn. J. Appl. Phys. 20 (1981) 321.

14) T. Kato, T. Matsumoto and T. Ishida: Jpn. J. Appl. Phys. 21 (1982) L667.

15) S. Kaneiwa, T. Takenaka, S. Yano, and T. Hijikata: J. Cryst. Growth 62 (1983) 498.

16) K. Hiramatsu, K. Tomita, N. Sawaki and I. Akasaki: Jpn. J. Appl. Phys. 23 (1984) 68.

17) B. de Cremoux: J. Physique 43 (1982) c5.

18) M. Quillec, C. Daguet, J. L. Benchimol and H. Launois: Appl. Phys. Lett. 40 (1982) 325.

19) K. Takahei and H. Nagai: Jpn. J. Appl. Phys. 20 (1981) L313.

20) S. Mukai: J. Appl. Phys. 54 (1983) 2635.

21) J. C. Mikkelsen Jr and J. B. Boyce:Phys. Rev. Lett. 49(1982)1412.

22) A. B. Chen and A. Sher: Phys. Rev. B 32 (1985) 3695.

23) S. Shirakata, M. Kondo, A. Tsushi, T. Nishino, Y. Hamakawa and T. Kariya: Jpn. J. Appl. Phys. 24 (1985) 524.

24) M. Kondo, S. Shirakata, A. Tsushi, T. Nishino and Y. Hamakawa: Jpn. J. Appl. Phys 24 (1985) 806.

25) M. Kondo, S. Shirakata, T. Nishino and Y. Hamakawa: J. Appl. Phys. 60 (1986) 3539.

26) S. Shirakata, M. Kondo, T. Nishino and Y. Hamakawa: Jpn. J. Appl. Phys. 25 (1986) 435.

27) S. Shirakata, Y. Fujiwara, M. Kondo, T. Nishino and Y. Hamakawa: Ext. Abst. 17th Conf. Solid State Devices and Mater., Tokyo, 1985 (Japan Business Center for Academic Societies, Tokyo, 1985)p.205.

28) S. Shirakata, Y. Fujiwara, M. Kondo, T. Nishino and Y. Hamakawa: J. Electronic Materials 15 (1986) 323.

29) Y. Fujiwara, S. Shirakata, T. Nishino, Y. Hamakawa and S. Fujita: Jpn. J. Appl. Phys. 25 (1986) 1628.

30) S. Shirakata, T. Nishino, Y. Hamakawa, T. Kato and T. Ishida: to be published in Jpn. J. Appl. Phys. Lett. 26 No. 2 (1987).

2. CRYSTAL GROWTH OF InGaPAs AND InGaP ALLOYS

2-1. Introduction

The crystal growth of InGaPAs alloys has been done mainly by liquid phase epitaxy (LPE) because high-quality InGaPAs epitaxial layers can be easily grown by a simple experimental apparatus with a horizontal furnace system and a conventional sliding graphite boat. A large number of LPE growth experiments have been focused on the growth lattice-matched to InP substrate, and the equilibrium phase diagrams and crystal growth conditions have been almost established.[1)]

On the other hand, the LPE growth of InGaPAs alloys lattice-matched to GaAs is now in the early stage of development. The LPE growth experiments of InGaPAs on GaAs have previously reported by several researchers.[2-10)] However, these experimental results have shown that the LPE growth of InGaPAs on GaAs substrate is difficult compared with that on InP substrate. Because of the high growth temperature of about 800°C, the evaporation of volatile element P from melt causes low reproducibility of the LPE growth due to the change in the saturation temperature[2,3)] and the reaction of P with the GaAs substrate.[4)] It has been found by Stringfellow[5)] that the composition pulling phenomena occur in this system due to the effect of the strain energy from the substrate. It is a great problem for the LPE growth of this quaternary alloy on GaAs substrate that the growth is largely affected by the existence of the immiscibility region.[6)] Furthermore, it has been found that, if the melt composition is not precisely controlled, the GaAs substrate is heavily melted back due to high

reactivity of the In melt to GaAs.[3,7] In view of above-mentioned problems, a systematic LPE growth experiment over the whole composition range is required.

In this Chapter, a systematic LPE growth of InGaPAs on the (100)GaAs substrate over the whole composition range is described. The two-phase melt method with excess GaP has been developed in order to perform the LPE growth reproducibly. The alloy compositions studied in this work are classified into two composition regions; compositions inside and outside of the immiscibility region. First, the LPE growth of $In_{1-x}Ga_xP_{0.96}As_{0.04}$ with compositions outside of the immiscibility region has been carried out, and some characteristics of this two-phase melt method have been investigated.[11,12] Next, the concept of immiscibility is described, and its influence on the LPE growth of $In_{1-x}Ga_xP_{0.7}As_{0.3}$ has been investigated comparing the two-phase melt method with the conventional supercooling method. The effect of the initial supercooling on the LPE growth inside the immiscibility region has been discussed.[13] The growth of InGaPAs LPE layer having various As compositions has been carried, and the LPE growth condition has been established over the whole composition range including the immiscibility region.

Finally, the solution growth of InGaP bulk crystals has been performed using the vapor-pressure controlled temperature difference method for the purpose of obtaining bulk InGaP alloys having crystal quality adequate for the characterization by the 3d-transition metal-related PL measurements described in Chapter 6.

2-2. Liquid phase epitaxy of InGaPAs lattice-matched to GaAs

2-2-1. Apparatus and procedure of liquid phase epitaxy

A series of single-crystal layers of InGaPAs have been grown on (100) GaAs substrate by a horizontal-type liquid phase epitaxial (LPE) furnace with a sliding boat[7]. The gas system and the structure of the graphite boat used for the LPE growth are shown in Fig. 2-1. The furnace is a three-zone gold-image furnace having a small thermal mass which enables us to control temperature precisely. The sliding boat is made of high purity graphite, and the temperature uniformity is within 0.5 °C along the boat. The melt temperature was monitored by a Pt-Pt.Ro thermocouple set inside the sliding boat.

A mirror-polished (100) oriented GaAs wafer doped with Cr or Si (8x8x0.38 mm^3 in size) was used as the substrate. The GaAs wafer was etched with HF to remove the oxidized surface layer, and then with hot Br-CH_3OH to remove the surface damaged layer. High-purity source polycrystals of InAs, InP, GaAs and GaP were added to In of 1g in weight. After the loading of the GaAs substrate, In melt and source polycrystals into the graphite boat, the reactor tube was evacuated to 10^{-5} Torr, and then purged by Pd-purified H_2 gas. The temperature of the furnace was raised to 800 or 820°C within 50 min. After the melt had been soaked for 60 min, it was cooled down to the growth temperature at a rate of 1.0°C/min. At the growth temperature, the substrate was brought into contact with the melt, and the temperature was lowered at the same rate during the growth period. After the growth, the melt was wiped off and the furnace was cooled down to room temperature rapidly.

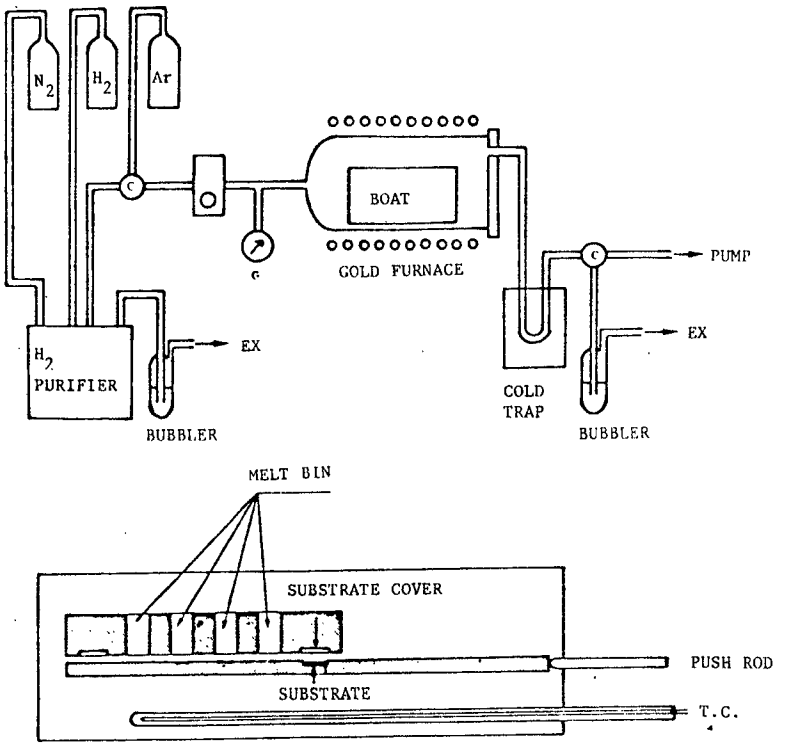

Fig. 2-1 LPE growth system used for the growth of InGaPAs alloy on GaAs. Upper figure shows the gas system of the LPE furnace and lower figure the graphite sliding boat.

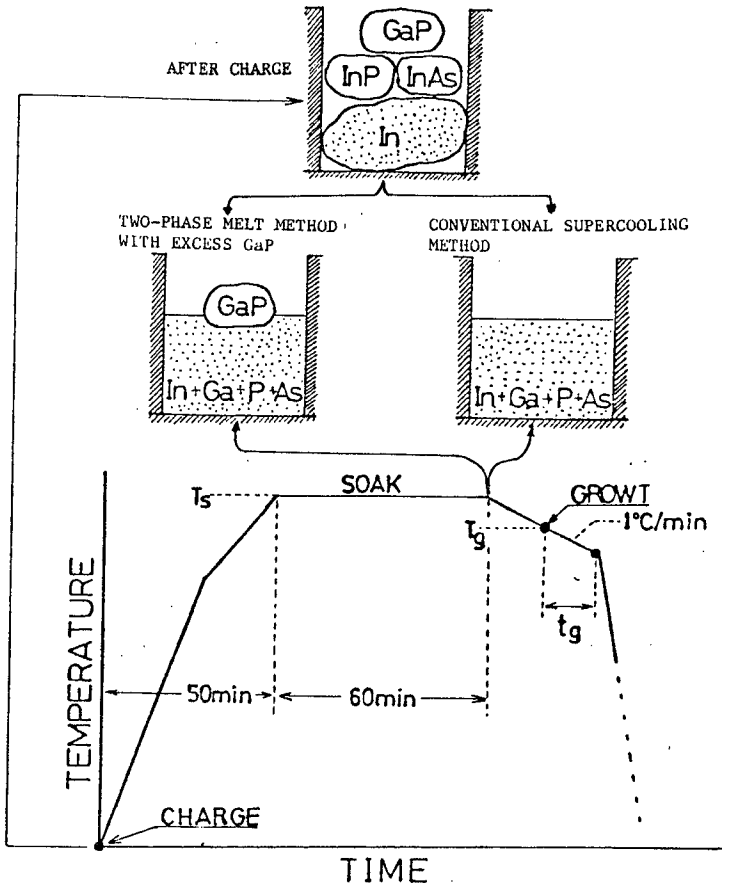

Fig. 2-2 Temperature sequence program used for LPE growth of InGaPAs on GaAs. The difference of the state of the melt between two-phase melt method and conventional supercooling method at the end of the soak period is schematically shown in the upper part of figure.

For the reproducible LPE growth of InGaPAs layers on GaAs substrate, the two-phase melt method with excess GaP has been employed.[11-13] In this growth method, GaP source crystals were charged in excess of the solubility, and the state of the melt at the end of the soak period is illustrated schematically in Fig. 2-2, comparing with that of the conventional supercooling method. The other procedures are the same as the conventional supercooling method.

The mismatch of the lattice constant perpendicular to the interface between InGaPAs LPE layer and GaAs substrate was measured by x-ray diffraction using the (400) reflection of CuKα line, and the solid composition of the InGaPAs LPE layer was determined by EPMA or analysis of the room-temperature photoluminescence peak.

2-2-2. Liquid phase epitaxy of $In_{1-x}Ga_xP_{1-y}As_y$ (y=0.04)

The LPE growth of $In_{1-x}Ga_xP_{0.96}As_{0.04}$ has been carried out in order to examine the characteristics of the two-phase melt method and find the optimum growth condition outside of the immiscibility region. In Fig. 2-3, the compositions of Ga and P in the liquid, X^l_{Ga} and X^l_P, from which InGaPAs LPE layers with uniform mirror-like surface have been grown, are plotted as a function of charged weight percentage of InP (InP/In). It can be seen in the figure that X^l_{Ga} decreases from 1.30 at% to 1.10 at% and X^l_P increases from 2.85 at% to 2.90 at%, as the charged InP/In increases from 2.10 wt% to 2.50 wt%. These results indicate that both X^l_{Ga} and X^l_P can be controlled by changing the charged InP/In when melts are charged with GaP poly-crystals in excess of their solubility. The solid compositions of InGaPAs LPE layers can also be controlled by changing charged InP/In. In Fig. 2-4, the

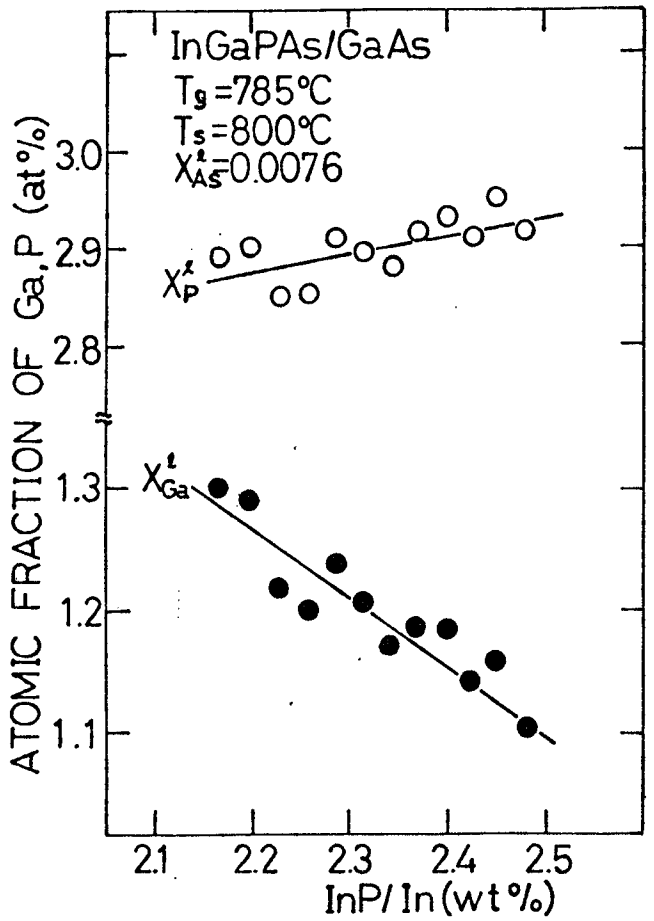

Fig. 2-3 Liquid compositions of Ga (X^{l}_{Ga}) and P (X^{l}_{P}) for growth of $In_{1-x}Ga_xP_{0.96}As_{0.04}$ LPE layer plotted as a function of the charged amount of InP (InP/In).

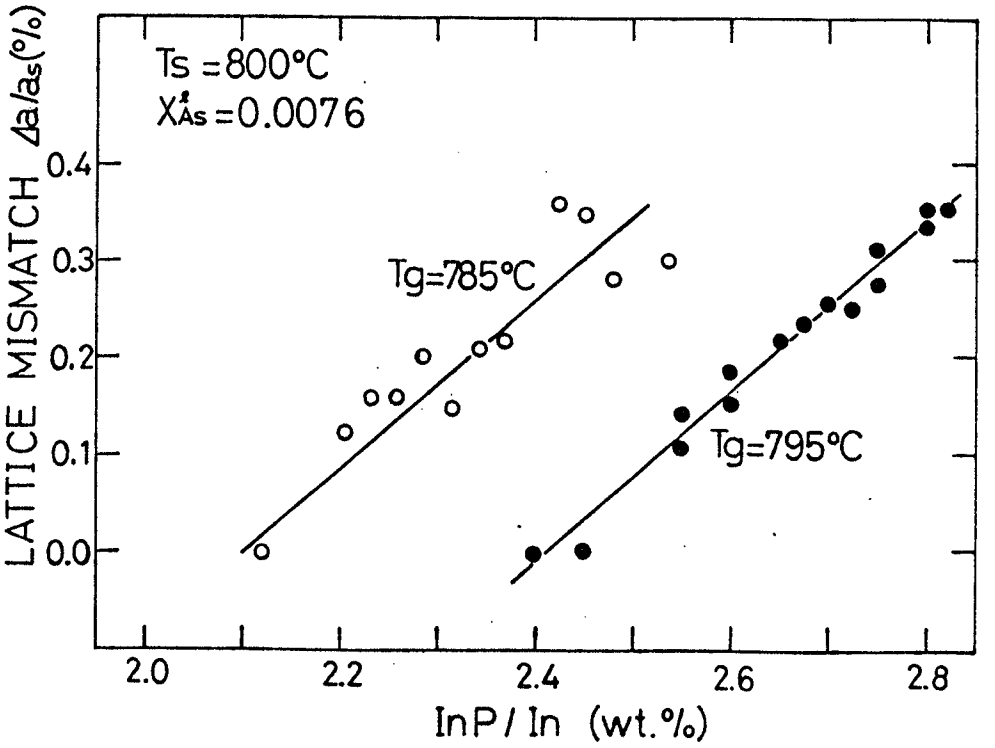

Fig. 2-4 Lattice mismatch between $In_{1-x}Ga_xP_{0.96}As_{0.04}$ LPE layer and (100) GaAs substrate plotted as a function of the charged amount of InP/In. Open circles and closed circles indicate results for growth temperature of 785°C and 795°C, respectively.

mismatch of the lattice parameter normal to the interface between InGaPAs LPE layer and GaAs substrate, $\Delta a/a$, is plotted as a function of charged InP/In. The results show that $\Delta a/a$ increases linearly as InP/In increases. The range of InP/In with which mirror-like InGaPAs LPE layers have been grown at 785°C is between 0.0% and 0.35%. Values of InP/In in the case of the growth temperature at 795°C which give the same $\Delta a/a$ as the case of 785°C are larger than that at 785°C by 0.3 wt%, as can be seen in Fig.2-4. The range of $\Delta a/a$ of InGaPAs LPE layers grown at 795°C (ΔT=5°C) is the same as that grown at 785°C (ΔT=15°C). Out of these ranges of InP/In, the GaAs substrate was heavily melted back and no LPE layer was grown.

In order to examine the liquid compositions of melts, the phase diagram has been calculated for the In-Ga-P-As quaternary system available for this study by using the well-known formula for the equilibrium condition with thermodynamical parameters previously reported.[15] Figure 2-5 shows the calculated liquidus isotherms with a temperature range between 780°C and 810°C, and iso-composition lines plotted for X^l_{As}=0.76 at%. The rectangular area shaded in this figure shows X^l_{Ga} and X^l_P with which InGaPAs LPE layers have successfully been grown at 785°C. It can be seen from the figure that the liquidus temperature of this area ranges from 796°C to 802°C of the calculated liquidus and agrees with the saturation temperature of 800°C.

As for solid compositions, EPMA measurements give the x value range between 0.54 and 0.56 for InGaPAs LPE layers successfully grown, and give a x value of 0.56 under the lattice-matched condition. The y values were 0.04 for all samples. The range of X^l_{Ga} corresponding to this range of x is between 1.10 at% and 1.30 at%, and somewhat larger

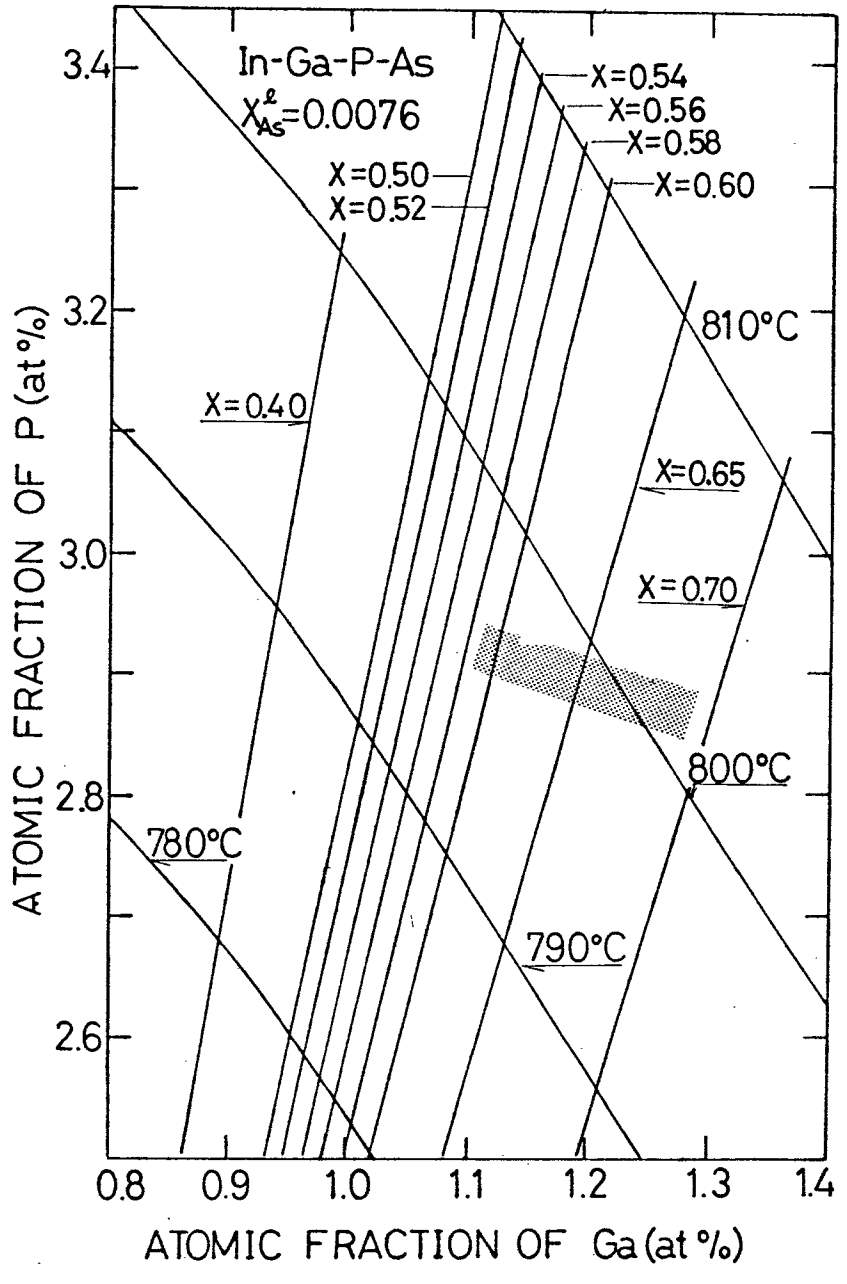

Fig. 2-5 Relations between X^{1}_{Ga} and X^{1}_{P} for X^{1}_{As}=0.76 at%. Calculated liquidus between 780°C and 810°C and iso-composition lines are shown. Rectangular area shaded in figure shows the liquid composition of the melt where $In_{1-x}Ga_{x}P_{0.96}As_{0.04}$ LPE layers have successfully grown.

than that predicted by these calculations being $1.06<X^{1}_{Ga}<1.08$ at%. The experimentally obtained growth range of X^{1}_{Ga} becomes wider than that predicted by these calculations, as can be seen in Fig. 2-5. These results are considered to be due mainly to the strain energy caused by lattice mismatch.[5,16,17]

In order to investigate characteristics of the melt, growth temperature (T_g) dependences of lattice mismatch and LPE layer thickness (d), and growth time (t_g) dependence of layer thickness have been measured with melt compositions unchanged. The growth temperature dependences of lattice mismatch and LPE layer thickness are shown in Fig. 2-6. Since the two-phase melt method has been used, the difference between growth temperature and soak temperature (T_s=800°C) shows supercooling (ΔT). It can be seen in the figure that $\Delta a/a$ increases, i.e. solid composition x, decreases as T_g decreases, and that d increases as ΔT increases. In Fig. 2-7, d is plotted as a function of t_g with ΔT of 5°C. As can be seen in Fig. 2-7, d increases with $t_g^{1/2}$. This shows that the growth occurs by the stepcooling-like mechanism, i.e. the diffusion limited growth, suggesting that the growth is not affected by microcrystal formation in the melt in spite of the existence of the solid phase of GaP contacting with the melt. This fact makes no discrepancy with the monotonous increase of d with ΔT. The decrease of LPE layer thickness with ΔT has been reported and suggested that microcrystals are formed in the melts supercooled by more than 8°C.[18] In the present study, such a decrease in d has not been observed with ΔT smaller than 15°C. Therefore, the decrease in x with decreasing T_g shown in Fig. 2-6 is not due mainly to microcrystal formation. The reason for this is

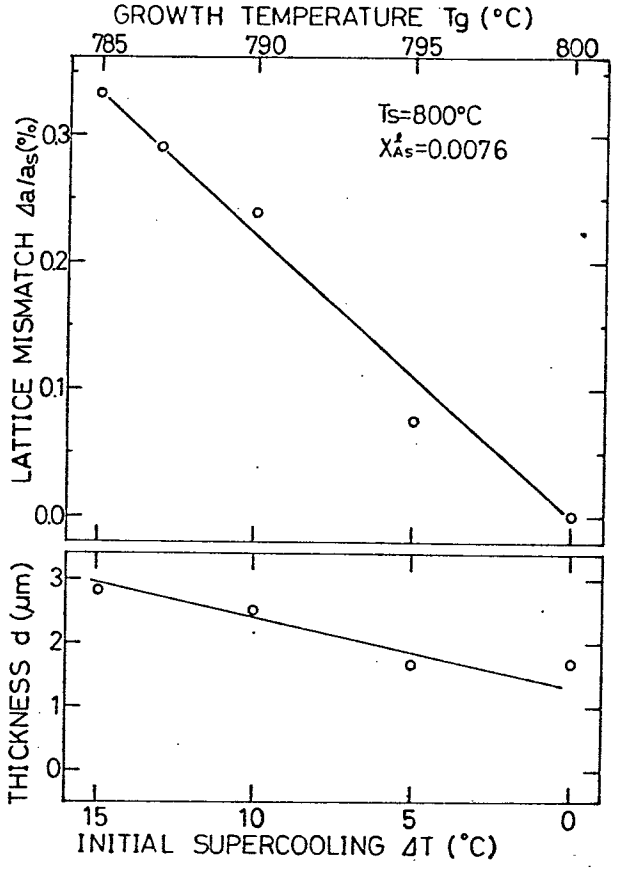

Fig. 2-6 Lattice mismatch ($\Delta a/a$) and $In_{1-x}Ga_xP_{0.96}As_{0.04}$ LPE layer thickness (d) plotted as a function of growth temperature (T_g). Saturation temperature (T_s) is 800°C, and X^l_{As} is 0.76 at%. Differences between T_s and T_g shows supercooling ΔT.

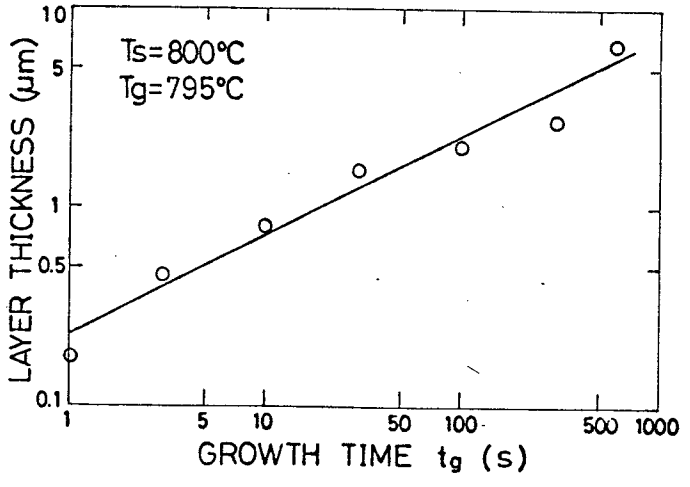

Fig. 2-7 Layer thickness of $In_{1-x}Ga_xP_{0.96}As_{0.04}$ LPE layers (d) plotted as a function of growth time (t_g).

considered to be the variation of the distribution coefficient of solutes, Ga and P, with ΔT under the non-equilibrium growth from the analysis of the growth path.[12] This may also cause the difference in the charged InP/In with the difference of growth temperature.

It has been said that a large initial supercooling such as 15°C is necessary in this system to prevent melt back of GaAs substrate.[10] In the conventional supercooling technique this was denied and it has been shown that ΔT=1°C is sufficient to obtain flat InGaPAs LPE layers.[2] In the present two-phase melt technique, the degree of supercooling is easily determined compared with the conventional supercooling technique, because the saturation at the soak period is automatically satisfied. While in the conventional supercooling method, saturation temperature is different from soak temperature and varies with sources charged. In order to ascertain this, several growth runs with a small initial supercooling have been done. After the soak period, the substrate was brought into contact with the melt without cooling and temperature was kept constant during the growth period of 5 mins. The interface between InGaPAs LPE layer and GaAs substrate was a little bit rough but the surface was flat. Therefore the melt is considered to be saturated or a little bit supercooled after the soak period. Samples grown without or with 2°C supercooling at a cooling rate of 1°C/min have shown the flat interface as well as flat surface. These results indicate that no large supercooling is necessary for the growth of InGaPAs LPE layers with this two-phase melt technique.

2-2-3. Liquid phase epitaxy inside the immiscibility region

In the LPE growth of $In_{1-x}Ga_xP_{1-y}As_y$ lattice-matched to GaAs, the growth is influenced by immiscibility.[19] The composition region influenced by immiscibility is called miscibility gap and defined by spinodal and binodal curves.[19-22] In this composition region, the crystal growth is unstable since the alloy tends to separate into two different compositions. The concept of immiscibility has been theoretically treated in terms of the free energy of alloys. If the free energy F for an $A_{1-x}B_xC_{1-y}D_y$ quaternary alloy plotted on the composition x,y-plane has a negative curvature direction as shown in Fig. 2-8, immiscibility occurs. The trace of inflection points for the free energy surface is called a spinodal curve, which represents the boundary between metastable and unstable regions. The spinodal curve is defined as;

$$\frac{\partial^2 F}{\partial x^2}\cdot\frac{\partial^2 F}{\partial y^2} - \left(\frac{\partial^2 F}{\partial x\cdot\partial y}\right)^2 = 0 \qquad (2\text{-}1)$$

When immiscibility occurs, the construction of a series of double tangent plane to the free energy surface is possible. The trace of tangent points is called a binodal curve, which represents the boundary between metastable and stable regions. On a set of binodal points, which can be connected by a tie line, chemical potentials are equal for two conjugate compositions, and hence solid-solid equilibrium is possible between them. A set of binodal points (x_1,y_1) and (x_2,y_2) is given by the following three independent equations;

$$\left.\frac{\partial F}{\partial x}\right|_1 = \left.\frac{\partial F}{\partial x}\right|_2 \qquad (2\text{-}2)$$

$$\left.\frac{\partial F}{\partial y}\right|_1 = \left.\frac{\partial F}{\partial y}\right|_2 \qquad (2\text{-}3)$$

$$-\left.\frac{\partial F}{\partial x}\right|_1 x_1 - \left.\frac{\partial F}{\partial y}\right|_1 y_1 + F(x_1,y_1) = -\left.\frac{\partial F}{\partial x}\right|_2 x_2 - \left.\frac{\partial F}{\partial y}\right|_2 y_2 + F(x_2,y_2). \qquad (2\text{-}4)$$

The free energy F per mole has been given by the strictly regular solution approximation[20,21] as

$$\begin{aligned} F = {} & \mu^0_{InP}(1-x)(1-y) + \mu^0_{InAs}(1-x)y + \mu^0_{GaP}x(1-y) + \mu^0_{GaAs}xy \\ & + \alpha_{InP-GaP}(1-x)x(1-y) + \alpha_{InAs-GaAs}(1-x)xy \\ & + \alpha_{InP-InAs}(1-x)(1-y)y + \alpha_{GaP-GaAs}x(1-y)y \\ & + RT\{ (1-x)\ln(1-x) + x\ln x + (1-y)\ln(1-y) + y\ln y \}, \end{aligned} \qquad (2\text{-}5)$$

where μ^0_{AB} is the chemical potential of a pure binary compound AB, α_{AB-AC} (α_{AB-CB}) is the pseudobinary interaction parameter for mixing between binary compound AB and AC (AB and CB), and RT is the product of gas constant and absolute temperature. Spinodal and binodal curves can be calculated by using equations (2-1)∿(2-5) and the relationship[20,21]:

$$\mu^0_{InP} + \mu^0_{GaAs} - (\mu^0_{GaP} + \mu^0_{InAs}) = W_Q = 3687.7 + 0.92T \text{ (cal/mol)}.$$

Calculated binodal curve and tie line with the corresponding spinodal curve for InGaPAs at a typical growth temperature of 820°C are shown in Fig. 2-9. It can be seen in the figure that compositions y between 0.22 and 0.45 are in the binodal curve when InGaPAs is lattice-matched to GaAs. It is therefore expected that the LPE growth of $In_{1-x}Ga_xP_{1-y}As_y$ with the composition range $0.22<y<0.45$ is influenced

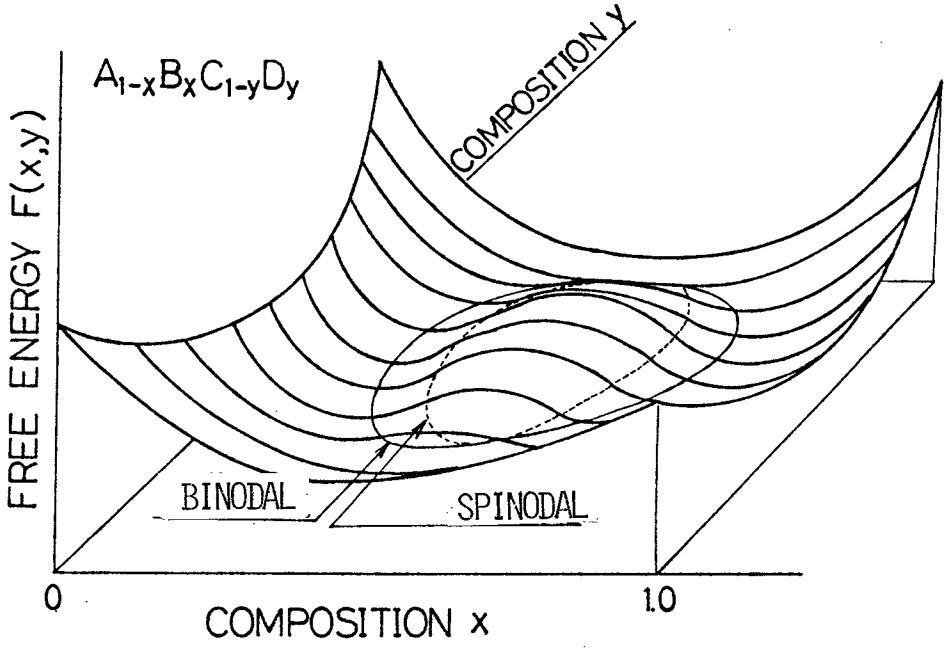

Fig. 2-8 Schematic representation of the free energy of the $A_{1-x}B_xC_{1-y}D_y$ alloy system having the immiscibility as a function of the composition x and y.

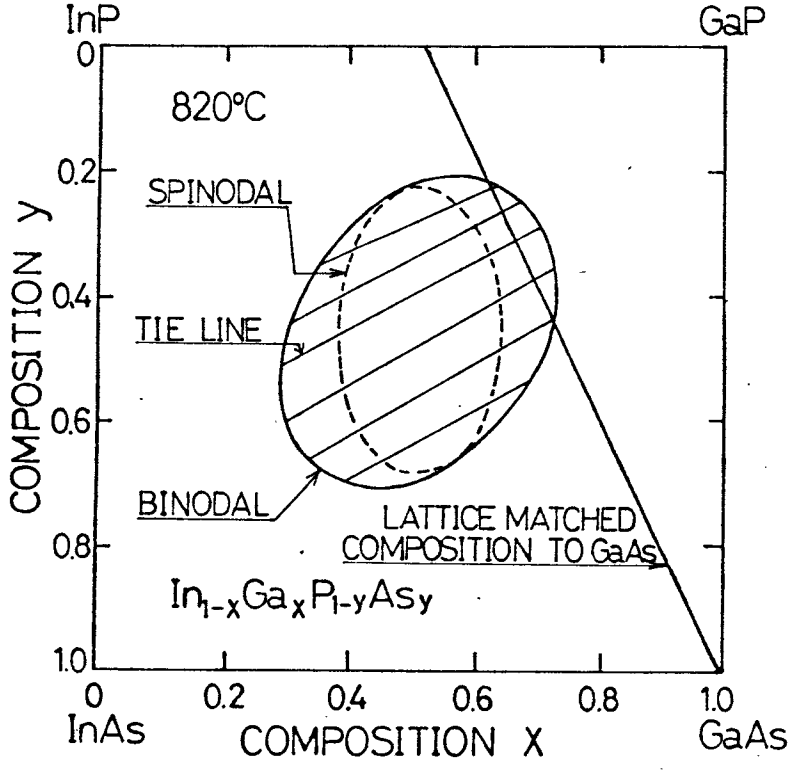

Fig. 2-9 Calculated spinodal and binodal curves for the InGaPAs system at 820°C. Chained and solid lines are calculated spinodal and binodal curves with its tie-lines at 820°C, respectively.

by immiscibility in contrast to that of $In_{1-x}Ga_xP_{0.96}As_{0.04}$ being less affected by immiscibility.

In order to find the optimum growth conditions for the LPE growth in the immiscibility region, firstly the LPE growth of $In_{1-x}Ga_xP_{0.7}As_{0.3}$ layers has been carried out using both the conventional supercooling technique and the two-phase melt technique with excess GaP. The growth time was 10 s.

In the conventional supercooling technique, InP, InAs and GaAs were used as sources, and they dissolved completely into In solution during the soak period as illustrated in Fig. 2-2. In this growth method, a change in X^1_{Ga} under a fixed X^1_P for the trimming of the lattice mismatch causes the variation in the degree of supercooling.

In the two-phase melt technique, GaAs, InAs and GaP were used as sources, in which GaP source poly-crystals were charged in excess of the solubility. In this method, since the excess GaP source crystal saturates the melt at soak temperature, the degree of supercooling defined as the difference between soak and growth temperatures can be kept constant independent of X^1_{Ga}.

The LPE growth was carried out under three conditions (A), (B) and (C) indicated in Table 2-1. In the LPE growth using the two-phase melt method under the growth condition (B), mirror-like $In_{1-x}Ga_xP_{0.7}As_{0.3}$ LPE layers have been obtained with the lattice mismatch between -0.24 and 0.30%. The liquid compositions, X^1_{Ga} and X^1_P, for such growth are plotted in Fig. 2-10 together with the calculated liquidus isotherms. As can be seen in the figure, the liquid composition of the melt soaked at 800°C is in good agreement with the calculated liquidus isotherm, indicating the melt beeing well

Table 2-1 Growth conditions used for the LPE growth of $In_{1-x}Ga_xP_{0.7}As_{0.3}$.

growth condition	growth method	T_{soak}(°C)	T_g(°C)	ΔT(°C)	X^l_{As}(at%)	X^l_P(at%)
(A)	supercooling	800	785		10.0	1.3
(B)	two-phase melt	800	795	5	10.0	
(C)	two-phase melt	823	820	3	11.5	

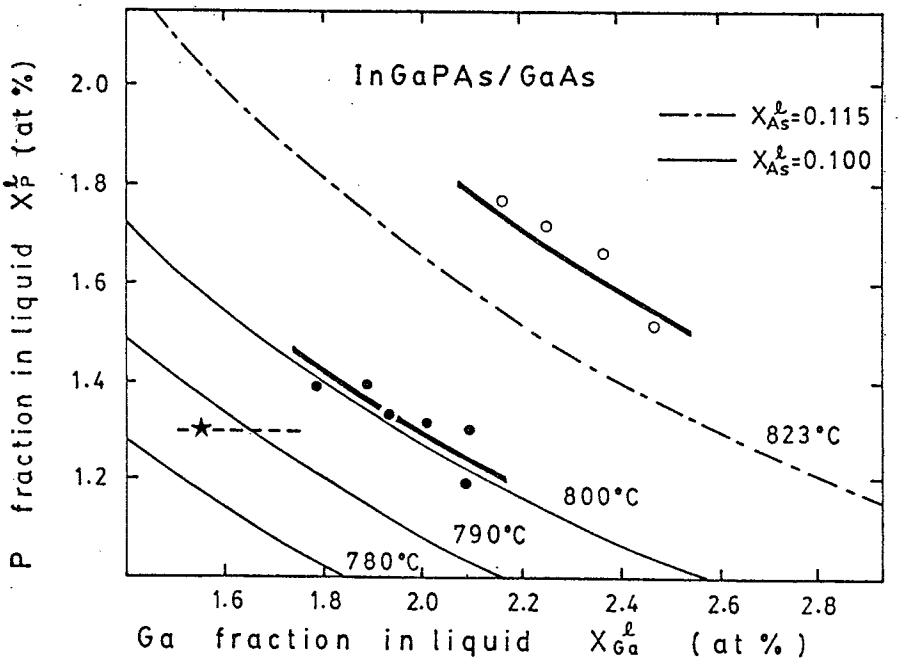

Fig. 2-10 Liquidus compositions plotted together with calculated liquidus isotherms for the growth of $In_{1-x}Ga_xP_{0.7}As_{0.3}$ LPE layer. Dashed line corresponds to growth condition (A), and star denotes the liquidus composition where solid is in equilibrium with liquid at 785°C. Closed and open circles correspond to conditions (B) and (C), respectively.

saturated at the soak temperature. The reason that the liquid composition of the melt soaked at 823°C is slightly larger than that calculated is mainly due to the loss of evaporated P due to higher soak temperature.

On the other hand, in the LPE growth using the conventional supercooling method under the condition (A), the range of lattice mismatch with successful growth is between 0.18 and 0.34 % which is much narrower compared with that for the two-phase melt method. Furthermore, the surface morphology changes critically depending on the lattice mismatch and therefore on X^1_{Ga}. Within the liquid composition range, $1.55 \leqq X^1_{Ga} \leqq 1.70$ at %, InGaPAs layers are uniform and mirror-like with flat surface and heterointerface, as shown in Fig. 2-11(b,e). Out of this composition region, the surface turns out to be rough. In the case of $X^1_{Ga} \leqq 1.55$ at %, the surface is rough like smoked glass. It has been observed that the GaAs substrate was partially dissolved into the melt and the InGaPAs LPE layer was grown like islands as can be seen in Fig. 2-11(d). This fact shows that the melt is slightly undersaturated.[2] On the other hand, when X^1_{Ga} is between 1.70 and 1.80 at %, the surface becomes smoky, and white and black sticks were sometimes observed on the surface, as can be seen in Fig.2-11(c). Such sticks are considered to be GaP-like and InAs-like crystals which were grown due to phase separation in the immiscibility region. At larger X^1_{Ga} than 1.80 at%, InGaPAs LPE layers have not been grown. These changes in the surface morphology are considered to be attributed to the change in the initial supercooling which is caused by the change of the liquid composition. This situation can be understood by comparing the liquid composition with the calculated

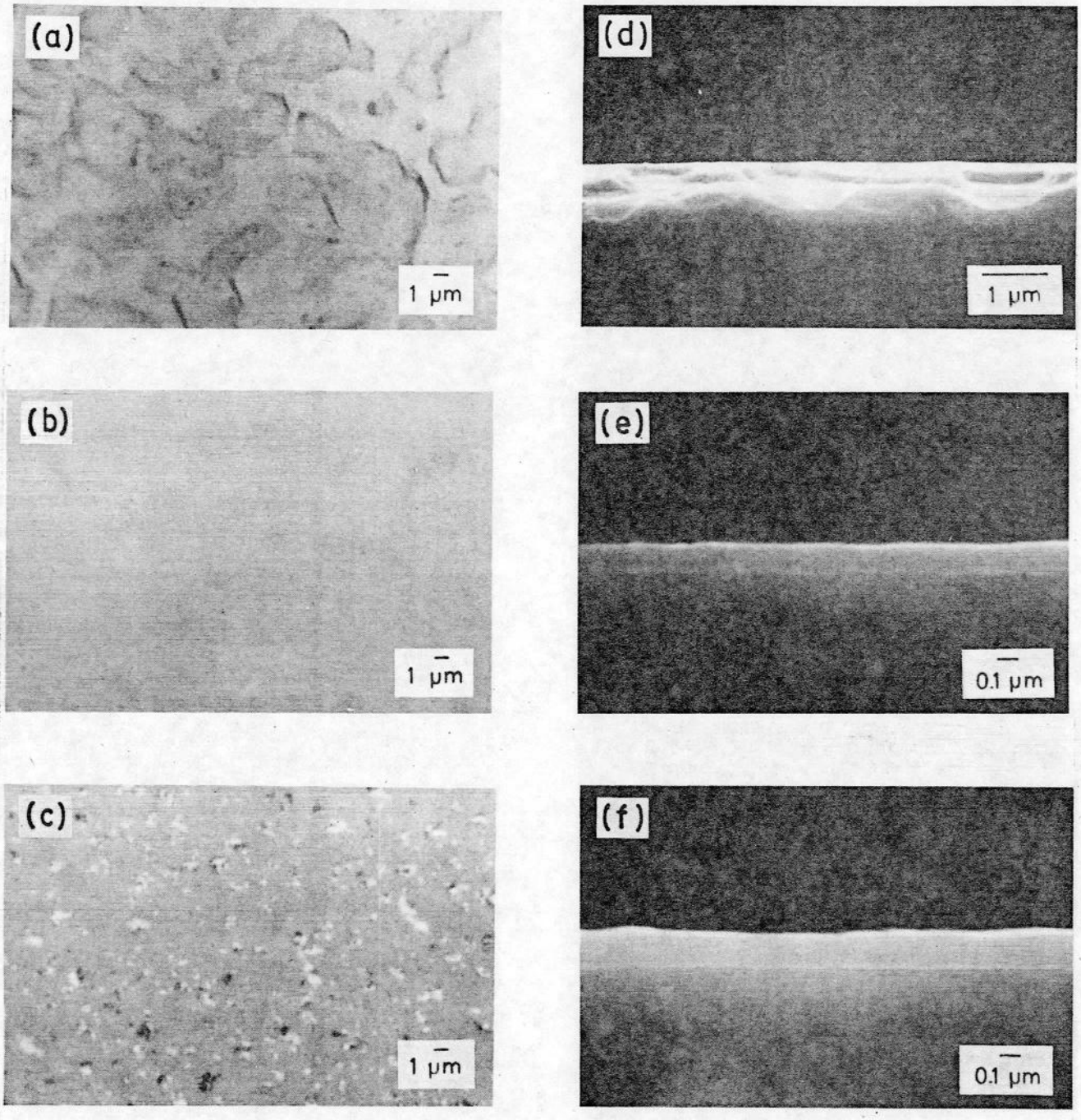

Fig. 2-11 Optical micrographs of front surface (a, b, c) and SEM images of cleaved cross-section (d, e, f) for $In_{1-x}Ga_xP_{0.7}As_{0.3}$ LPE layers. X^l_{Ga} is 1.50 (a, d), 1.60 (b, e) and 1.75 at % (c, f), respectively.

liquidus. In Fig. 2-10, the dashed line represents the trace of the liquid composition used in the LPE growth by the conventional supercooling method. The star plot in the same figure indicates the liquid composition in which the melt is saturated at the growth temperature of 785°C under X^1_P of 1.3 at%. The difference of the liquidus temperature between the point in the dashed line and the star indicates the initial supercooling ΔT. It follows that ΔT changes from 0 to 10°C when X^1_{Ga} is changed from 1.55 to 1.74 at%, indicating that the LPE growth is very sensitive to ΔT. It is considered from the above result that ΔT of 3∿5°C is necessary for obtaining flat-surface InGaPAs LPE layers. Such ΔT sensitivity in the LPE growth has not been observed in the LPE growth of $In_{1-x}Ga_xP_{0.96}As_{0.04}$ in which the composition is outside of the binodal. It is also noted here that the crystal quality of $In_{1-x}Ga_xP_{0.7}As_{0.3}$ LPE layers changes critically depending on ΔT as described in Chapter 3.

Next, the LPE growth has been examined under various X^1_{As} using the two-phase melt method under the condition (C) in which the ΔT has been chosen as 3°C suitable for the LPE growth in the immiscibility region based on the above discussions. In the case of $X^1_P > X^1_{Ga}$, sources of InP, InAs and GaP were used, while GaAs, InP and GaP were used in the case of $X^1_P < X^1_{Ga}$. The liquid and solid compositions with the successful growth of LPE layers under various X^1_{As} are shown in Figs. 2-12 and 2-13, respectively. In Fig. 2-13, the calculated spinodal and binodal curves with tie lines at 820°C are also shown. It is noted that the growth of InGaPAs LPE layer on GaAs substrate was possible over a large composition range even for compositions calculated to be in the immiscibility region. However, the surface of

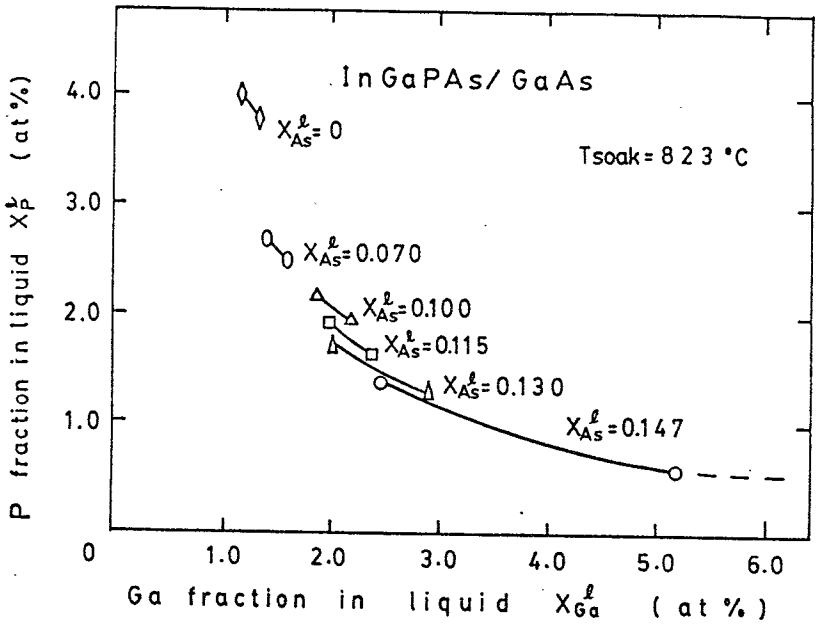

Fig. 2-12 Liquid compositions, X^{1}_{Ga} and X^{1}_{P}, plotted for various X^{1}_{As} in successful growth of InGaPAs LPE layers.

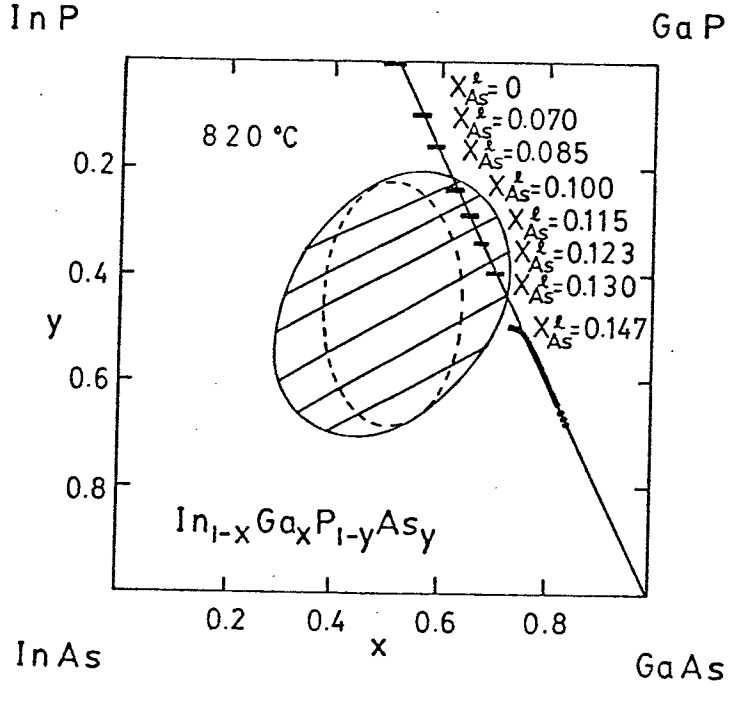

Fig. 2-13 Solid compositions of $In_{1-x}Ga_xP_{1-y}As_y$ LPE layers grown from melts having various X^{1}_{As}.

LPE layers grown in the immiscibility region was mirror-like only when the growth time was shorter than 10 s corresponding to an epitaxial layer thickness of ∿0.3 μm. The surface of the layers grown with larger growth time rapidly turned rough, and the source melt was usually left on the surface with the growth time longer than 20 s. In the present study, the growth of LPE layers thicker than 0.3 μm was impossible in the immiscibility region, while in the outside of the region LPE layers thicker than 3 μm were easily grown. These results can be interpreted in terms of the elastic energy induced from substrate such as strain energy due to lattice mismatch. The negative curvature in the free energy surface shown in Fig. 2-8 which produces immiscibility is considered to be cancelled in the presence of strain energy due to lattice mismatch which has parabolic dependence with respect to composition change along the tie line.[23,24] As long as the epitaxial layer is thin and grows coherently on substrate, spinodal decomposition does not occur due to strain energy. When epitaxial layers grow thicker and the strain energy is relaxed due to the formation of misfit dislocations,[25] the influence of immiscibility on the LPE growth becomes larger and the growth of uniform LPE layers becomes difficult due to spinodal decomposition. From these results and discussion, it is concluded that the LPE growth of InGaPAs alloys in the immiscibility region is possible with an aid of the elastic energy from substrate.

It is noted in Fig. 2-12 that the successful growth range is extraordinarily large at X^l_{As}=14.7 at %, compared with other X^l_{As} values. In the case of X^l_{As}<14.7 at %, the solid As composition y is almost constant as X^l_{Ga} increases, while in the case of X^l_{As}=14.7 at

%, y increases in proportion to the increase in X^{l}_{Ga} and InGaPAs layer keeps lattice-matching with substrate, as shown in Fig. 2-13. This is caused by increase of the distribution coefficient of As with increase of X^{l}_{Ga} corresponding to a changing in the liquidus from In-rich solution to Ga-rich one.

2-3. Solution growth of bulk InGaP alloys

The bulk crystals of InGaP alloys have been synthesized by the vapor-pressure controlled temperature-difference solution-growth method[26,27] using a multi-zone vertical furnace. The growth has been carried out in a sealed quartz tube. The outline of the growth apparatus is schematically shown in Fig. 2-14. The In or In+Ga solvents have been charged in the upper part of the quartz ampoule together with source poly-crystals of InP and GaP, which is placed in the high temperature region of the furnace. The red phosphorus is charged in the lower end of the quartz tube which is placed in the low temperature region for the purpose of applying the phosphorus vapor pressure. The growth has been carried out under a constant growth temperature at 960°C with a temperature gradient of 10°C/cm. The growth occurs by the diffusion of Ga and P to the lower part of the ampoule by the temperature difference and then supersaturated. The liquid composition of the solution has been controlled by changing the phosphorus vapor pressure. The amount of dissolved GaP source poly-crystals into the In melt is determined automatically according to the P vapor pressure, and the liquid composition can be maintained at a constant value. Even if the liquid composition of Ga decreases according to the crystal growth, the GaP source poly-crystal supplies Ga into the liquid to make the liquid composition of the melt constant, and therefore the growth of bulk InGaP alloys with uniform alloys composition is expected.

After the growth for 7∿10 days, poly-crystalline InGaP bulk alloys of ∿1g in weight with grain size of 3∿5 mm have been obtained.

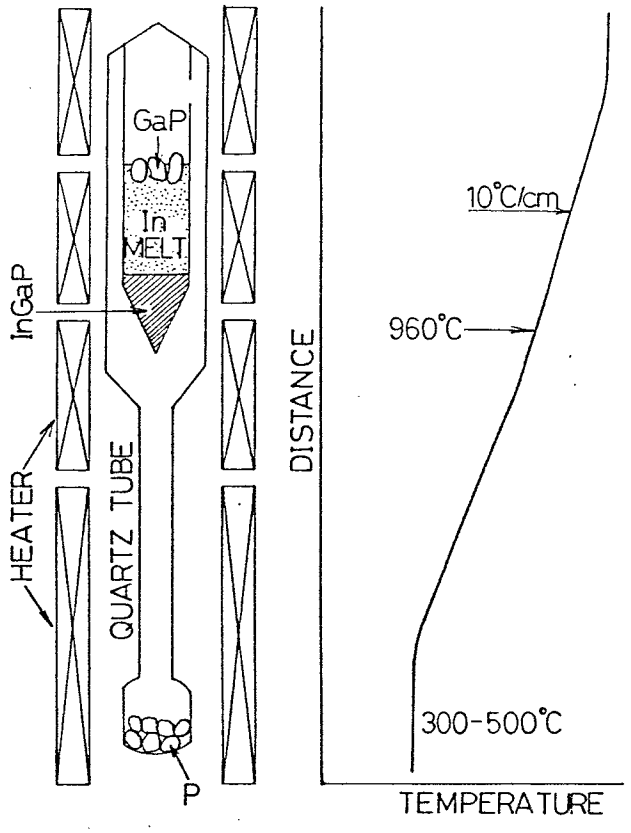

Fig. 2-14 Vertical multizone furnace and temperature profile used for the growth of bulk InGaP alloys.

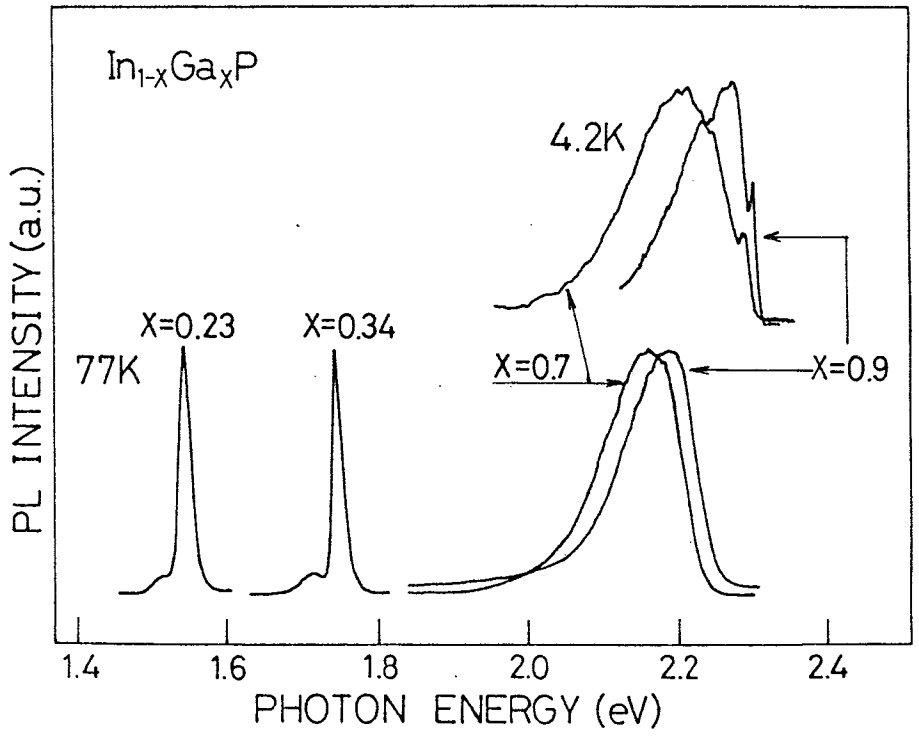

Fig. 2-15 Near-band edge PL spectra of bulk InGaP alloys.

The composition of $In_{1-x}Ga_xP$ alloys has been determined using both a powder x-ray diffraction method and EPMA. $In_{1-x}Ga_xP$ alloys with the composition x between 0.23 and 0.99 have been grown, and it has been verified that the alloy composition x decreases from 0.99 to 0.23 when the phosphorus temperature is changed from 300 to 550°C, indicating that the alloy composition is controlled by changing the P vapor pressure. The variation of composition is ∿1% within the grain.

All InGaP alloys are n-type, and the room temperature carrier concentrations and Hall mobility are 1∿2 x 10^{16} cm^{-3} and 400∿700 $cm^2/V.s$, respectively, for samples with x between 0.23 and 0.47. The near-band edge PL spectra obtained for these InGaP alloys are shown in Fig. 2-15. The FWHM values of the near-band edge emission measured at 77K are 14∿17 meV for InGaP alloys with direct band gap. The sharp emission peak at 2.3 eV observed at 4.2K for $In_{1-x}Ga_xP$ with x of 0.7 and 0.9 having indirect band gap is considered to be due to bound exciton recombination. These features of the near-band edge emission show that good quality InGaP bulk alloys have been grown.

2-4. Summary

The LPE growth of InGaPAs single crystal layers on GaAs substrate has been investigated. For the reproducible LPE growth of this alloy system, the two-phase melt method with excess GaP was proposed. LPE growth conditions such as growth temperature, supercooling and growth time about the two-phase melt method were examined, the results showing that the accurate setting of supercooling is possible independent of the liquid composition of Ga, which enabled the reproducible LPE growth of InGaPAs on GaAs even in the immiscibility region. The relationship between the liquid and solid compositions has been made clear, and the results were compared with the calculated phase diagram. In the immiscibility region, it has been found that the crystal growth is sensitive to the degree of supercooling, and that the supercooling of 3∿5°C is necessarily for the LPE growth. By using the two-phase melt method, InGaPAs LPE layers have been successfully grown over the whole composition range even in the immiscibility region. However, in the immiscibility region, the LPE layer thicker than 0.3 μm has not been grown, the result suggesting that the strain energy from substrate plays an important role in the LPE growth.

The solution growth of bulk $In_{1-x}Ga_xP$ alloys was carried out using the vapor-pressure controlled temperature difference method. Bulk crystals with composition $0.23<x<0.99$ have been grown, and were characterized by Hall effect and PL measurements, the results showing that the bulk InGaP alloys have good crystal quality.

REFERENCES

1) K. Nakajima: Semiconductors and Semimetals, eds. W. T. Tsang (Academic Press, New York) Vol. 8, Chap. 1, p. 1.

2) K. Hiramatsu, K. Tomita, N. Sawaki and I. Akasaki: Jpn. J. Appl. Phys. 23 (1984) 68.

3) A. Suzuki, H. Kyuragi, S. Matsumura and H. Matsunami: Jpn. J. Appl. Phys. 19 (1980) L207.

4) A. Suzuki, T. Murakami, Y. Kuriyama and H. Matsunami: Jpn. J. Appl. Phys. 21 (1982) L363.

5) G. B. Stringfellow: J. Appl.Phys. 43 (1972) 3455.

6) S. Mukai: J. Appl. Phys. 54 (1983) 2635.

7) S. Mukai, M. Matsuzaki and J. Shimada: Jpn. J. Appl. Phys. 19 (1980) L505.

8) T. Kato, T. Matsumoto and T. Ishida: Jpn. J. Appl. Phys. 21 (1982) L667.

9) S. Kaneiwa, T. Takenaka, S. Yano and T. Hijikata: J. Cryst. Growth 62 (1983) 498.

10) H. Kawanishi and T. Suzuki: Jpn. J. Appl. Phys. 23 (1983) L52.

11) S. Shirakata, M. Kondo, A. Tsushi, T. Nishino, Y. Hamakawa and T. Kariya: Jpn. J. Appl. Phys. 24 (1985) 524.

12) M. Kondo, S. Shirakata, A. Tsushi, T. Nishino and Y. Hamakawa: Jpn. J. Appl. Phys. 24 (1985) 806.

13) M. Kondo, S. Shirakata, T. Nishino and Y. Hamakawa: J. Appl. Phys. 60 (1986) 3539.

14) A. Suzuki, H. Kyuragi, S. Matsumura and H. Matsunami: Jpn. J. Appl. Phys. 19 (1980) L207.

15) M. B. Panish and M. Ilegems: Progress in Solid Srate Chemistry (Pergamon, Oxford, 1972) Vol.7, p. 39.

16) B. de Cremoux, P. Hirtz and J. Ricciardi: Proc. 1980 Int. Symp. Gallium Arsenide & Related Compounds (Inst. Phys., London, 1981) p.115.

17) P. K. Bhattacharya and S. Srinivasa: J. Appl. Phys. 54 (1983) 5090.

18) S. Mukai, M. Matsuzaki and J, Shimada: Jpn. J. Appl. Phys. 20 (1981) 321.

19) B. de Cremoux: J. Physique 43 (1982) c5.

20) K. Onabe: NEC Res. and Develop. 72 (1984) 1.

21) K. Onabe: Jpn. J. Appl. Phys. 22 (1983) 663.

22) G. B. Stringfellow: J. Cryst. Growth 58 (1982) 194.

23) M. Quillec, C. Daguet, J. L. Benchinol and H. Launois: Appl. Phys. Lett. 40 (1982) 325.

24) M. Ishikawa and R. Ito: Jpn. J. Appl. Phys. 23 (1984) L21.

25) J. W. Matthews, A. E. Blakeslee and S. Mader: Thin Solid Films 33 (1976) 253.

26) H. Itoh, K. Hara, A. Tanaka and T. Sukegawa: Appl. Phys. Lett. 19 (1971) 348.

27) T. Kato, A. Shimizu and T. Ishida: Jpn. J. Appl. Phys. 13 (1974) 1481.

3. PHOTOLUMINESCENCE AND ELECTROREFLECTANCE OF InGaPAs/GaAs

3-1. Introduction

For practical applications of InGaPAs layers grown on GaAs to optoelectronic devices as visible-light laser diode, the lattice-matching condition is important.[1,2] However, due to the difference of thermal expansion between InGaPAs and GaAs,[3] InGaPAs LPE layers precisely lattice-matched to GaAs at room temperature grow under the lattice-mismatched condition which introduces defects and misfit dislocations during the growth. Therefore, the characterization of InGaPAs LPE layers in terms of lattice mismatch at both room and growth temperatures is required. Another important problem is the crystal quality of InGaPAs LPE layers grown under the influence of immiscibility.[4-7] This problem is serious for fabrication of a visible-light laser diode operating at the 720 nm wavelength region,[8-10] because the growth of the active layer is affected by immiscibility. In fact, degradation of the crystal quality of LPE layers grown in the immiscibility region has been reported such as extraordinarily broadened near-band edge PL.[11] However, the detailed examination on the crystal quality of InGaPAs LPE layers grown in the immiscibility region, such as growth condition and lattice mismatch dependence of the crystal quality has not been carried out.

For the characterization of the crystal quality and impurity, photoluminescence (PL) measurements have been conventionally used.[12] By measurements of the band-to-band emission, one can characterize the crystal quality from the full-width at the half maximum (FWHM). PL

spectra are very sensitive to impurities or defects, and therefore PL spectra are widely used to characterize them involved in the crystal. However, PL spectra are sometimes obscured by the superposition of several PL lines or bands with different origins. On the other hand, electroreflectance (ER) spectra, which have been widely used for the determination of the band-gap energy, are less affected by impurities or defects.[13,14] Such ER measurement is powerful, since the crystal quality can be studied using the broadening parameter (Γ) in ER spectra as well as the precise band-gap energy.[15,16] By using these two characterization techniques complementally, one can make a clear picture to the crystal quality and impurities in InGaPAs LPE layers.

In this Chapter, the results of a systematic measurement of PL and ER spectra in InGaPAs LPE layer on GaAs over the whole composition range are discussed. First, the crystal quality and residual impurities in $In_{1-x}Ga_xP_{0.96}As_{0.04}$ are examined as a function of temperature and lattice mismatch.[17,18] Next, PL and ER spectra in InGaPAs LPE layers grown inside the immiscibility region are examined in connection with the crystal growth condition, composition dependence and lattice-mismatch dependence, and the influence of immiscibility on the crystal quality of InGaPAs LPE layers is discussed.[18,19]

3-2. Experimental procedure

3-2-1. Photoluminescence (PL)

The photoexcitation source was a cw Ar^+ laser operating at 514.5 nm with a beam diameter of about 1 mm. The luminescence taken from the irradiated surface was analyzed by a SPEX 1704 monochromator equipped with a 600 grooves/mm grating blazed at 1.25 μm and detected by a cooled photomultiplier. The detector output was fed to an EG&G PAR 124A lock-in amplifier and processed with a computer controlled signal-averaging system to improve the signal-to-noise ratio. The block diagram of the averaging system is shown in Fig. 3-1.

3-2-2. Electroreflectance (ER)

ER spectra were measured by both the Shottky-barrier and electrolyte methods. For Shottky-barrier ER, $Au/In_{1-x}Ga_xP_{0.96}As_{0.04}$ Shottky-barriers were fabricated by the evaporation of the semi-transparent Au film with sheet resistance of 1~5 K ohm/□ on the lightly etched (with $H_2SO_4:H_2O_2:H_2O=6:1:1$ solution at 70°C for 90 s) surface of an InGaPAs LPE layer after the formation of the ohmic contact to GaAs substrate. For electrolyte ER measurements, the sample was immersed in the 1N KCl aquenous solution. To both the Shottky-barrier diode and the sample in electrolyte, the modulating voltage with 200 Hz superposed on DC bias was applied, to modulate the surface electric field of both the samples. The nearly normal reflection alignment with the reflection angle smaller than 30° was used for both the ER measurements. The reflected light intensity was

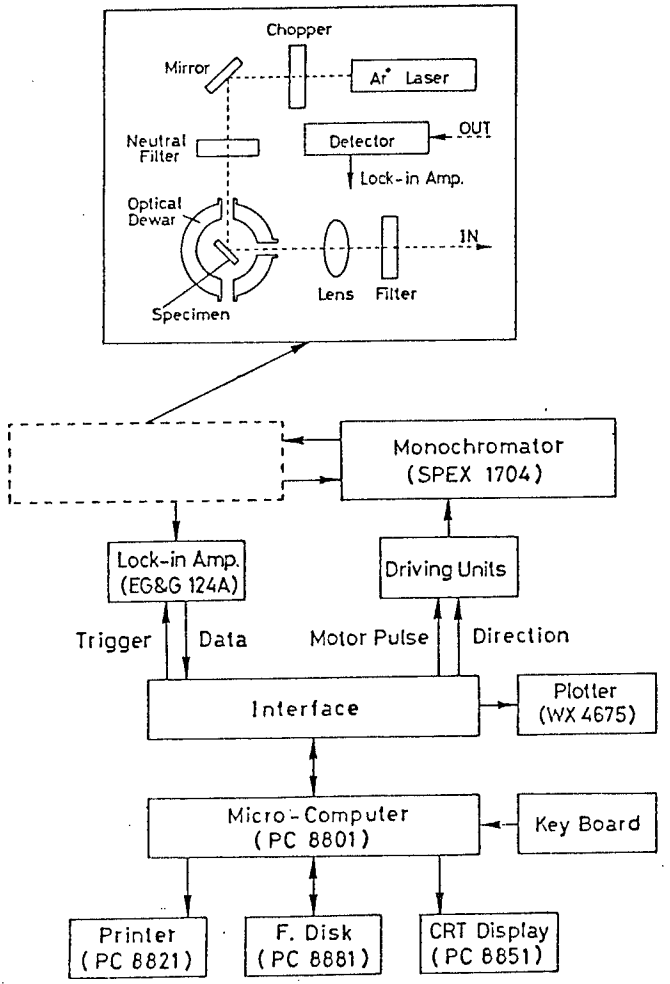

Fig. 3-1 Block diagram of photoluminescence measurement system used in this work.

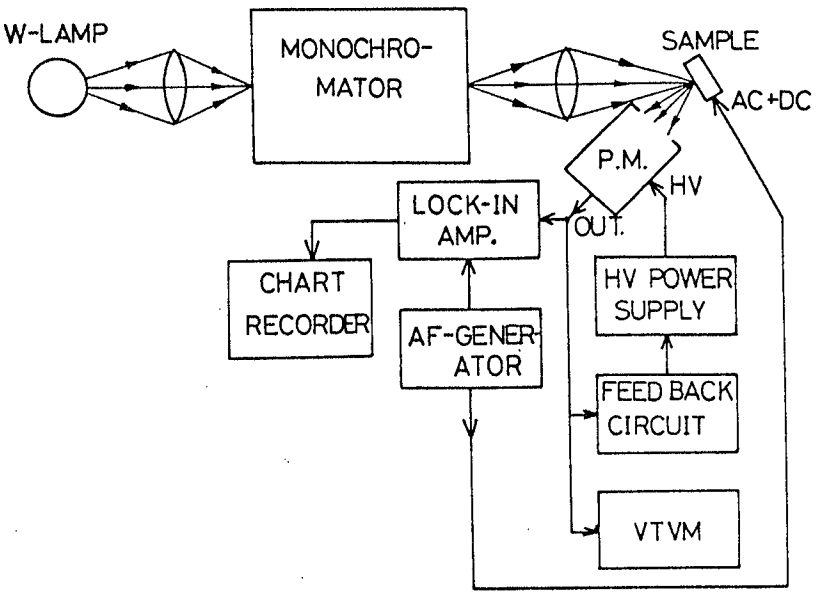

Fig. 3-2 Block diagram of electroreflectance measurement system used in this work.

detected by a HTV R-955 photomultiplier (PM). The ER signal ($\Delta R/R$) was obtained by the phase-sensitive detection of the AC component (proportional to the change in reflectivity, ΔR) through a PAR HR-8 lock-in amplifier under the condition that the DC component (proportional in reflectivity R) was kept constant by the electronic feed-back circuit which controls the high-voltage to PM and hence the sensitivity of PM. The block diagram of the ER measurement system is presented in Fig. 3-2.

ER measurements of InGaPAs LPE layers were carried out under the low-field condition. The low-field ER spectra were analyzed using the three-point adjusting method as follows.[16] The band-gap energy E_i and the broadening parameter Γ can be determined using the following equations:

$$E_i = E_A + (E_B - E_A)f(\rho) \qquad (3\text{-}1)$$

$$\Gamma = (E_B - E_A)g(\rho) \qquad (3\text{-}2)$$

$$\rho = -(\Delta R/R)_B/(\Delta R/R)_A, \qquad (3\text{-}3)$$

where A and B mean the lower- and higher- energy side peaks in ER spectra, and functions $f(\rho)$ and $g(\rho)$ are given by Aspnes et al.[15,16] The broadness of an ER spectrum is characterized by the broadening parameter Γ which is included in the dielectric function and is usually treated as the parameter of the so-called Lorentzian-type broadening.[14-16] In general, experimentally obtained ER spectra are affected by broadening effects coming from crystal imperfections other than the intrinsic life-time broadening effect. Therefore, the

magnitude of Γ can be sometimes considered to be a measure of the quality of the crystal under consideration.

3-3. PL and ER spectra in LPE $In_{1-x}Ga_xP_{1-y}As_y$ (y=0.04)

PL and ER spectra in $In_{1-x}Ga_xP_{0.96}As_{0.04}$ have been measured in order to characterize the crystal quality and impurities involved in the crystals grown outside the immiscibility region. Samples measured are all undoped n-type LPE layers with carrier concentration of $10^{15}\sim10^{16}$ cm^{-3} and electron Hall mobility of 1000∿1200 cm^2/Vs at room temperature.

3-3-1. PL and ER spectra at room temperature

Figure 3-3 shows typical room-temperature PL and ER spectra in the near-band edge region taken for an $In_{1-x}Ga_xP_{0.96}As_{0.04}$ LPE layer with Δa/a of 0.21%. Both the ER spectra taken by the Schottky-barrier and the electrolyte modulation techniques show the same line shape with no significant difference. The magnitude of the ER signal intensity (ΔR/R) was of the order of 10^{-4} with the peak-to-peak modulation voltage (V_{pp}) of 0.5 V. The ER line shape showed no change for the modulation voltage ranging from 0.1 to 0.5 V, and the ΔR/R amplitudes change linearly with the modulation voltage up to 0.5 V, these results suggesting that the ER spectra are in the low-field regime. The band-gap energy E_0 and broadening parameter Γ obtained by the three-point adjustment-method for these low-field ER spectra[15,16] do not change with V_{pp} lower than 0.5 V. The precise band-gap energy E_0 obtained by the three-point-adjustment method, 1.885 eV, is shown

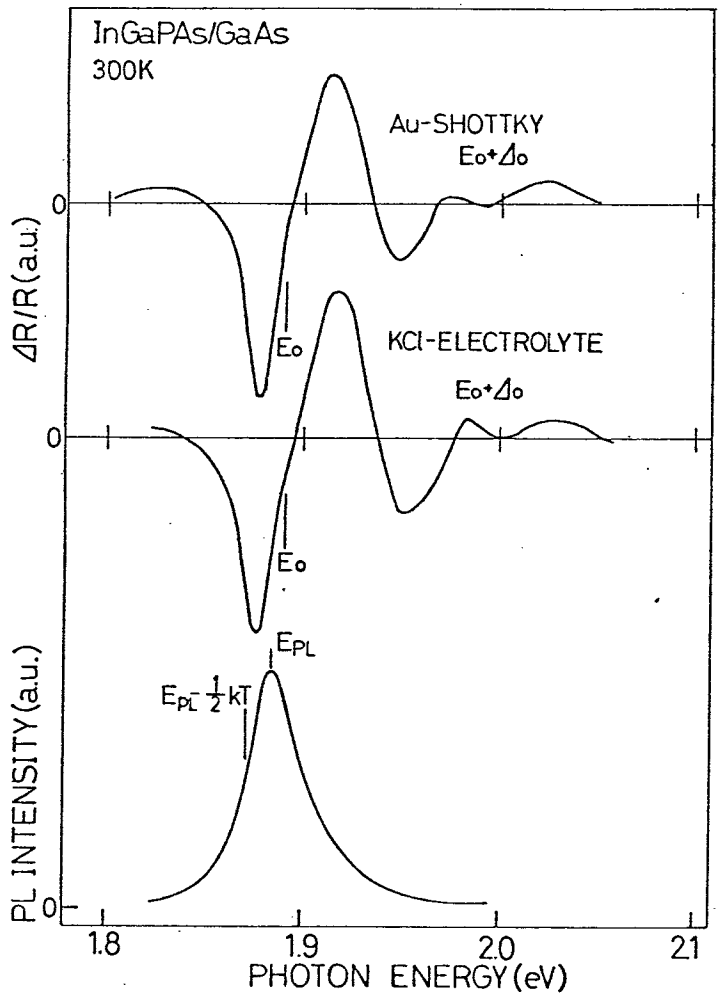

Fig. 3-3 ER and PL spectra of $In_{1-x}Ga_xP_{0.96}As_{0.04}$ LPE layer with $\Delta a/a$ of 0.21 % measured at room temperature. ER spectra were measured with V_{pp} of 0.5V. The band-gap energy obtained by the three-point adjustment method is indicated as E_0.

in the figure. The structure near 2.0 eV is due to the spin-orbit split-off band ($E_0+\Delta_0$), and the spin-orbit splitting energy Δ_0 is estimated to be about 100 meV.

The typical near-band-edge PL spectrum, as shown in Fig. 3-3, exhibits a single band peaked at 1.883 eV with the FWHM value of 34 meV. This spectral line shape resembles quite well that of $In_{1-x}Ga_xP_{0.99}As_{0.01}$ previously reported, where the PL band was attributed to band-to-band (B-B) transitions from the line shape analysis.[20-22] When the radiative recombination is dominated by B-B transitions, the peak energy should be larger than the energy gap with 13 meV at room temperature because the PL theory gives the peak photon energy at $h\nu=E_0+kT/2$, where k is the Boltzmann constant and T is temperature.[12] As can be seen in Fig. 3-3, the PL peak energy, E_{PL}=1.883 eV, is slightly smaller than the band-gap energy E_0 (1.885eV) obtained by the ER spectra analysis. Therefore, this near-band edge PL band cannot be considered due to pure B-B transitions. PL band by band-to-impurity (B-I) transitions gives the same spectral line shape as B-B transitions, but the peak energy is smaller by the amount of the activation energy of an impurity involved. Based on these results, this near-band edge emission is largely influenced by the donor-to-valence band transitions with the donor activation energy of 15 meV. These behaviors have been observed for all samples with different lattice mismatch at the temperature range between 80K and 300K, as shown in the following section.

3-3-2. Temperature dependence

Figure 3-4 shows PL spectra taken at various temperatures between 4.2 and 280K. The PL spectra are dominated by two peaks when temperature is lower than 40K. The main peak is the near-band edge emission corresponding to the PL peak shown in Fig. 3-3, and another is a small peak at the photon energy of about 60 meV lower than the main peak. When temperature is higher than 74K, only the main peak can be observed. The small peak is considered to be a donor-to-acceptor pair (D-A pair) emission, since the peak shifts to higher energy as the excitation intensity increases. From the temperature dependence of the line shape, this small peak is composed of two different peaks, as can be seen from the spectra taken in the temperature range between 17 and 37K. These two PL bands may be due to D-A pair emissions having the different activation energies, which are probably caused by some residual impurities such as Zn and two unidentified donors. In Fig. 3-5, the peak energy of the main peak E_{PL} and the value of E_{PL}-kT/2 are plotted as a function of temperature together with the precise band-gap energy obtained by ER measurements. Near room temperature, E_{PL} is very close to E_0 with only a slight difference of 1∿2 meV. As temperature decreases, the difference between E_0 and E_{PL} increases, however, E_{PL}-kT/2 is always about 15 meV smaller than E_0 over the temperature range between 80 and 300K. The temperature coefficients of E_0 and E_{PL}-kT/2 are estimated to be 4.1×10^{-4} and 4.0×10^{-4} eV/K, respectively.

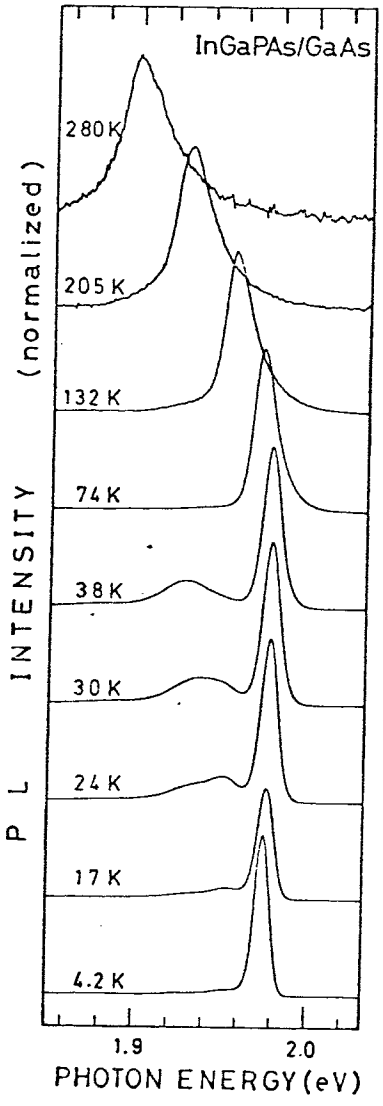

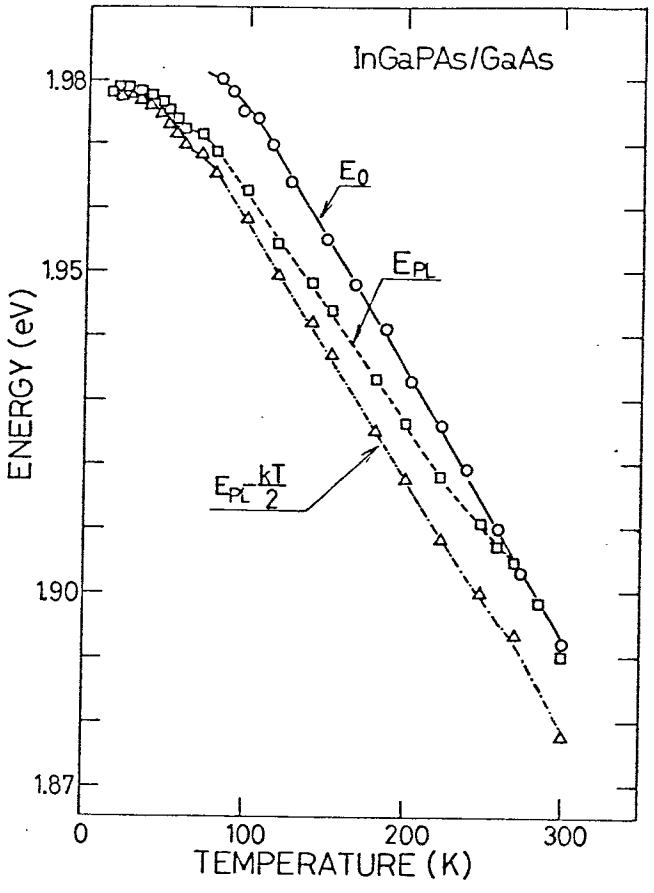

Fig. 3-5 PL peak energy (E_{PL}) and E_{PL} minus kT/2 (E_{PL}-kT/2) of $In_{1-x}Ga_xP_{0.96}As_{0.04}$ LPE layer plotted as a function of temperature together with band-gap energy (E_0) obtained by Au-Shottky ER measurements.

Fig. 3-4 PL spectra of $In_{1-x}Ga_xP_{0.96}As_{0.04}$ LPE layer taken at various temperatures between 4.2K and 280K. Spectra are normalized by each peak intensity.

3-3-3. Lattice mismatch dependence

In Fig. 3-6, photoluminescence spectra for the near-band edge emission at 77K are shown for various samples having different lattice mismatch. In Fig. 3-7, the FWHMs of the main peak at 77 and 300K are plotted as a function of lattice mismatch $\Delta a/a$ together with the broadening parameter Γ determined from ER spectra. The FWHM is small when the lattice mismatch is in the range between 0% and 0.24%, and abruptly increases when $\Delta a/a$ exceeds 0.3%. The FWHM tends to be the minimum when $\Delta a/a$ is around 0.2%. The behavior of the FWHM value is in good agreement with that of Γ in ER spectra, indicating that the crystal quality of $In_{1-x}Ga_xP_{0.96}As_{0.04}$ LPE layer is best at $\Delta a/a$ of 0.2%, corresponding to the lattice-matching at the growth temperature of 785°C.[3] Figure 3-8 shows the energies of the main peak at 77K and 300K as a function of $\Delta a/a$. At both temperatures, PL peak energy decreases linearly as $\Delta a/a$ increases in the region between 0% and 0.3%. However, the peak energy at 77K decreases abruptly when $\Delta a/a$ exceeds 0.3%. At room temperature, a slight decrease in photon energy from a linear line was observed, when $\Delta a/a$ exceeds 0.3%. Samples with $\Delta a/a$ exceeding 0.3% have shown large FWHM and the surfaces of such samples were rough. Because of large lattice mismatch in these samples, a lot of defects have been introduced by stress from the interface region to the InGaPAs LPE layer and no B-B emission has been observed. These results show that the best quality $In_{1-x}Ga_xP_{0.96}As_{0.04}$ LPE layer is obtained when both the lattices are matched at the growth temperature.

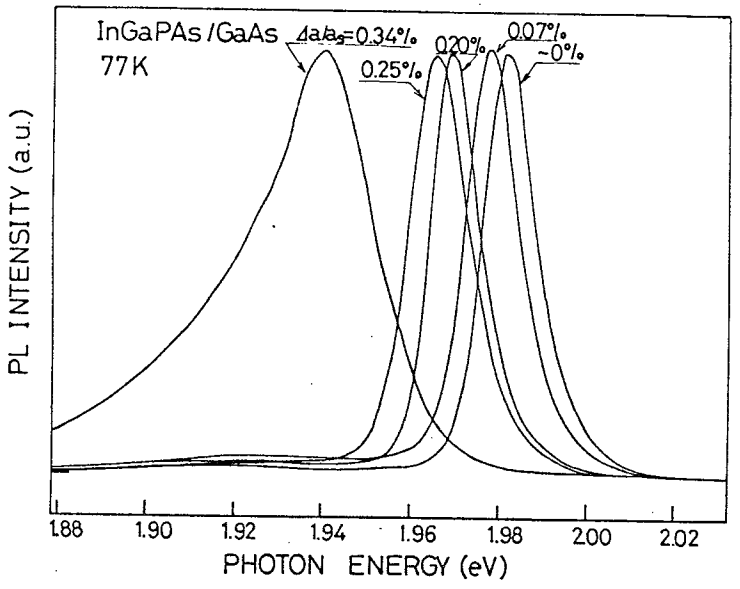

Fig. 3-6 PL spectra of $In_{1-x}Ga_xP_{0.96}As_{0.04}$ LPE layers with different lattice mismatch at 77K.

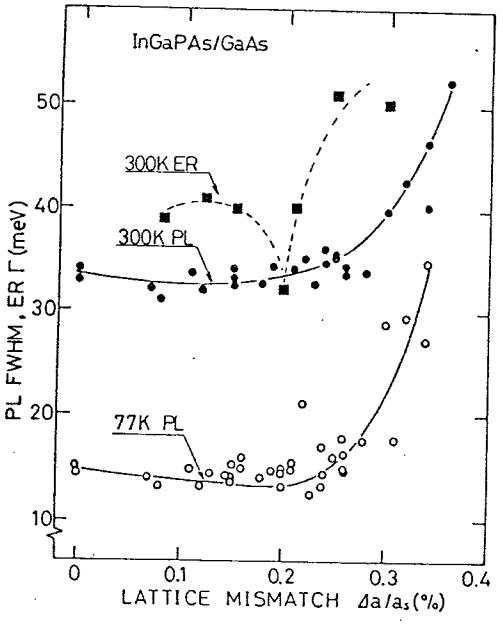

Fig. 3-7 FWHM values of near-band-edge PL and broadening parameters in ER spectra of $In_{1-x}Ga_xP_{0.96}As_{0.04}$ LPE layers plotted against lattice mismatch.

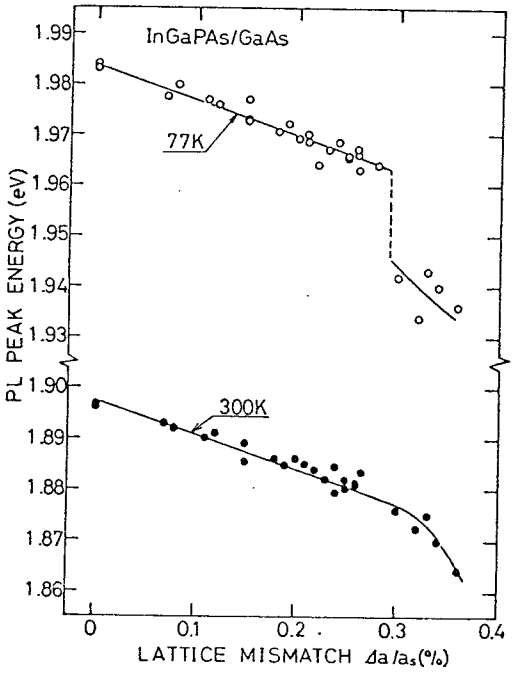

Fig. 3-8 Peak energy of near-band edge PL plotted as a function of lattice mismatch.

3-4. Effect of immiscibility on PL and ER spectra

As has been discussed in Section 2-3-2, the LPE growth of InGaPAs lattice-matched to GaAs is affected by immiscibility in the composition region $0.22<y<0.45$. In this composition region, the crystal growth of InGaPAs alloy with uniform alloy composition under the thermal equilibrium is considered to be impossible because InGaPAs alloy is stable with respect to the free energy when the alloy is phase-separated to the two binodal compositions.[4-6] However, as has been shown in Section 2-2-3, the successful LPE growth has been possible inside the immiscibility region on GaAs substrate. The reasons for the LPE growth inside the immiscibility domain are considered to be due to forces such as supercooling, strain energy due to lattice mismatch and energy of defect formation.[23,24] Therefore, the crystal quality of InGaPAs LPE layers grown inside the immiscibility domain is considered to be influenced more or less by immiscibility.

In Fig. 3-9, PL spectra measured at 77K from InGaPAs LPE layers grown outside ($In_{1-x}Ga_xP_{0.96}As_{0.04}$) and inside ($In_{1-x}Ga_xP_{0.7}As_{0.3}$) the immiscibility region are shown. As can be seen in the figure, the near-band edge PL peak of $In_{1-x}Ga_xP_{0.7}As_{0.3}$ is much broad compared with that in $In_{1-x}Ga_xP_{0.96}As_{0.04}$. Furthermore, a broad strong PL band is observed about 200 meV below the near-band edge PL peak in $In_{1-x}Ga_xP_{0.7}As_{0.3}$. These characteristic features of PL spectra in InGaPAs LPE layers show that the crystal quality degrades inside the immiscibility region.

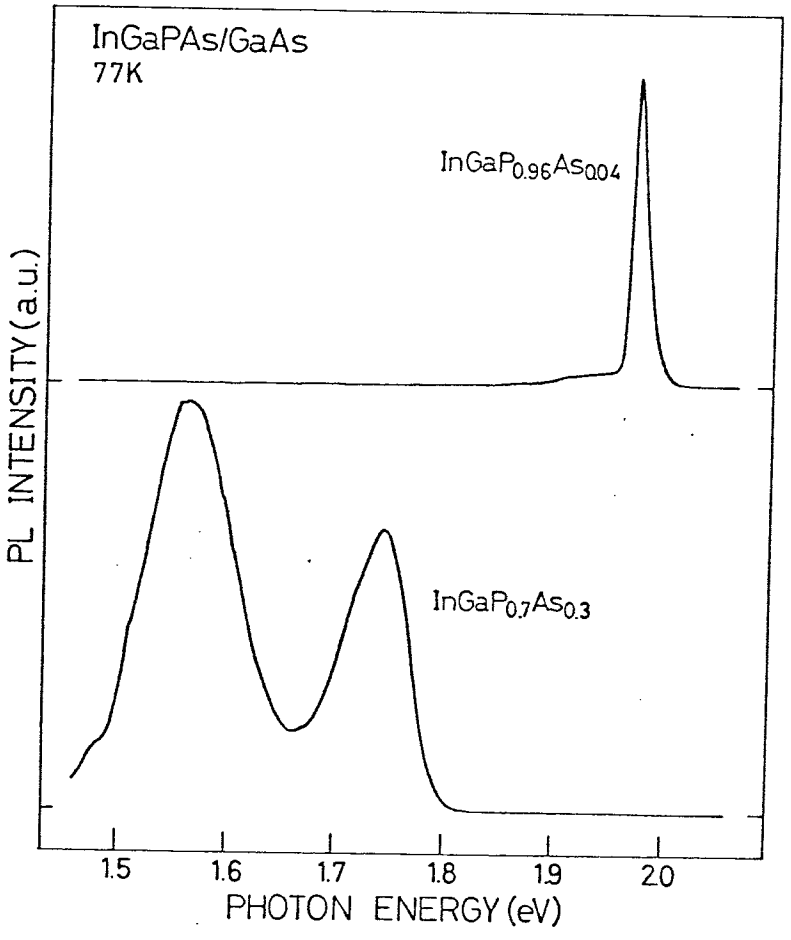

Fig. 3-9 PL spectra of $In_{1-x}Ga_xP_{0.96}As_{0.04}$ (upper figure) and $In_{1-x}Ga_xP_{0.7}As_{0.3}$ (lower figure) LPE layers measured at 77K.

3-4-1. Effect of growth condition

As has been described in Section 2-2-3, the LPE growth of InGaPAs on GaAs inside the immiscibility region is greatly affected by the degree of the initial supercooling. It is also expected that the crystal quality of InGaPAs LPE layers depends on the LPE growth conditions such as the degrees of the initial supercooling. Two series of LPE layers with different lattice mismatch, one grown by the conventional supercooling (CS) method and another by the two-phase melt (TPM) method, which are described in Section 2-2-3, have been measured to examine effects of the initial supercooling on the crystal quality of grown layers. The $In_{1-x}Ga_xP_{0.7}As_{0.3}$ LPE layers grown by these two growth methods have lattice mismatch ranging 0.18-0.34 % for the CS method and $-0.24 \sim +0.30$ % for the typical TPM method. The ER spectra measured for $In_{1-x}Ga_xP_{0.7}As_{0.3}$ LPE layers show low-field ER line shape, as shown in Fig. 3-10. The ER spectra of the LPE layers grown by the CS method are broader than those grown by the TPM method. Moreover, the spectrum becomes broadened when $\Delta a/a$ was small, and the narrow spectrum was observed when $\Delta a/a$ was large ($\Delta a/a \sim 0.28$ %). Contrary to this, the ER spectrum of $In_{1-x}Ga_xP_{0.7}As_{0.3}$ LPE layers grown by the TPM method showed a narrow line shape as indicated in the upper part of Fig. 3-10, and did not show remarkable changes in its line shape when $\Delta a/a$ was changed from -0.25 to 0.25 %.

In Fig. 3-11, the broadening parameters estimated from these ER spectra are plotted as a function of $\Delta a/a$. A clear difference between these two growth methods is seen. The Γ value of $In_{1-x}Ga_xP_{0.7}As_{0.3}$ LPE layers grown by the CS method increases drastically from 35 to 80 meV when $\Delta a/a$ is changed from 0.34 to 0.18%. Whereas, the Γ values of

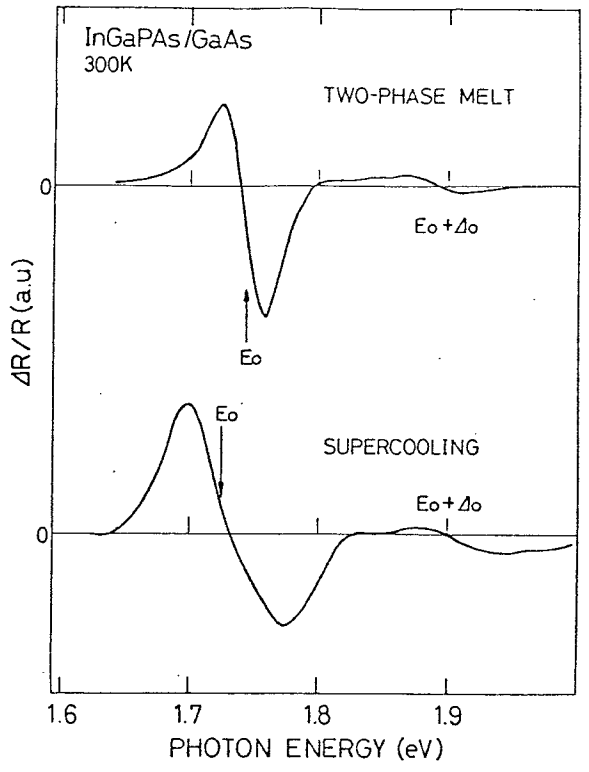

Fig. 3-10 Electrolyte ER spectra of $In_{1-x}Ga_xP_{0.7}As_{0.3}$ LPE layers. The upper curve is for typical LPE layers grown by the TPM method, and the lower curve for LPE layers grown by the CS method.

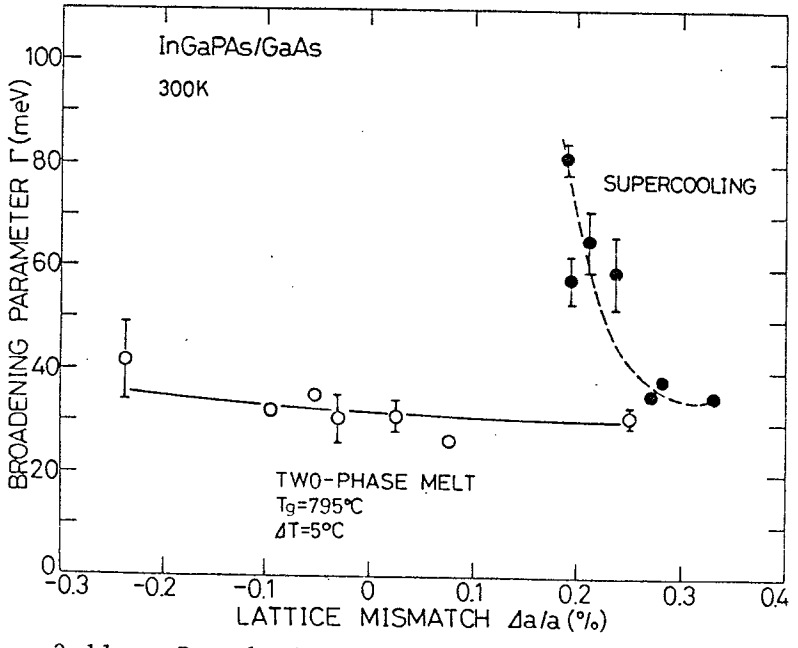

Fig. 3-11 Broadening parameters obtained from electrolyte ER spectra of $In_{1-x}Ga_xP_{0.7}As_{0.3}$ LPE layers plotted against lattice mismatch. The open circle plots for LPE layers grown by the TPM method, and the closed circle plots for LPE layers grown by the CS method.

$In_{1-x}Ga_xP_{0.7}As_{0.3}$ LPE layers grown by the TPM method are nearly constant, 28-32 meV, with the change of $\Delta a/a$ from -0.25 to 0.25 %. The reason of different behaviors in the Γ-$\Delta a/a$ relationship between the two growth methods is considered to be due to the difference in the supercooling between two growth methods as has been discussed in Section 2-2-3. In the CS method, the supercooling ΔT changes from ~10°C to 5°C when $\Delta a/a$ changes from 0.18% to 0.3%. Whereas in the TPM method, all $In_{1-x}Ga_xP_{0.7}As_{0.3}$ LPE layers have been grown from melts supercooled at ~5°C, independent of $\Delta a/a$. These results show that the crystal quality of $In_{1-x}Ga_xP_{0.7}As_{0.3}$ LPE layer is very sensitive to ΔT.

In Fig. 3-12, the FWHM values of the near-band-edge PL in $In_{1-x}Ga_xP_{0.7}As_{0.3}$ LPE layers are plotted as a function of $\Delta a/a$ together with those of $In_{1-x}Ga_xP_{0.96}As_{0.04}$ LPE layers. The behavior of the FWHM values agrees with that of Γ of ER. It can be seen that the FWHM values of the near-band-edge PL in $In_{1-x}Ga_xP_{0.96}As_{0.04}$ LPE layers grown with ΔT of 5°C and 15°C have the same dependence on $\Delta a/a$ at both 77K and 300K. These facts indicate that the crystal quality of $In_{1-x}Ga_xP_{0.96}As_{0.04}$ LPE layers grown outside of the immiscibility region is almost insensitive to ΔT in contrast to the case of $In_{1-x}Ga_xP_{0.7}As_{0.3}$ LPE layers.

3-4-2. Alloy composition dependence

In Fig. 3-13, the FWHM values of the near-band edge PL in InGaPAs LPE layers lattice-matched to GaAs measured at 77K are plotted as a composition y. The InGaPAs LPE layers grown by the TPM method at 820°C have been used for PL measurements. It can be seen in the

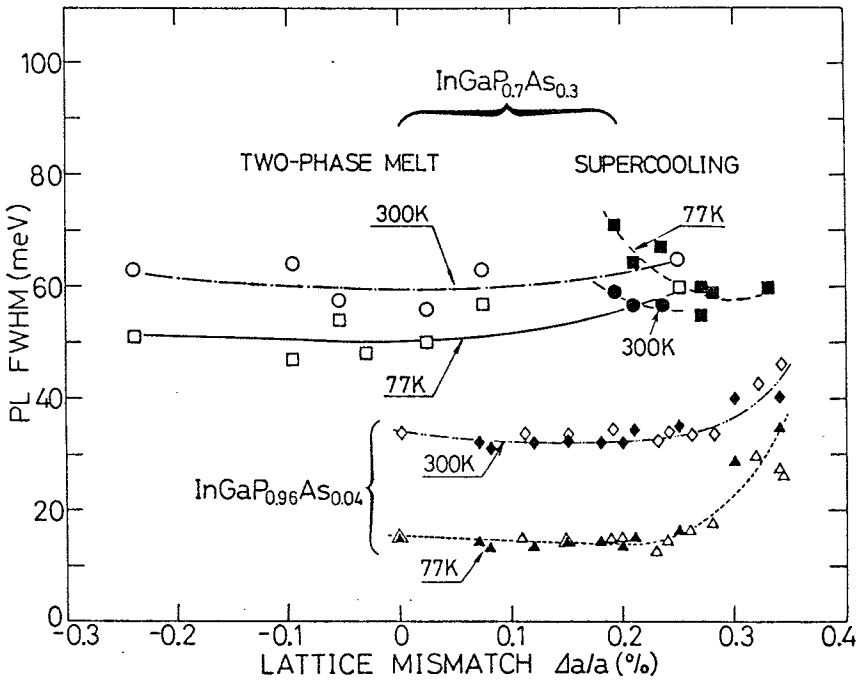

Fig. 3-12 FWHM values of near-band-edge PL of $In_{1-x}Ga_xP_{0.7}As_{0.3}$ and $In_{1-x}Ga_xP_{0.96}As_{0.04}$ LPE layers plotted against lattice mismatch. Open circle and square denote FWHM of $In_{1-x}Ga_xP_{0.7}As_{0.3}$ grown by the TPM method, and closed circle and square for $In_{1-x}Ga_xP_{0.7}As_{0.3}$ grown by the CS method. Open triangle and rhombus denote FWHM of $In_{1-x}Ga_xP_{0.96}As_{0.04}$ grown by the TPM method with ΔT of 5°C, and closed triangle and rhombus for FWHM of $In_{1-x}Ga_xP_{0.96}As_{0.04}$ grown by the TPM method with ΔT of 15°C.

figure that the FWHM value increases gradually with composition y, and has the maximum value of 57 meV with y around 0.34. The FWHM value then decreases abruptly when y is increased from 0.45, and has a small value of 14∿18 meV with y larger than 0.5. The composition y inside the calculated binodal isotherm at 820°C, i.e. the immiscibility region, is between 0.22 and 0.45, and therefore the composition y of the InGaPAs LPE layers having the large FWHM value is in good agreement with the immiscibility region. Two reasons can be considered for the increase in FWHM of the near-band edge PL peak. One reason is the variation of the band gap[11] due to the spinodal decomposition.[25-27] Another reason is the superposition of PL component due to shallow defects to that due to band-to-band transitions, because the energy due to lattice defects introduced during the LPE growth can stabilize immiscibility.[23,24] In order to clarify whether this large FWHM of the near-band edge PL peak is due to the variation of the band-gap or not, the broadness of ER spectra has been examined. The broadening parameter Γ obtained for $In_{1-x}Ga_xP_{0.7}As_{0.3}$ LPE layers grown by the TPM method is nearly constant, 28∿32 meV, independent of $\Delta a/a$, as has been discussed in the previous Section. This Γ value is comparable with the thermal energy kT of 26 meV at room temperature and also comparable with the Γ value of 35 meV obtained for $In_{1-x}Ga_xP_{0.96}As_{0.04}$ LPE layer which has been grown much less affected by immiscibility. This fact shows that the variation of the energy gap for InGaPAs LPE layers grown inside the immiscibility region is negligible, and therefore the large FWHM of the near-band edge PL peak is not due to the variation of the band-gap caused by spinodal decomposition.

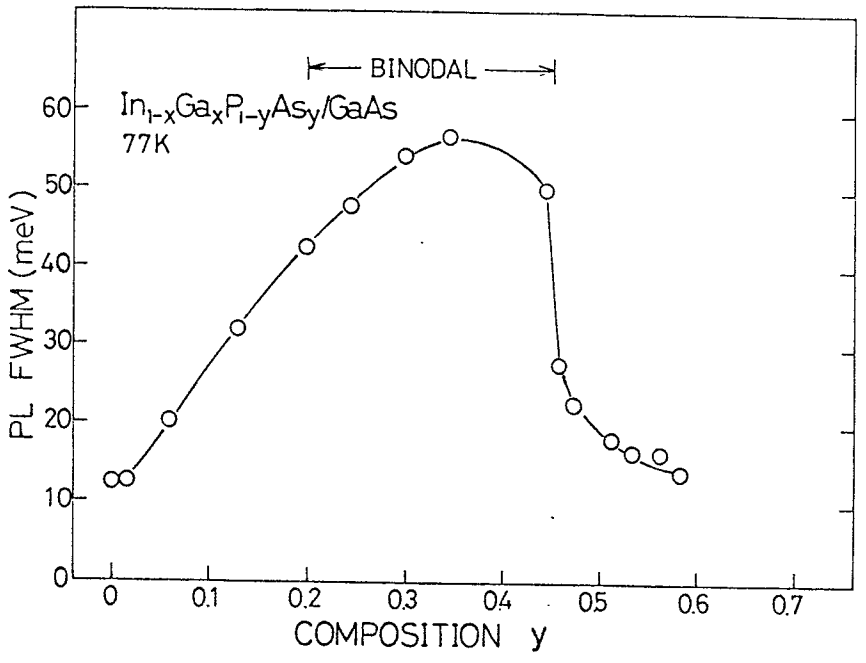

Fig. 3-13 FWHM values of near-band edge PL of $In_{1-x}Ga_xP_{1-y}As_y$ LPE layers lattice-matched to GaAs plotted as a function of composition y.

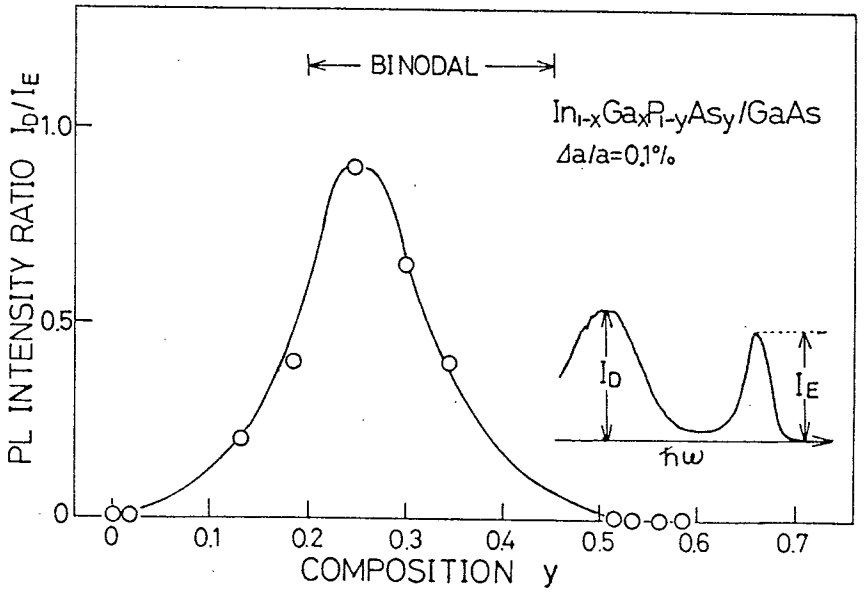

Fig. 3-14 Normalized intensity of PL band observed ∿200 meV below near-band edge PL plotted as a function of composition y. Lattice mismatch is 0.1% for all samples.

In Fig. 3-14, the intensity of the PL band observed at lower energy side normalized by the near-band edge PL for $In_{1-x}Ga_xP_{1-y}As_y$ LPE layers with $\Delta a/a$ of 0.1% is plotted as a function of composition y. It can be seen in the figure that the PL intensity becomes larger within the binodal, showing that this PL band is also attributed to immiscibility. This PL band is not due to the PL corresponding to InGaPAs having binodal composition which has been grown due to spinodal decomposition, because no ER peak has been observed in the energy region of this PL band. Furthermore, this PL peak intensity is strong only when InGaPAs LPE layer is excited by the light with photon energy larger than that of the near-band edge PL. Therefore, the origin of this PL band is considered to be the PL due to defects which are introduced into InGaPAs LPE layer during the growth. It has been also found that this PL band strongly depends on lattice mismatch. Figure 3-15 shows PL spectra of $In_{1-x}Ga_xP_{0.7}As_{0.3}$ taken with various lattice mismatches. In Fig. 3-16, the intensity of the PL band normalized by that of the near-band edge PL is plotted as a function of lattice mismatch. It is noted in these figures that this PL band is strong with positive $\Delta a/a$, and has the minimum value with $\Delta a/a$ around -0.05%, indicating that the crystal quality is not so good with $\Delta a/a$ of 0.14% where lattices are matched at the growth temperature in contrast to the case for $In_{1-x}Ga_xP_{0.96}As_{0.04}$ as has been shown in Section 3-3. The FWHM of the near-band edge PL has the same behavior as the PL band. These behavior can be interpreted as follows. The degree of immiscibility is larger with respect to alloy composition with positive $\Delta a/a$ as shown in the upper part of Fig. 3-17. It is known that the LPE growth in the immiscibility region is stabilized by

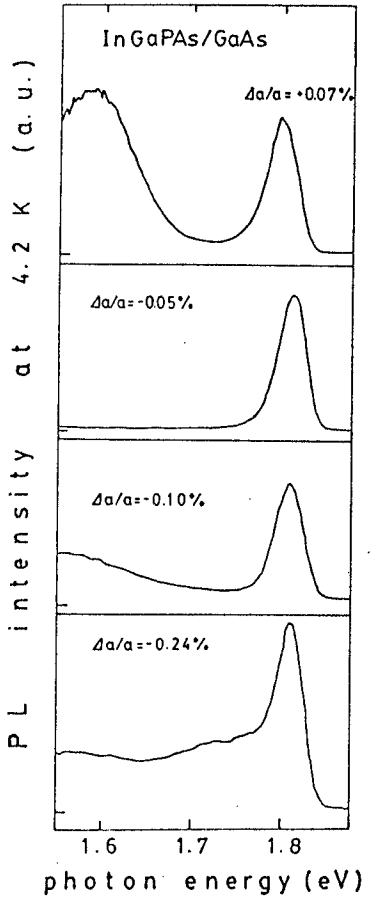

Fig. 3-15 PL spectra of $In_{1-x}Ga_xP_{0.7}As_{0.3}$ LPE layers with various lattice mismatch measured at 4.2K.

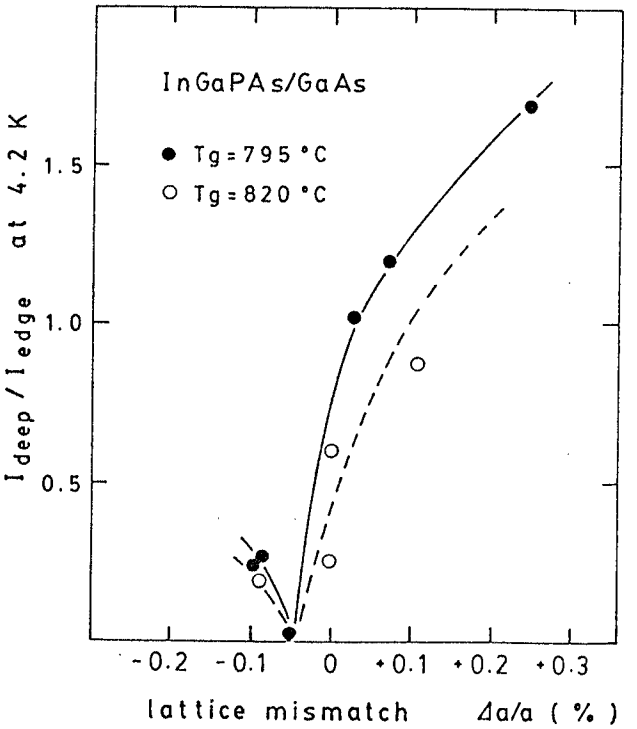

Fig. 3-16 Normalized intensity of PL band observed ∿200 meV below near-band edge PL plotted as a function of lattice mismatch. Closed and open circles are for $In_{1-x}Ga_xP_{0.7}As_{0.3}$ LPE layers grown at 795 and 820°C, respectively.

the strain energy due to lattice mismatch at the growth temperature.[23,24] Therefore, the magnitude of free energy due to immiscibility which can not be cancelled by the strain energy should be compensated by the energy of defects such as dislocations introduced during the growth in order to grow with no spinodal decomposition. However, the strain energy is easily relaxed by the formation of misfit dislocations when the growth layer thickness reaches a critical point,[28] as shown in the middle part of Fig. 3-17. In this critical point, the strain energy becomes the maximum, and immiscibility is most effectively canceled. Therefore, it is expected that a number of defects introduced due to immiscibility is the smallest at this critical point, as shown in the lower part of Fig. 3-17. If a PL band is attributed to defects introduced by immiscibility, the lattice mismatch of -0.05% where the PL intensity becomes the minimum, corresponds to the critical point. In fact, the critical thickness[28] calculated using the lattice mismatch at the growth temperature (corresponding to the lattice mismatch of -0.05% at room temperature) fairly agrees with the epitaxial layer thickness being 0.2∿0.3 μm. It is considered from these results and discussion as mentioned above that the strain energy due to lattice mismatch plays an important role in the crystal quality and the LPE growth under the influence of immiscibility.

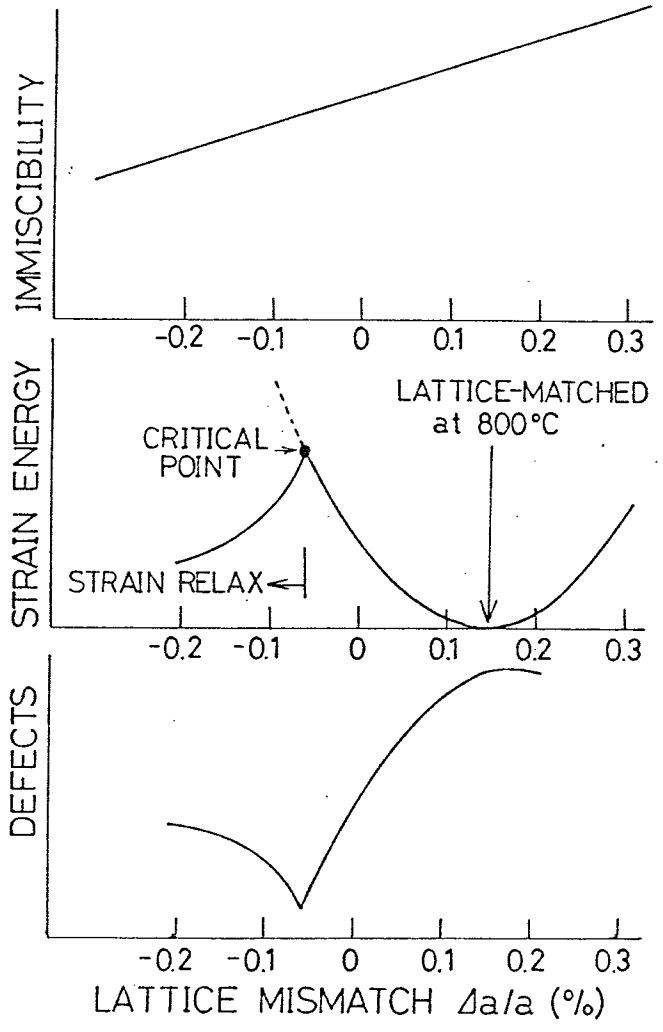

Fig. 3-17 Model for introduction of defects in the immiscibility region.

3-5. Summary

Photoluminescence and electroreflectance in $In_{1-x}Ga_xP_{0.96}As_{0.04}$ have been investigated. The band-gap energy estimated from the near-band edge PL analysis is smaller than the precise band-gap energy obtained by ER measurement, the results suggesting that the near-band edge PL is not due to pure band-to-band transitions. The FWHM of the near-band edge PL peak and the broadening parameter Γ in ER spectra have been measured as a function of lattice mismatch, and this result indicates that the best quality $In_{1-x}Ga_xP_{0.96}As_{0.04}$ LPE layer can be obtained under the lattice matching condition at the growth temperature.

The influence of immiscibility on PL and ER spectra in $In_{1-x}Ga_xP_{1-y}As_y$ LPE layer has been investigated. The Γ value of ER spectra in $In_{1-x}Ga_xP_{0.7}As_{0.3}$ LPE layer grown by the conventional supercooling method is large and varies drastically depending on the lattice mismatch in contrast to the small Γ values of that grown by the two-phase melt method, and this shows that the crystal quality is sensitive to the initial supercooling in the LPE growth under the influence of immiscibility. PL spectra have been measured on InGaPAs LPE layers having various As compositions y and lattice mismatch. The FWHM of the near-band edge PL peak is extraordinarily large inside the immiscibility region. The small broadening parameter in ER spectra shows that the large FWHM in PL spectra is not due to the distribution of the band-gap energy due to the spinodal decomposition but due to defects incorporated under the influence of immiscibility. The PL band $\sim$200 meV below the near band edge PL band observed only in the

immiscibility composition region depends on lattice mismatch, and its intensity becomes the minimum with $\Delta a/a$ of -0.05% which is different from the lattice-matching condition at growth temperature. This fact indicates that the strain energy due to lattice mismatch plays an important role in the LPE growth in the immiscibility region, and defects are introduced into the LPE layer when immiscibility is not stabilized by the strain energy due to lattice mismatch.

REFERENCES

1) H. C. Caysey, Jr, M. B. Panish: Heterostructure Lasers, (Academic Press, New York, 1978).

2) H. Kressel and J. K. Butler: Semiconductor Lasers and Heterojunction LEDs, (Academic Press, New York, 1977).

3) Z. R. Zytkiewicz and Z. Kalinski: Phys. Status Solidi a 57 (1980) 489.

4) B. de Cremoux: J. Physique 43 (1982) c5.

5) G. B. Stringfellow: J. Cryst. Growth 58 (1982) 194.

6) K. Onabe: Jpn. J. Appl. Phys. 22 (1983) 663.

7) K. Onabe: Jpn. J. Appl. Phys. 21 (1982) 797.

8) K. Wakao, H. Nishi, T. Kusunoki, S. Isozumi and S. Ohsaka: Appl. Phys. Lett. 44 (1984) 1035.

9) S. Kaneiwa, H. Takiguchi, T. Hayakawa, S. Yamamoto, H. Hayashi, S. Yano and T. Hijikata: Appl. Phys. Lett: 46 (1985) 455.

10) S. Mukai, H. Yajima and J. Mukai: Jpn. J. Appl. Phys. 20 (1981) L729.

11) S. Mukai: J. Appl. Phys. 54 (1983) 2635.

12) H. B. Webb and E. W. Williams: Semiconductors and Semimetals, eds. R. K. Willardson and A. C. Beer (Academic Press, New York, 1972) Vol. 8, Chap. 4, p. 238.

13) M. Cardona: Modulation Spectroscopy (Academic Press, New York, 1969).

14) Y. Hamakawa and T. Nishino: Optical Properties of Solids: New Developments, ed. B. O. Seraphin (North-Holland, Amsterdam,1976) Chap. 6.

15) D. E. Aspnes: Surf. Sci. 37 (1983) 418.

16) D. E. Aspnes and J. E. Rowe: Phys. Rev. Lett. 27 (1971) 188.

17) S. Shirakata, M. Kondo, A. Tsushi, T. Nishino, Y. Hamakawa and T. Kariya: Jpn. J. Appl. Phys. 24 (1985) 524.

18) S. Shirakata, M. Kondo, T. Nishino and Y. Hamakawa: Jpn. J. Appl. Phys. 25 (1986) 435.

19) M. Kondo, S. Shirakata, T. Nishino and Y. Hamakawa: J. Appl. Phys. 60 (1986) 3539.

20) S. Mukai, M. Matsuzaki and J. Shimada: Jpn. J. Appl. Phys. 20 (1981) 321.

21) A. Suzuki, H. Kyuragi, S. Matsumura and H. Matsunami: Jpn. J. Appl. Phys. 19 (1980) L207.

22) H. Kyuragi, A. Suzuki, S. Matsumura and H. Matsunami: Appl. Phys. Lett. 37 (1980) 723.

23) M. Quillec, C. Daguet, J. L. Benchimol and H. Launois: Appl. Phys. Lett. 40 (1982) 325.

24) M. Ishikawa and R. Ito: Jpn. J. Appl. Phys. 23 (1984) L21.

25) S. Mahajan, B. V. Dutt, H. Temkin, R. J. Cava and W. A. Bonner: J. Cryst. Growth 68 (1984) 589.

26) S. N. G. Chu, S. Nakahara, K. E. Strege and W. D. Johnston, Jr: J. Appl. Phys. 57 (1985) 4610.

27) A. G. Norman and G. R. Booker: J. Appl. Phys. 56 (1985) 4715.

28) J. W. Matthews, A. E. Blakeslee and S. Mader: Thin Solid Films 33 (1976) 253.

4. PHOTOLUMINESCENCE OF TRANSITION METAL IMPURITIES IN III-V SEMICONDUCTORS AND THEIR ALLOYS

4-1. Introduction

The 3d-transition metal (TM) impurities form deep-acceptor levels in semiconductors. Most of TM impurities are important for III-V compound semiconductor technology because TM impurities have been widely used to compensate residual shallow donors for semi-insulating substrate materials, such as Cr in GaAs.[1] On the other hand, TM impurities such as Ni deteriously affect minority carrier properties and degrade the efficiency of light emitting devices.[2] From these reasons, properties of TM impurities in III-V semiconductors have been intensively studied by means of electron spin resonance (ESR), deep-level transient spectroscopy (DLTS) and optical spectroscopic measurements as photoluminescence (PL) and optical absorption. It is well known that low-temperature PL spectra due to TM impurities in III-V compounds show very sharp characteristic zero-phonon lines accompanied with broad phonon replicas in their low-energy side in the near-infrared region. Such emissions arise from electronic transitions between the 3d-electron levels of a TM atom split by a crystal field at the cation site of the zincblende crystal lattice. It is known that these PL spectra are sensitively affected by perturbation acting on the TM luminescent center through the crystal field. For example, the energy levels of 3d electrons split or shift in the application of stress to the crystal.[3] Also, the energy levels are largely affected by the presence of a vacancy or an

impurity in the vicinity of the TM luminescent center,[4] which is called a complex, and this is characteristic of the strongly localized 3d electrons in TM atoms. In view of such perturbation sensitivity of TM luminescent centers in III-V semiconductors, a study of III-V semiconductors via the TM-related luminescence is considered to be very effective for the characterization of stress or defects in III-V semiconductors and their alloys. In this Chapter, some fundamental behaviors of 3d-electrons in the zincblende type lattice with T_d symmetry are briefly presented based on the crystal field theory. A survey of TM-related PL spectra in III-V compounds and alloys is presented, and the basic characteristics of these spectra are briefly discussed.

4-2. Crystal field splitting

The main feature of 3d-transition metal impurities in III-V semiconductors is a crystal field splitting of the terms in 3d-electrons.[5,6] First, we consider the case that a TM impurity with one 3d-electron occupies the cation site in the zincblende lattice of III-V compounds as shown in Fig. 4-1. The TM impurity is then tetrahedrally coordinated by four anions (ligands) which produce the electrostatic field (crystal field) at the cation site. A 3d-electron of the TM ion which has orbitally fivefold degenerated eigenfunctions, d_{xy}, d_{yx}, d_{zx}, $d_{x^2-y^2}$ and d_{z^2} in a free space interacts with the crystal field at the cation site, where the subscript denotes the base of the wavefunction. The atomic orbitals d_{xy}, d_{yz} and d_{zx} are located in the vicinity of ligands and their interactions (repulsion) are

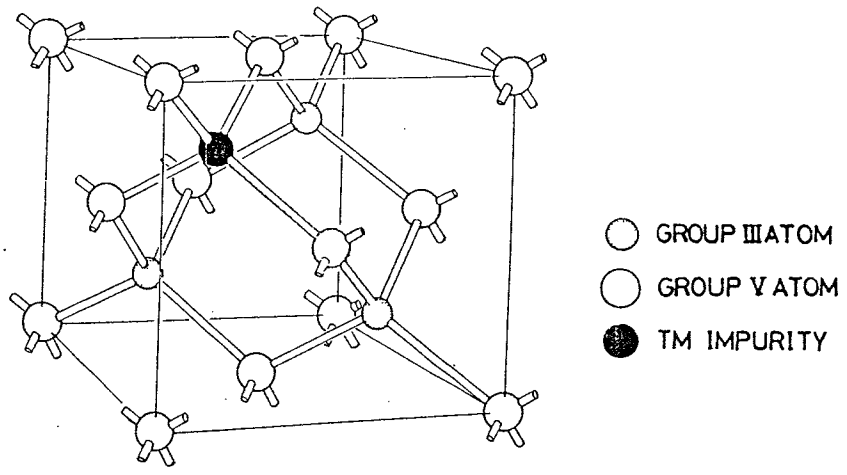

Fig. 4-1 3d transitiom metal impurity occupying group III atom site in III-V compound having zincblende lattice.

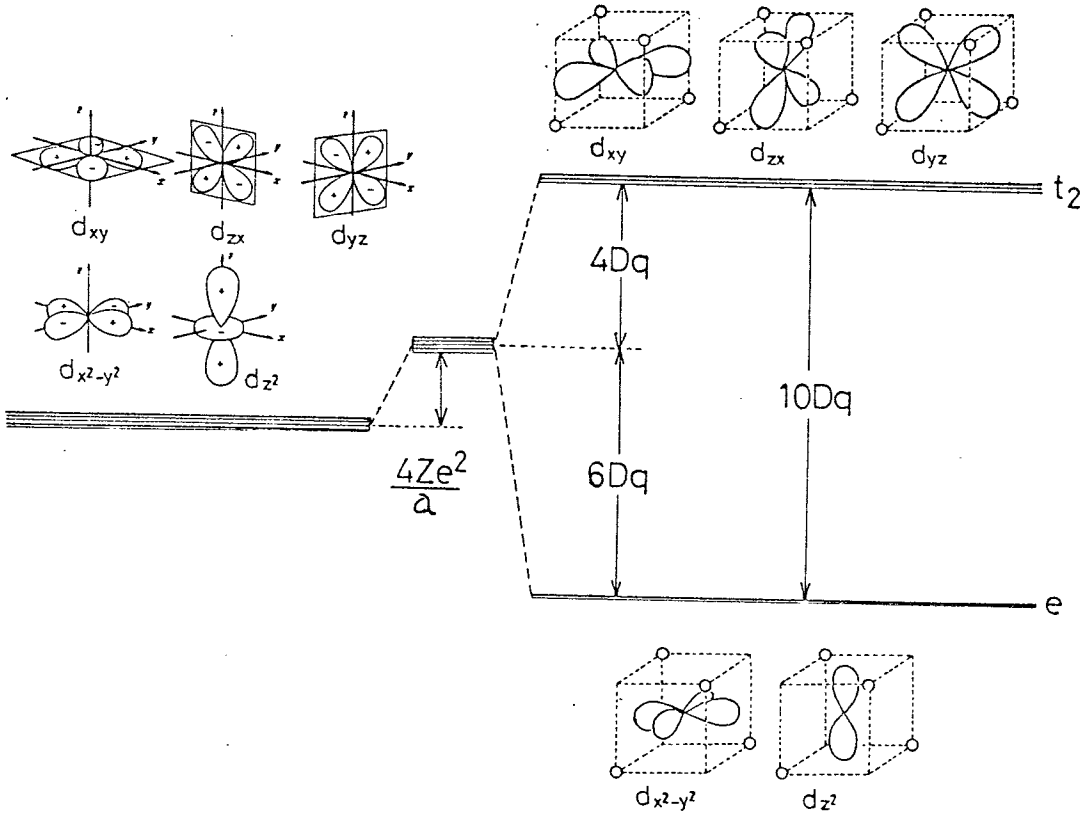

Fig. 4-2 Splitting of 3d-electron level in TM impurity due to tetrahedral crystal field. Wafefunctions of 3d-electron of a free ion and that in a zincblende lattice are schematically shown.

strong, whereas the other orbitals $d_{x^2-y^2}$ and d_{x^2} are subjected to weaker electrostatic repulsion by ligands because of larger distance between them. Consequently, there are two groups of electrons for different energies. The group of electrons on the orbitals d_{xy}, d_{yz} and d_{zx} has higher energy compared with that of the group of electrons on the orbitals $d_{x^2-y^2}$ and d_{z^2} according to the degree of interaction. Therefore, partial lifting of the fivefold degeneracy occurs in the crystal field with T_d symmetry, and triply and doubly degenerated orbitals of 3d-electrons which are called t_2 or e orbitals, respectively, appear as shown in Fig.4-2. The energy difference between t_2 and e levels is called the crystal field splitting and conventionally denoted by 10 Dq or Δ_{CF}. The energy of an unsplit level of a TM impurity at the cation site in lattice is not equal to that in free space by $4Ze^2/a$ because of the average energy of repulsion of 3d-electron from negative ligands,[6] where Z is the atomic number, e the electron charge and a the distance between TM atom and ligand.

Next, we deal with 3d-TM impurities having more than one electrons, and then we have to take Coulomb interactions between 3d-electrons into account. The states of these electrons under such interactions are characterized by a term with total angular momentum, L, and total spin, S. The terms are generally described by L, where L=S, P, D, F, G, H and I, depending on the value of the atomic orbital quantum number. The terms for the ground states of a series of TM impurities in the case of the $3d^n$ electron configuration are summarized in Table 4-1 together with the crystal field splitting scheme of terms.

Table 4-1 Electron configurations and terms of TM impurities in tetrahedral crystal field.

free TM ion		TM ion in zincblende lattice									
Sc	$3d^1 4s^2$	Sc^{3+}	Sc^{2+}	Sc^{+}	Sc^{0}						
Ti	$3d^2 4s^2$	Ti^{4+}	Ti^{3+}	Ti^{2+}	Ti^{+}	Ti^{0}					
V	$3d^3 4s^2$	V^{5+}	V^{4+}	V^{3+}	V^{2+}	V^{+}	V^{0}				
Cr	$3d^5 4s^2$	Cr^{6+}	Cr^{5+}	Cr^{4+}	Cr^{3+}	Cr^{2+}	Cr^{+}	Cr^{0}			
Mn	$3d^5 4s^1$	Mn^{7+}	Mn^{6+}	Mn^{5+}	Mn^{4+}	Mn^{3+}	Mn^{2+}	Mn^{+}	Mn^{0}		
Fe	$3d^6 4s2$					Fe^{4+}	Fe^{3+}	Fe^{2+}	Fe^{+}	Fe^{0}	
Co	$3d^7 4s^2$						Co^{4+}	Co^{3+}	Co^{2+}	Co^{+}	Co^{0}
Ni	$3d^8 4s^2$							Ni^{4+}	Ni^{3+}	Ni^{2+}	Ni^{+}
electron configuration		$3d^0$	$3d^1$	$3d^2$	$3d^3$	$3d^4$	$3d^5$	$3d^6$	$3d^7$	$3d^8$	$3d^9$
spin S		0	1/2	1	3/2	2	5/2	2	3/2	1	1/2
term ^{2S+1}L		^1S	^2D	^3F	^4F	^5D	^6S	^5D	^4F	^3F	^2D
splitting scheme of terms in T_d crystal field		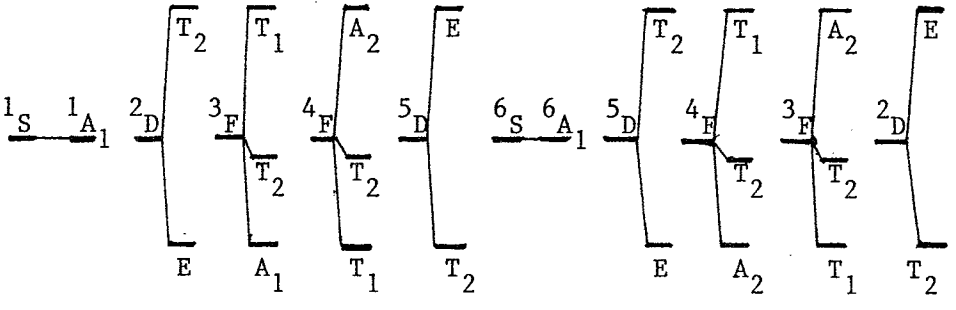									

4-3. Transition metal related luminescence

4-3-1 Cr in GaAs

Figure 4-3 shows a typical Cr-related PL spectrum in GaAs. The PL spectrum is dominated by a series of sharp zero-phonon lines in the 0.839 eV region accompanied with a broad phonon side band in their low-energy side.[7,8] This emission is attributed to $^5E \rightarrow {}^5T_2$ intracenter transitions of the Cr^{2+} ion at a Ga site in the GaAs lattice. Previous analyses of Zeemann effect[9,10] and uniaxial stress effect[3] on these zero-phonon lines have shown that this emission is subjected to trigonal perturbation along the <111> direction, and these results have shown that the PL spectra arise from the Cr^{2+} center forming a complex with unknown impurity or defect. Recent

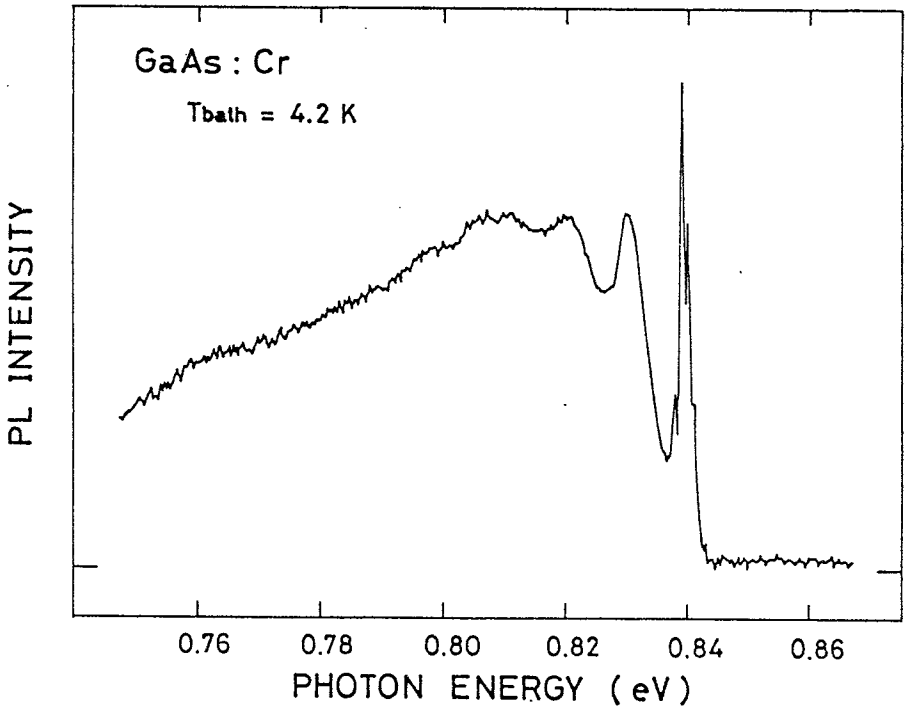

Fig. 4-3 Cr-related PL spectrum in GaAs measured at 4.2K.

detailed analysis of these lines has shown that the perturbation is due to an arsenic vacancy in the nearest neighbor site of the Cr center.[11] The ground state ^5D of the Cr^{2+} free-ion splits into two ^5E (excited state) and $^5T_2$ (ground state) by the cubic crystal field of the GaAs lattice. Furthermore, the ground state $^5T_2$ splits into six levels, and the excited ^5E state splits into five levels by the C_{3v} axial field and also the spin-orbit interaction.[3] Between these excited and ground states, radiative intracenter transitions are possible. Most of the PL lines in the 0.839 eV region observed by high-resolution PL shown in Fig. 4-4 have been well assigned with these intracenter transitions. Following Lightowler's nomenclature,[12,13] these PL lines correspond in order from high energy to line B',B, C, D, E', E, F, G, H' and H, respectively. These transitions are indicated by vertical arrows in the energy level scheme shown in Fig. 4-5. As can be seen in Fig. 4-4, the Cr-related PL spectrum in GaAs is dominated by a strong line-G and other week lines. The effect of uniaxial stress on these PL lines has been precisely investigated.[3] Recently, the residual stress in plastically bent GaAs wafer has been successfully characterized with respect to the magnitude and direction by measuring splitting and shift of the line-G, and the results have shown that this line-G can be used for the characterization of stress with high sensitivity.[14,15] Changes in energy levels of the Cr center by the perturbation of compressive uniaxial stress along [100] and [111] axes are shown in Fig. 4-6. It can be seen from this figure that the dominant line G splits into two lines G_1 and G_2 under stress for [100] axis, and into three lines G_1, G_2 and G_3 for [111] axis. The stress

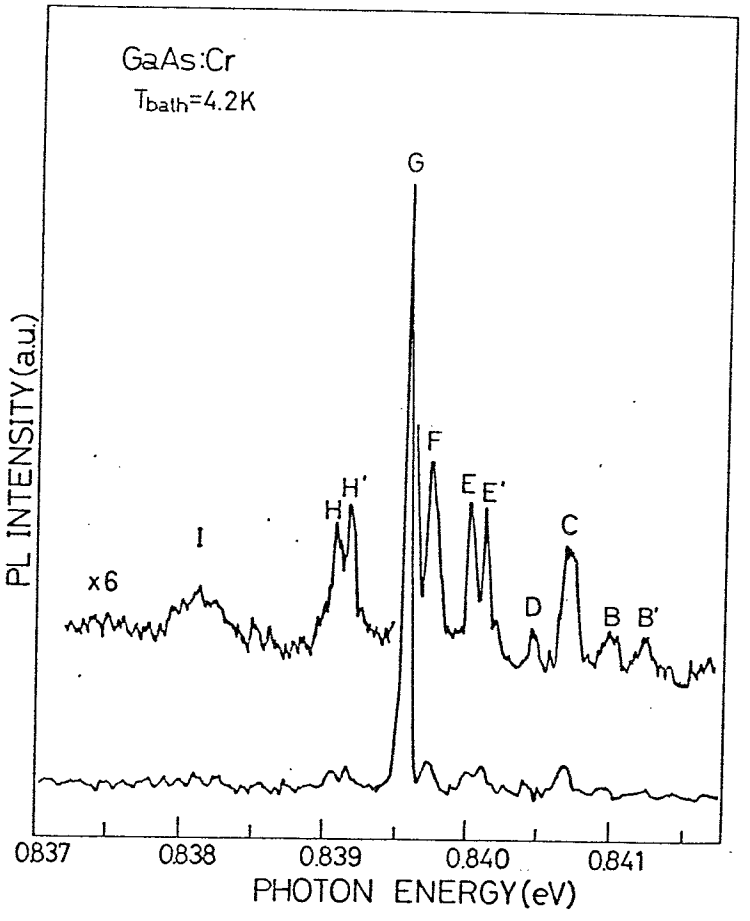

Fig. 4-4 High resolution Cr-related PL spectrum in GaAs in the 0.839 eV energy region. The notation follows Lightowler's nomenclature.[12)]

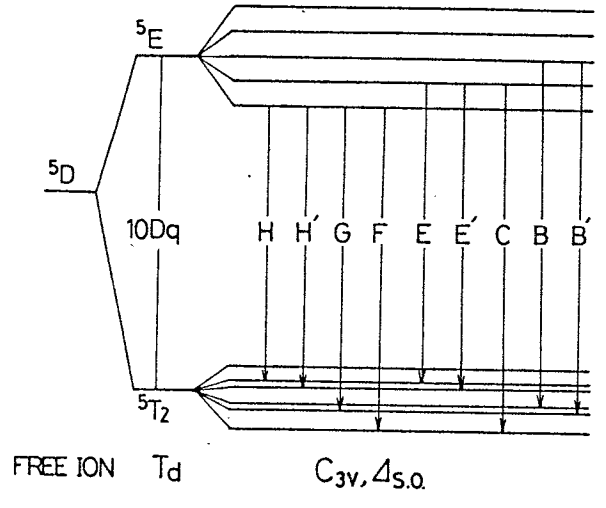

Fig. 4-5 Schematic representation of energy levels of Cr^{2+} in GaAs which cause the emission in the 0.839 eV energy region. Vertical arrows show transitions corresponding to PL lines in Fig. 4-4.

sensitivity of these PL lines has been applied to the characterization of the interface stress at InGaPAs/GaAs heterostructure[16,17] and details are presented in Chapter 5.

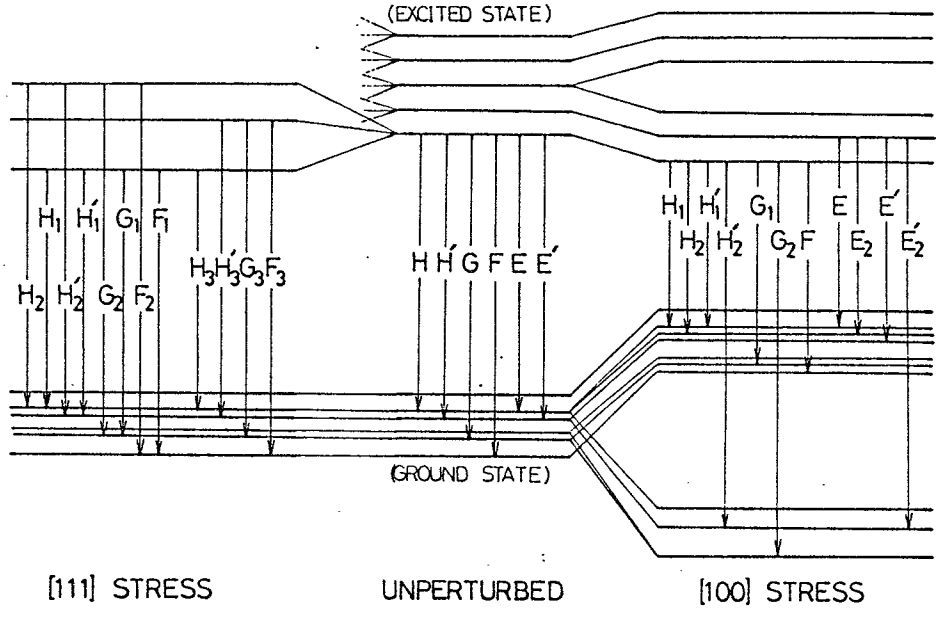

Fig. 4-6 Schematic representation of Cr-related energy levels in GaAs under [111] and [100] compressive uniaxial stress.

4-3-2. V, Cr, Co and Ni in GaP

The PL spectra related to TM impurities in GaP have been intensively studied because they generally make a shunt pass of minority carriers and degrade the emission efficiency of light emitting diodes.[2] All TM-related PL spectra in GaP are represented by sharp zero-phonon lines and their phonon replicas. TM impurities can be classified into two groups. One group is TM impurities in which the emissions are due to isolated centers such as V, Fe and Co. Another group is TM impurities such as Cr and Ni which easily form complexes with shallow donors or defects. It has been also reported that, in Cr and Ni impurities, the charge states associated with the radiative transitions can easily change under the illumination of the below-gap light.[18,19] The TM (V, Cr, Co and Ni)-related PL spectra in GaP are shown in Figs. 4-7, 4-8, 4-9 and 4-12, respectively.

Vanadium (V)

The V-related PL spectrum in GaP is dominated by the zero-phonon line A_0 at 0.791 eV, and weak phonon replicas are observed in the low-energy side, as can be seen in Fig. 4-7. This emission has been assigned due to the transition $^3T_2(F) \rightarrow {}^3A_2(F)$ of the isolated V^{3+} center by measurements of Zeemann effects,[20] PL excitation spectra[21] and time resolved PL characteristics.[22]

Cromium (Cr)

The Cr-related PL spectrum in GaP is shown in Fig. 4-8. The spectrum is composed of the zero-phonon line at 1.03 eV and a strong broad phonon side band in the lower-energy side. As can be seen in

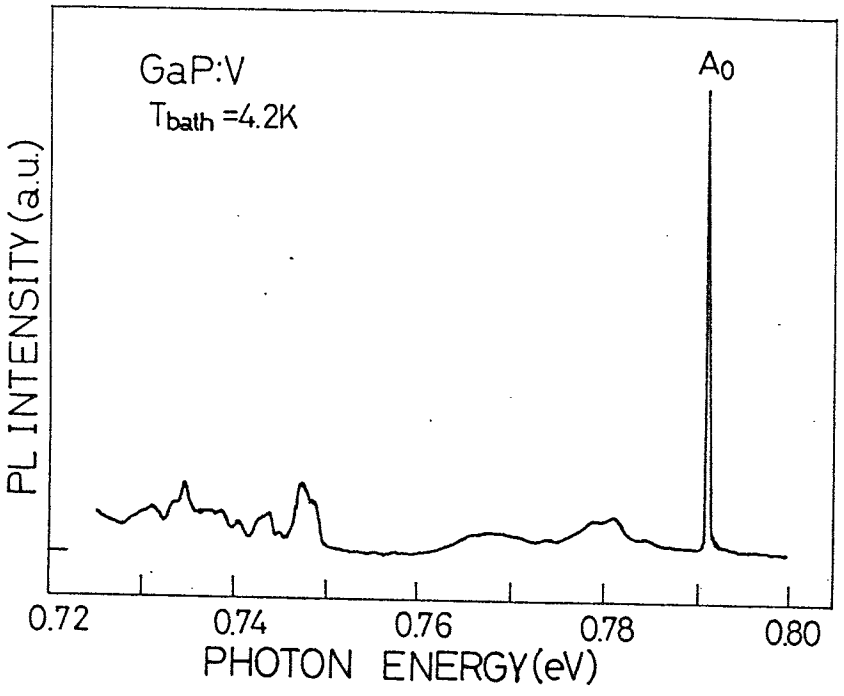

Fig. 4-7 V-related PL spectrum in GaP measured at 4.2K.

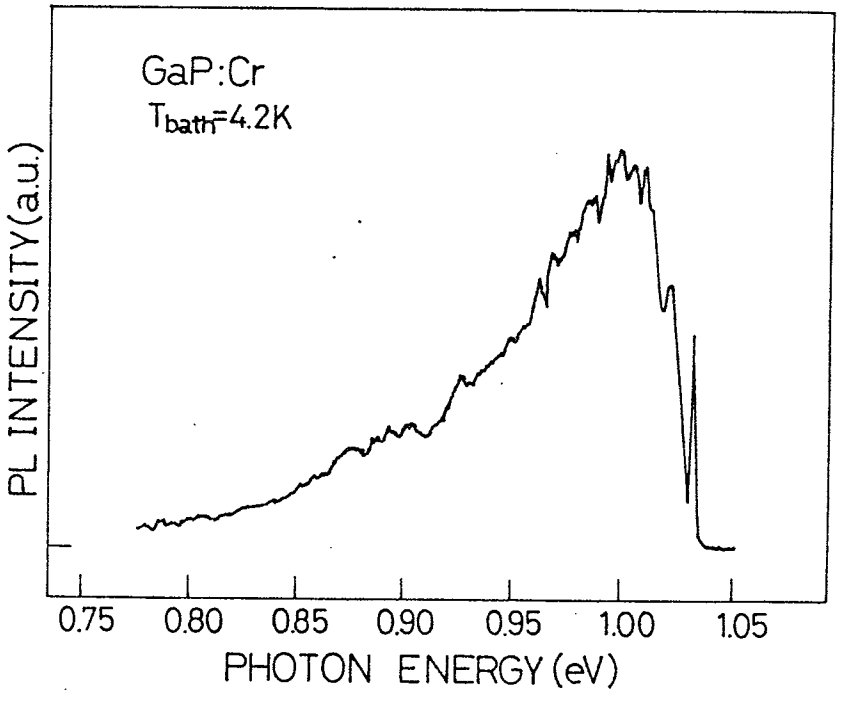

Fig. 4-8 Cr-related PL spectrum in GaP measured at 4.2K

the figure, the phonon coupling in the transition is very strong compared with other TM impurities. This emission has primarily been assigned to the $^5T_2 \rightarrow {}^5E$ internal transition of the substitutional Cr^{2+}.[23,24] Zeemann measurements for PL spectra have shown that the Cr center giving rise to the structure at 1.03 eV has tetragnal symmetry and subsequently it was concluded that the responsible transition is the $^4T_2(F) \rightarrow {}^4T_1(F)$ internal transition of the substitutional Cr^{3+}.[18] It is noted that the charge states and the associated radiative transitions are different from those in GaAs.

Cobalt(Co)

The Co-related PL spectra are shown in Fig. 4-9. The sharp PL lines at 0.559 and 0.519 eV are the zero-phonon line and its local-mode phonon replica, respectively. Weak broad bands around 0.55 and 0.53 eV are TA and LA phonon replicas, respectively. The PL lines have been well assigned to $^4T_2(F) \rightarrow {}^4A_2(F)$ transitions of the isolated Co^{2+} center by the measurements of Zeemann effect,[25] PL excitation (PLE) spectra[26] and uniaxial stress effect.[27] The decay time of this PL line obtained in this work is 270 μs in good agreement with the previously reported value.[22] A small mixing parameter of 0.06 obtained from the decay time supports the assignment that the radiative transitions occur between multiplets A and T. It is also characteristic of Co in GaP that the excited state of Co^{2+} can be easily observed by PLE spectrum. In Fig. 10, the PLE spectrum for the PL line at 0.559 eV is shown. The PLE spectrum is dominated by the zero-phonon line at 1.52 eV, and the PLE spectrum has been assigned due to the transitions $^4A_2(^4F) \rightarrow {}^4T_1(^4P)$ by Bishop et al.[26] The broad

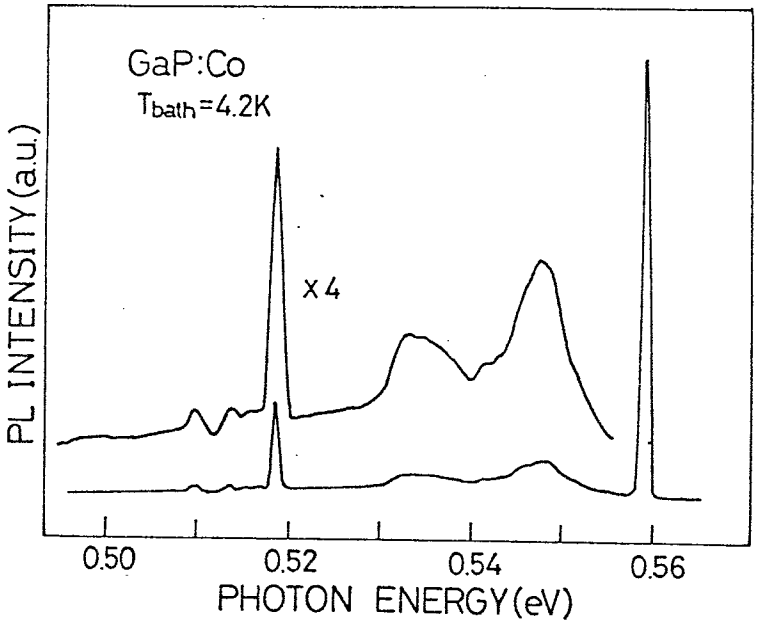

Fig. 4-9 Co-related PL spectrum in GaP measured at 4.2K.

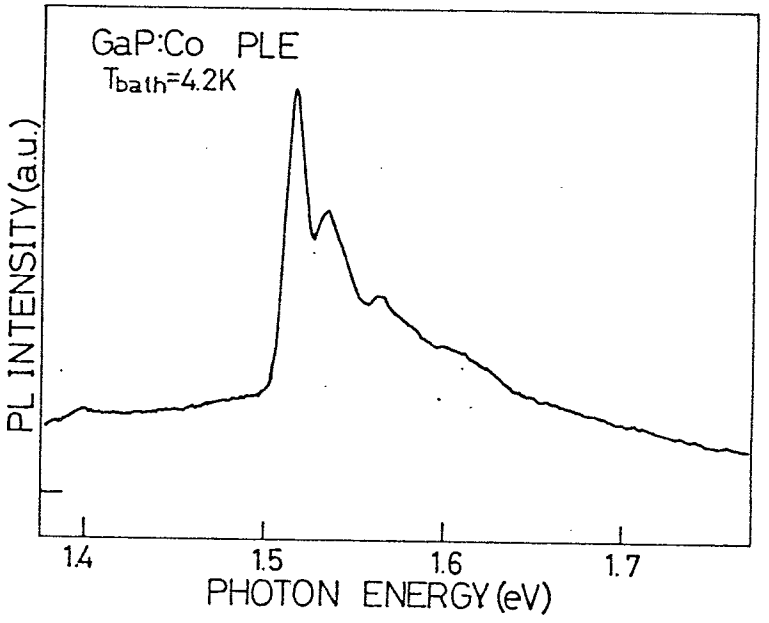

Fig. 4-10 PLE spectrum for Co-related 0.559eV PL line in GaP. The peak at 1.52 eV is due to transition $^4A_2(^4F) \rightarrow {}^4T_1(^4P)$ in Co^{2+}.

PLE and absorption band around 1.2 eV due to $^4A_2(^4F) \rightarrow {}^4T_1(^4F)$ transitions have been also reported.[26] The energy level of Co^{2+} in GaP is schematically shown in Fig. 4-11, where transitions corresponding to PL and PLE are indicated by vertical arrows. From the fact that these PL and PLE spectra correspond well to the multiplet arising from the Co^{2+}, the assignment of the PL transition is considered to be well confirmed. Similar PL and PLE spectra have been observed in both InP[28] and GaAs[29], and the charge state state associated with the radiative transitions has been confirmed to be Co^{2+} in both InP and GaAs. The Co-related PL spectra in ternary semiconducting alloys, InGaP and GaAsP, are discussed in detail in Chapter 6.

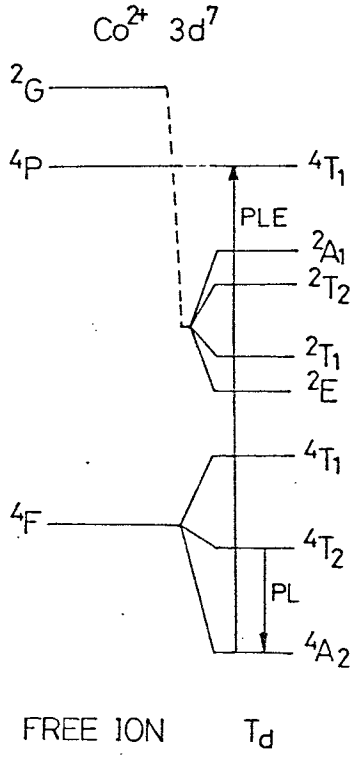

Fig. 4-11 The energy level scheme of Co^{2+} ion in GaP lattice. Vertical arrows show transitions corresponding to PL and PLE spectra shown in Figs. 4-9 and 4-10, respectively.

Nickel (Ni)

The Ni impurity is well known as a persistent contaminant in device grade VPE GaP which degrades the efficiency of light emitting diodes making the shunt pass of minority carrier.[2] The Ni-related PL spectrum is shown in Fig. 4-12. The PL line at 0.663 eV denoted as A_0 is a zero-phonon line and lines A_1 and A_2 are local-mode phonon replicas. The PL line has been assigned to $^2E \rightarrow {}^2T_2$ transitions of a Ni^+ center.[2,26,30,31] It is noted that the charge state of the Ni impurity in GaP can be easily changed under the illumination of the below-gap light. Also, it is noted that the Ni impurity forms a complex with shallow donor impurities, and PL lines due to the Ni-S and Ni-Ge complex centers have been reported.[4] Especially in GaAs, Ni impurity forms a complex with S, Se, Te, Si and Sn and the PL lines due to these complexes have been reported, although the PL line due to an isolated Ni center has never been observed.[4]

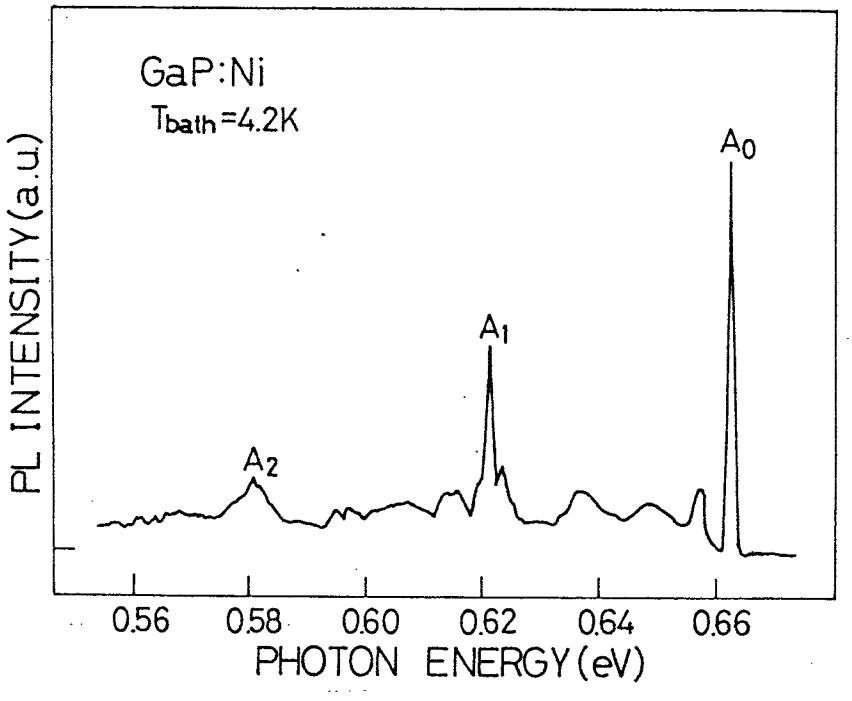

Fig. 4-12 Ni-related PL spectrum in GaP measured at 4.2K.

4-4. Cr in GaAsP and AlGaAs

In contrast to intensive studies of the TM-related PL spectra in III-V binary compounds, very few has been reported on TM-related PL spectra in III-V semiconducting alloys; Cr-related PL spectra in GaAsP [32] and AlGaAs [33-35] alloys.

In $GaAs_{1-x}P_x$ alloys, it has been reported that the Cr-related PL spectra show broad PL bands with no zero-phonon line over the whole composition range, and the peak position of the broad band changes abruptly with composition between 0.65 and 0.75. The disappearance of the zero-phonon line has not been made clear.[32] The abrupt change in the PL energy has been considered to be the change in the charge states of Cr center.

In $Al_xGa_{1-x}As$ alloys, the Cr-related PL spectra have been reported for AlGaAs LPE layers grown on GaAs substrate. Deveaud et al. have measured the Cr-related PL spectra in AlGaAs alloys with the composition x between 0.11 and 0.38 using Cr-diffused AlGaAs LPE layers.[33] They have observed broad PL bands centered around 0.78 eV with no zero-phonon line, and these broad bands have been interpreted due to the isolated Cr^{2+} center which is different from that in GaAs being the Cr^{2+}-V_{As} complex center. On the other hand, Kocot et al. have doped Cr impurities during the LPE growth and reported the Cr-related PL spectra with zero-phonon lines at 0.84 eV which are almost the same position as that in GaAs.[34,35] Such discrepancy is considered to be arisen from the fact that these PL spectra have been taken using thin epitaxial layers grown on GaAs substrate and that effects of the substrate can not be ignored.

As mentioned above, the investigation of the TM-related PL spectra in III-V semiconducting alloys is now in the starting point. Studies of TM impurities in III-V semiconducting alloys are important mainly due to the following reasons. One reason is that the systematic investigation of the characteristic properties of TM centers, such as charge states and crystal field parameters which are closely related to the host material is possible under the gradually changing the environment of TM center by changing alloy composition. Furthermore, the change in the alloy composition also changes the crystal symmetry at the TM center, the band structure of the host material and the crystal field strength. Another reason is that the characterization of the local atomic structure of semiconducting alloy is possible because the wave-functions of 3d electrons are strongly localized in space. This characterization is discussed in Chapter 6.

However, there are difficulties in the measurement of the TM-related PL spectra in semiconducting alloys. Most of III-V semiconducting alloys are epitaxial thin films grown on a binary compound substrate, and the growth of compositionally uniform bulk alloys is rather difficult. The measurement on epitaxial samples is unacceptable because stress due to lattice mismatch shifts and splits the energy levels of TM impurities.[16,17] Furthermore, the TM-related PL lines from the epitaxial layer are obscured by other PL components from the substrate. This problem should be overcomed by PL measurements on bulk-grown semiconducting alloys. The author has grown compositionally uniform bulk InGaP alloys as described in Section 2-3, and systematic investigations on the TM-related PL are described in detail in Chapter 6.[36]

4-4. Summary

The general features of photoluminescence related to TM impurities in III-V semiconductors have been described.

First, the crystal field splitting of 3d electrons in TM impurities occupying the zincblende crystal lattice has been briefly discussed based on the crystal field approach. Second, low-temperature PL spectra related to TM impurities have been shown. The Cr-related PL spectra in GaAs have been described in connection with the energy level scheme caused by the trigonal crystal field and perturbation under uniaxial stress. The TM (V, Cr, Co and Ni)-related PL spectra have been presented and the associated charge state and the energy levels have been described. Finally, the literatures of TM-related PL spectra in III-V semiconducting alloys have been cited, and the significance and problems in the characterization of alloy semiconductors by TM-related PL measurement have been discussed.

REFERENCES

1) U. Kaufmann and J. Shneider: Festkorperprobleme-Advance in Solid State Physics (Vieweg, Braunschwing, 1980) Vol.XX p87.

2) P. J. Dean, A. M. White, B. Hamilton, A. R. Peaker and R. M. Gibb: J. Phys. D 10 (1977) 2545.

3) J. Barrau, F. Voillot, M. Brousseau, J. C. Brabant and G. Poiblaud: J. Phys. C 14 (1981) 3447.

4) H. Ennen, U. Kaufmann ans J. Schneider: Appl. Phys. Lett. 38 (1981) 355.

5) E. M. Omel'yanovskii and V. I. Fistul': Transition Metal Impurities in Semiconductors (Adam Hilger Ltd, Bristol, 1983).

6) S. Sugano, Y. Tanabe and H. Kamimura: Multiplets of Transition-Metal Ions in Crystal (Academic Press, New York & London, 1070).

7) H. J. Stocker and M. Schmidt: J. Appl. Phys. 47 (1976) 2450.

8) W. H. Koshel, S. G. Bishop and B. D. McCombe: Solid State Commun. 19 (1976) 521.

9) C. Uihlein and L Eaves: Phys. Rev. B 26 (1982) 4473.

10) F. Voillot, J. Barrau, M. Brousseau and J. C. Brabaut: J. Phys. C 14 (1981) 1855.

11) Y. Fujiwara, A. Kojima, T. Nishino and Y. Hamakawa: J. Luminescence 31&32 (1984) 451.

12) E. C. Lightowlers, M. O. Henry and C. M. Penchina: Proc. 14th Int Conf. Physics of Semiconductors, Edinburgh, 1978 (Inst. of Phys., Bristol & London, 1979) p.307.

13) J. Barrau, D. X. Thanh, M. Brousseau, J. C. Brabant and F. Voillot: Solid State Commun. 44 (1982) 395.

14) Y. Fujiwara, A. Kojima, T. Nishino, Y. Hamakawa, K. Yasutake, M. Umeno and H. Kawabe: Ext. Abst. 16th Int. Conf. Solid State Devices and Mater., Kobe, 1984 (Japan Business Center for Academic Societies, Tokyo, 1984) p.177.

15) Y. Fujiwara, T. Nishino and Y. Hamakawa: Appl. Phys. A 41 (1986) 115.

16) S. Shirakata, Y. Fujiwara, M. Kondo, T. Nishino and Y. Hamakawa: Ext. Abst. 17th Conf. Solid State Devices and Mater., Tokyo, 1985 (Japan Business Center for Academic Societies, Tokyo, 1985)p.205.

17) S. Shirakata, Y. Fujiwara, M. Kondo, T. Nishino and Y. Hamakawa: J. Electronic Materials 15 (1986) 323.

18) D. P. Halliday, W. Ulrici and L. Eaves: J. Phys. C 19 (1986) L683.

19) H. Ennen and U. Kaufmann: J. Appl. Phys. 51 (1980) 1615.

20) G. Aszodi and U. Kaufmann: Phys. Rev. B 32 (1985) 7108.

21) B. Clejaud, C. Naud, B. Deveaud, B. Lambert, B. Plot, G. Biemond, C. Benjeddou, G. Guillot and A. Nouailhat: J. Appl. Phys. 58 (1985) 4207.

22) C. Benjeddou, A. Nouailhat and G. Guillot: Abst. 5th."Lund" Int. Conf. Deep-Level Impurities in Semicond. (1985) p.4.

23) U. Kaufmann and W. H. Koschel: Phys. Rev.B 17 (1978) 2081.

24) P. J. Williams, L. Eaves, P. E. Simmounds, M. O. Henry, E. C. Lightowlers and C. Uihlein: J. Phys. C 15 (1982) 1337.

25) J. Weber, H. Ennen, U. Kaufmann and J. Schneider: Phys. Rev. B 21 (1989) 2394.

26) S. G. Biship, P. J. Dean, P. Porteous and D. J. Robbins: J. Phys. C 13 (1980) 1131.

27) W. Hayes, J. F. Ryan, C. L. West and P. J. Dean: J. Phys. C 13 (1980) L149.

28) M. S. Skolnick, P. R. Tapster, P. J. Dean, R. G. Humphreys, B. Cockayne, W. R. MacEwan and J. M. Noras: J. Phys. C 15 (1982) 3333.

29) B. Deveaud, B. Lambert, P. Auvray, A. M. Hennel, B. Clerjaud and C. Naud: J. Phys. C 19 (1986) 1251.

30) U. kaufamnn, W. H. Koschel and J. Scneider: Phys. Rev. B 19 (1979) 3343.

31) W. Hayes, J. F. Ryan, C. L. West and P. J. Dean: J. Phys. C 12 (1979) L815.

32) Y. Fujiwara, A. Kojima, T. Nishino and Y. Hamakawa: Jpn. J. Appl. Phys. 23 (1984) L4.

33) B. Deveaud, B. Lambert, H. L'haridon and G. Picoli: J. Luminescence 24&25 (1981) 273.

34) K. Kocot and G. L. Pearson: Solid State Commun. 25 (1978) 113.

35) K. Kocot, R. A. Rao and G. L. Pearson: Phys. Rev. B 19 (1979) 2059.

36) S. Shirakata, T. Nishino, Y. Hamakawa, T. Kato and T. Ishida: to be published in Jpn. J. Appl. Phys. Lett. 26, No. 2 (1987).

5. INTERFACE STRESS AT InGaPAs/GaAs HETEROINTERFACE

5-1. Introduction

Much attention has been recently paid to effects of the interface stress on semiconductor heterojunction devices. The interface stress induced by lattice mismatch in heteroepitaxy plays an important role in the interfacial electrical properties as well as the physical properties of an epitaxially grown layer. In general, the interface stress at heterojunctions has been estimated by a strain-stress analysis in connection with lattice mismatch obtained by x-ray diffraction measurements[1]. However, such a method does not enable us to obtain precisely the magnitude of stress at hetero-interfaces, since such stress is easily relaxed by the formation of misfit dislocations[2-4], and the analyzed region is too large as compared with the interface region. In recent years, Raman scattering has come to be used to characterize stress at heterointerfaces such as silicon-on-sapphire (SOS)[5] and InGaAs/GaAs[6]. Raman spectra are, however, insensitive to stress. The detection limit is about 100 MPa (10^9 dyn/cm^2)[7], and therefore such Raman measurements are restricted to heterointerfaces with extremely large stress.

From these points of view, a new powerful technique for characterization of the interface stress at heterojunctions has been strongly desired. As has been discussed for the Cr-related PL spectrum in GaAs in Chapter 4, the Cr-related PL line at 0.839 eV is very sensitive to stress and has been used for the characterization of the residual stress in plastically bent GaAs wafer.[8,9]

In this Chapter, the author has applied this PL method to the characterization of the interface stress at heterostructure.[10,11] Studies have been made on $In_{1-x}Ga_xP_{1-y}As_y$ ($y \cong 0.04$)/GaAs heterojunction prepared by the LPE method as has been described in Chapter 2.[12,13] The systematic PL measurements on the Cr-related zero-phonon PL line have been done for a series of (100) or (111) oriented InGaPAs/GaAs:Cr heterostructures varying the lattice mismatch. From the shift and splitting of this PL line, the interface stress at InGaPAs/GaAs heterostructure has been obtained and discussed comparing with that calculated. Furthermore, this characterization technique has been successfully applied for AlGaAs/GaAs:Cr and ZnSe/GaAs:Cr heterostructures.

5-2. PL spectra at InGaPAs/GaAs heterointerface

With the photo-excitation through a thin InGaPAs LPE-layer ($Eg \cong 2.0$ eV at 4.2 K) by the 514.5 nm (2.41 eV) line of the Ar^+-laser, PL spectra from GaAs substrate could be clearly observed as well as from InGaPAs LPE-layer. In Fig.5-1, a typical PL spectrum of the InGaPAs/GaAs:Cr heterostructure is shown, where the spectrum is not corrected by the wavelength response of the measurement system. The PL line at 1.98 eV is the near-band edge PL of InGaPAs LPE layer, and PL lines bellow 1.52 eV are from the GaAs substrate. The PL intensity from GaAs substrate was comparable with that from InGaPAs LPE-layer. It is noted here that the Cr-related PL line at 0.839 eV is strong enough to measure with high resolution for stress characterization at heterointerface.

It is important to note here the estimation of the interface region to be measured by this PL method. The interface region is considered to be determined mainly by the penetration depth of the exciting radiation and the diffusion length of photoexcited carriers. The penetration depth is about 0.1 μm at 4.2 K for the excitation light of 514.5 nm used here,[15] and the diffusion length of the photoexcited carriers is estimated to be about 0.5 μm from the Einstein relation, considering that the recombination time of photoexcited carriers is shorter than 1 ns.[16] Therefore, this method characterizes the interface stress in the GaAs substrate region within 1 μm from the InGaPAs/GaAs heterointerface.

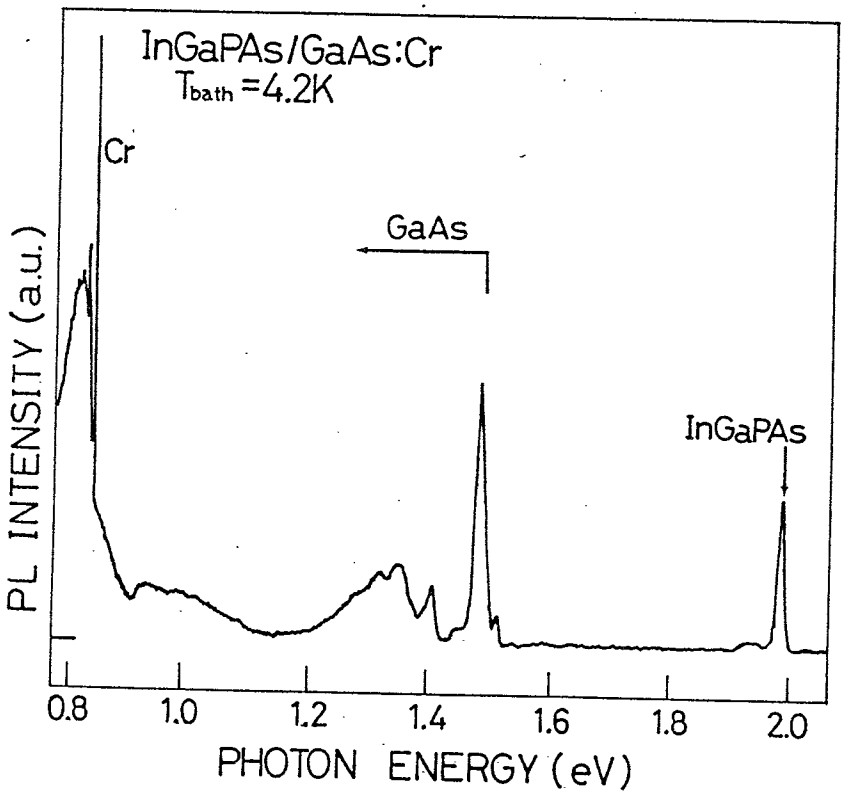

Fig. 5-1 PL spectrum from InGaPAs/GaAs:Cr heterostructure.

5-3. Effects of interface stress on energy level of Cr in GaAs

In GaAs:Cr, the well-known sharp zero-phonon PL lines are observed in the 0.839 eV region. The details of this PL lines are described in Section 4-3-1. The energy level scheme of this luminescent center is illustrated in Fig. 5-2. The strongest PL line "G" at 0.8396 eV has been used for the interface stress measurement in this work, and the corresponding transition is indicated by arrows in the energy level scheme in Fig. 5-2.

In the LPE growth of InGaPAs on (100)GaAs substrate, if the thickness of the epitaxial layer (d_e) is much smaller than that of the substrate (d_s) and also the lattice mismatch ($\Delta a/a>0$) between them is not so large, the lattice of the epitaxial layer is tetragonally deformed due to biaxial compressive stress parallel to [100] or [010] axis, T^e_{xx} and T^e_{yy}, and then the GaAs substrate suffers biaxial tensile stress, T^s_{xx} and T^s_{yy}, to satisfy the balance of force and moment. This situation is shown in Fig. 5-3(a). The biaxial tensile stress can be decomposed into compressive uniaxial stress and tensile hydrostatic pressure components with the same magnitude using stress tensor as

$$\begin{bmatrix} T^s_{xx} & 0 & 0 \\ 0 & T^s_{yy} & 0 \\ 0 & 0 & 0 \end{bmatrix} = \begin{bmatrix} P & 0 & 0 \\ 0 & P & 0 \\ 0 & 0 & P \end{bmatrix} + \begin{bmatrix} 0 & 0 & 0 \\ 0 & 0 & 0 \\ 0 & 0 & -T^s_{zz} \end{bmatrix} \qquad (5\text{-}1)$$

where $T^s_{xx}=T^s_{yy}=T^s_{zz}=P$, as shown in Fig. 5-3(b). Therefore, effects of biaxial tensile stress on the Cr energy levels in GaAs are also decomposed into tensile hydrostatic pressure and compressive uniaxial

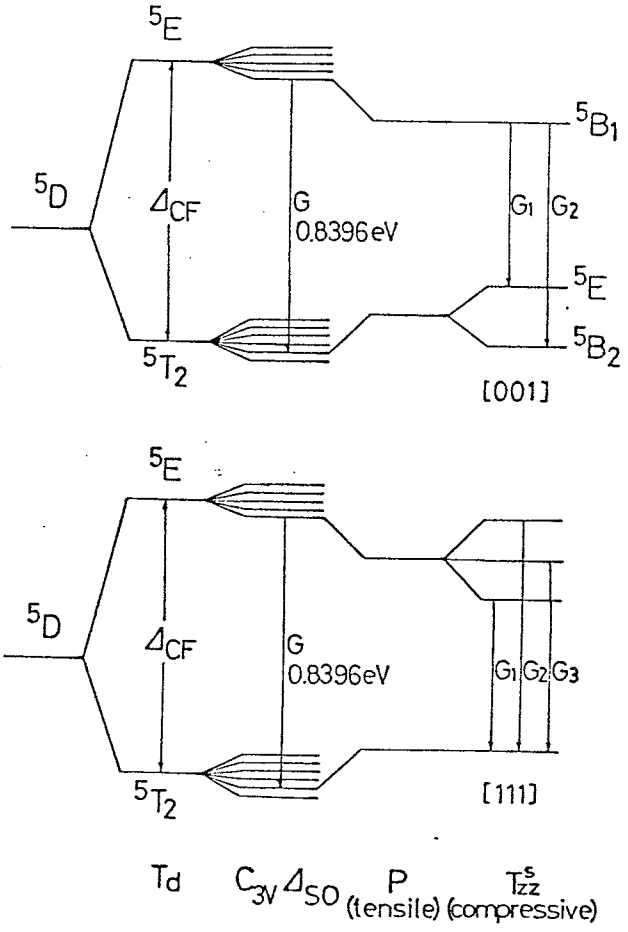

Fig. 5-2 Level scheme of ^5D state of Cr-ion in GaAs. Upper and lower correspond to case for (100) and (111) oriented GaAs:Cr, respectively. Vertical arrows show radiative transitions of the well-known 0.839 eV PL lines. Notations G1, G2, and G3 follow Ref. (19).

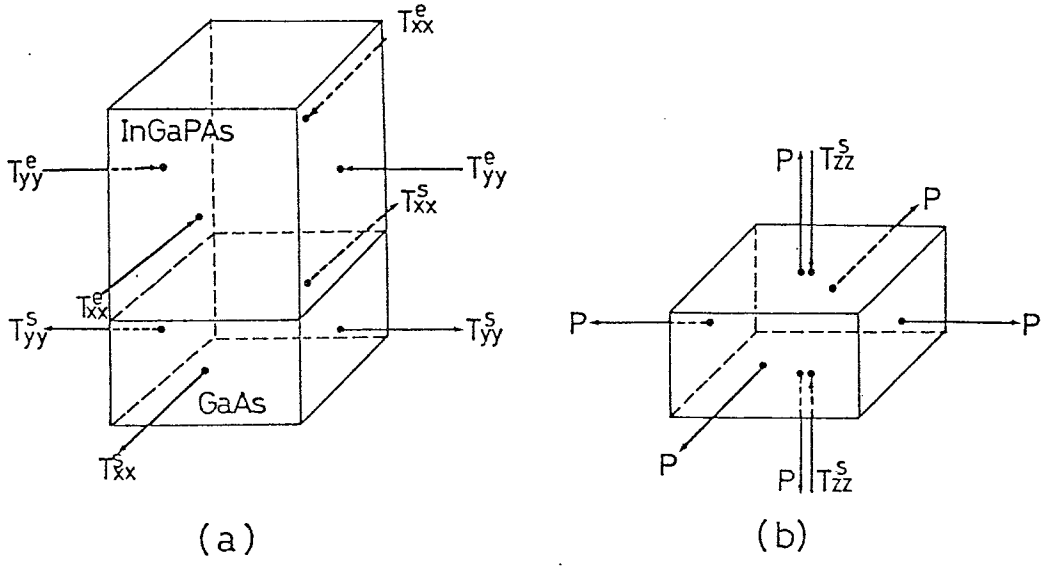

Fig. 5-3 Tetragonal distortion due to biaxial stresses onto InGaPAs epi-layer and GaAs substrate. Note that biaxial stress is decomposed into hydrostatic pressure and uniaxial stress.

stress components. It can be considered that tensile hydrostatic pressure makes the crystal-field splitting between the ^5E and $^5T_2$ levels of a Cr^{2+} in GaAs smaller, because the crystal field decreases generally with increasing lattice constant.[17,18] Compressive uniaxial stress causes a lifting of degeneracy in the energy levels due to the reduction of site symmetry of the Cr center. The ground state energy level for the G- transition splits into two levels (transitions corresponding to G1 and G2 in Fig. 5-2) under [001] stress, and the excited state level splits into three levels (transitions corresponding to G1, G2 and G3 in Fig. 5-2) under [111] stress.[19] These effects of the tensile biaxial stress on the energy-level scheme of G line in GaAs:Cr are indicated for (100) and (111) orientated GaAs in Fig. 5-2. One can estimate the magnitude of stress acting on the GaAs substrate by the LPE growth of InGaPAs, using the following formula by Reinhart,[20]

$$T^s=\frac{1}{3\rho(d_e+d_s)d_s}\left(\frac{d_e^3}{S^e}+\frac{d_s^3}{S^s}\right)+\frac{X^s+d_s}{S^s\rho} \tag{5-2}$$

$$\rho=(d_e+d_s)\left\{1+\frac{1}{3}\left(\frac{S^e}{d_e}+\frac{S^s}{d_s}\right)\left(\frac{d_e^3}{S^e}+\frac{d_s^3}{S^s}\right)(d_e+d_s)^{-2}\right\}\left(\frac{\Delta a_f}{a}\right)^{-1} \tag{5-3}$$

$$S^i=S_{11}+S_{12} \quad i=e,\ s \tag{5-4}$$

where T^s is the stress in the substrate, ρ the radius of curvature, $\Delta a_f/a$ the lattice mismatch in the free space, S_{ij} the elastic compliance and X^s the position from the heterointerface. In (100) $In_{0.46}Ga_{0.54}P_{0.97}As_{0.03}$/GaAs:Cr with $\Delta a_f/a$ of 0.1%, d_e of 3 μm and d_s of 380 μm, the stress acting on the GaAs substrate is estimated to be 3.8

MPa. This magnitude of stress yields a splitting of 0.2 meV in G-line using previously reported uniaxial stress data.[19)]

5-4. Cr-related luminescence at InGaPAs/GaAs heterostructure

5-4-1. Peak shift and splitting

Figures 5-4(a) and (b) show Cr-related PL spectra of GaAs in the 0.839 eV region for (100) and (111)B InGaPAs/GaAs:Cr heterostructure with different lattice mismatch together with the PL spectrum of a GaAs:Cr semi-insulating wafer. It can be seen in the figure that G-line in GaAs:Cr shifts to lower energy and its full width at half maximum (FWHM) becomes larger as the lattice mismatch perpendicular to the interface ($\Delta a/a$) increases. Furthermore, for (111)B InGaPAs/GaAs:Cr with $\Delta a/a$ of 0.28%, new lines appear in the low and high energy sides of G-line.

The shift of the main peak to lower energy is due to the tensile hydrostatic pressure component of the biaxial interface stress existing at InGaPAs/GaAs:Cr heterostructure, as mentioned previously. However, the GaAs:Cr substrate suffers heat treatment at 800°C for 1 h in an ambient of H_2 before the LPE growth, and therefore the substrate surface suffers thermal damage, which can be seen as the appearance of a new line at 1.412 eV as shown in Fig. 5-1.[21)]

In order to clarify that the observed peak shift is not due to such thermal damage of the substrate surface but to the interface stress, two experiments have been done. First, the shift of the G-line has been measured with respect to $\Delta a/a$. In Figs. 5-5 and 5-6, the energy shift of G-line is plotted as a function of $\Delta a/a$ for (100) and (111)B

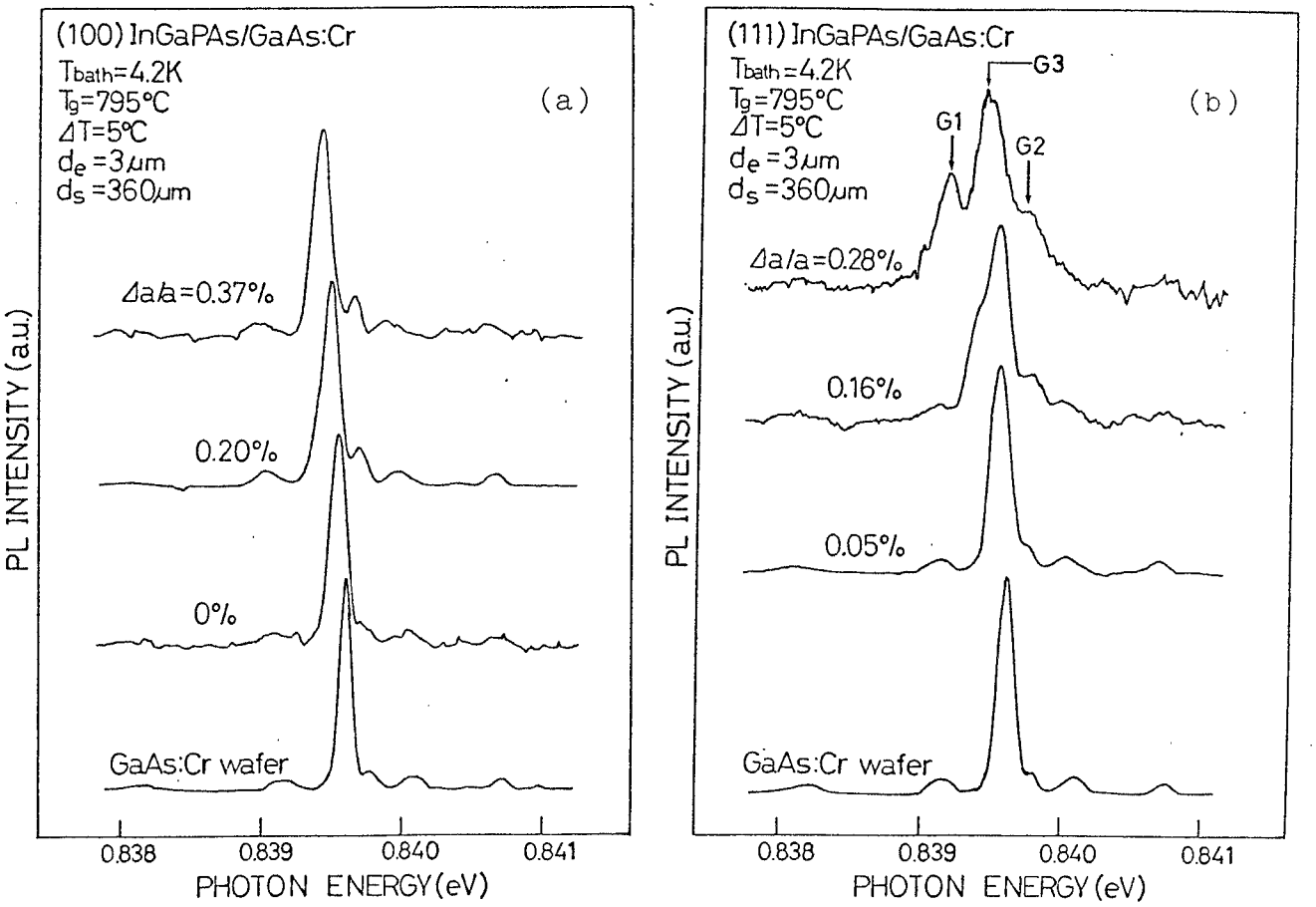

Fig. 5-4 Cr-related PL spectra of GaAs from InGaPAs/GaAs:Cr heterostructure with various lattice mismatch, where (a) and (b) show case for (100) and (111)B samples, respectively.

InGaPAs/GaAs:Cr, respectively. The magnitude of the shift increases monotonously as $\Delta a/a$ increases for both (100) and (111)B oriented samples. Secondly, the peak shift has been measured as a function of the InGaPAs LPE layer d_e, which was changed by successive etching. The result is shown in Fig. 5-7. The PL peak shift becomes smaller as d_e decreases and becomes zero when d_e is zero. It has also been found that this PL peak shift is inversely proportional to the substrate thickness d_s. Therefore, this PL peak shift to lower energy is proportional to the thickness ratio d_e/d_s. With the assumptions $d_e \ll d_s$ and $S^e \cong S^s$, equations (5-2) and (5-3) are approximated as,

$$T^s = (4/S^e)(d_e/d_s)(\Delta a_f/a). \qquad (5\text{-}5)$$

Compared with this equation and experimental observations mentioned above, we can conclude that the PL peak shift observed for InGaPAs/GaAs:Cr is caused by the tensile hydrostatic pressure component of the interface stress due to the lattice mismatch between InGaPAs and GaAs.

In Figs. 5-5 and 5-6, it can be seen that the peak shift of $\sim$0.04 meV is observed even in samples with $\Delta a/a$ of 0%. This may be due to the lattice mismatch $\Delta a/a$ at 4.2 K which is caused by difference in thermal expansion of InGaPAs and GaAs during cooling down for PL measurements from room temperature to 4.2 K. The difference in lattice mismatch between 300 K and 4.2 K is estimated to be 0.056 and 0.043% for (100) and (111) oriented surfaces, respectively, taking the temperature dependence of the thermal expansion coefficient into account. The magnitude of the observed PL peak shift at $\Delta a/a$ of 0% agrees roughly with the shift expected by this thermal effect.

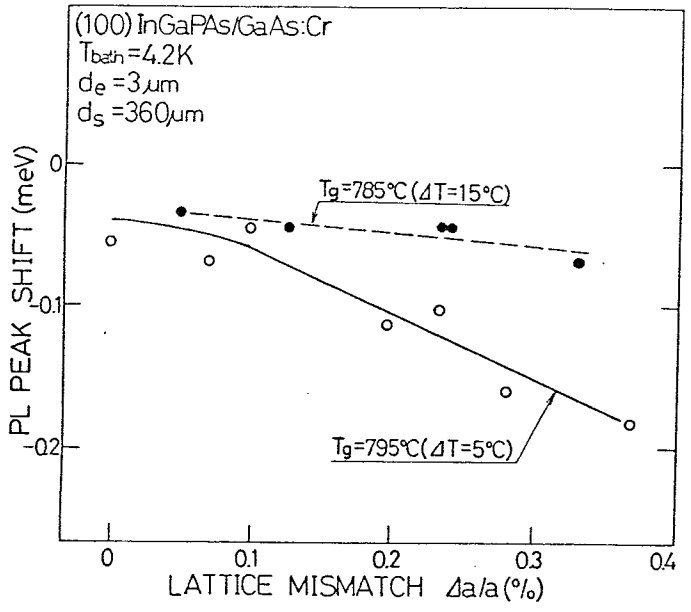

Fig. 5-5 Peak shift of Cr-related PL line from (100)InGaPAs/GaAs:Cr heterostructure as a function of lattice mismatch.

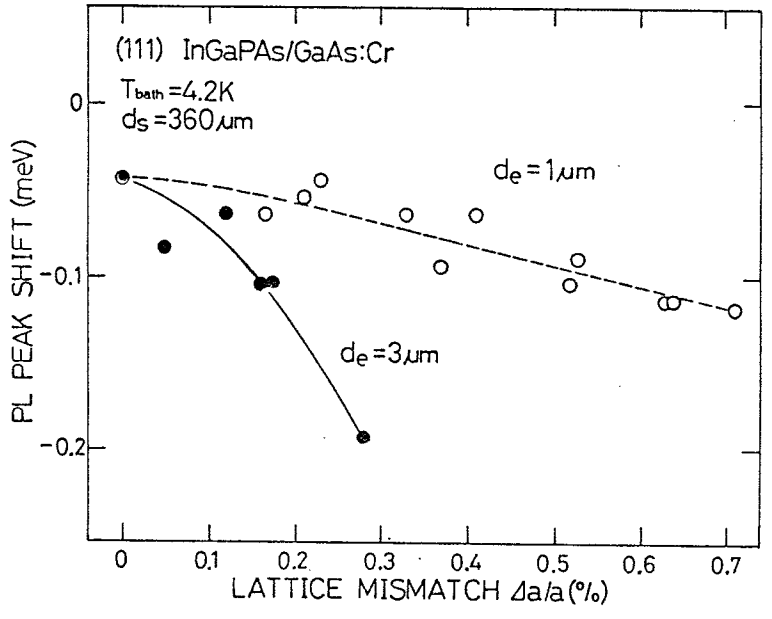

Fig. 5-6 Peak shift of Cr-related PL line plotted as a function of lattice mismatch for (111)B InGaPAs/GaAs:Cr heterostructure.

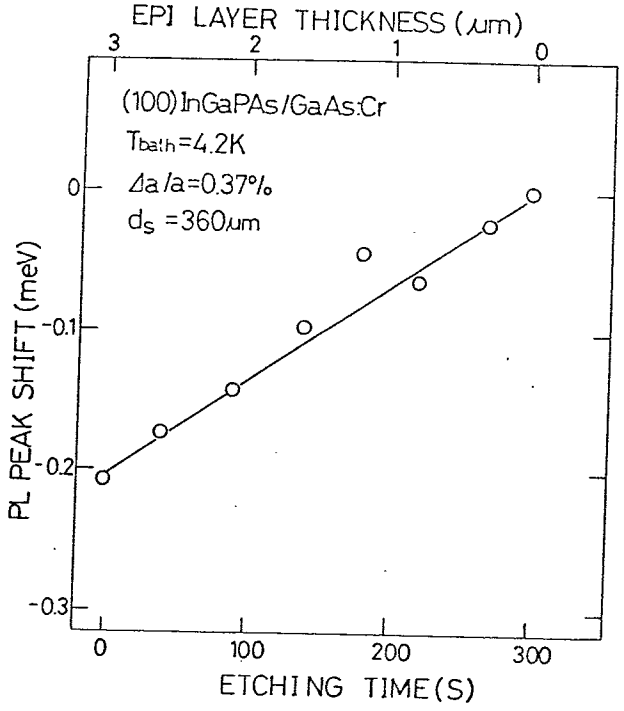

Fig. 5-7 Peak shift of Cr-related PL line plotted as a function of epi-layer thickness for (100)InGaPAs/GaAs:Cr with Δa/a of 0.37%.

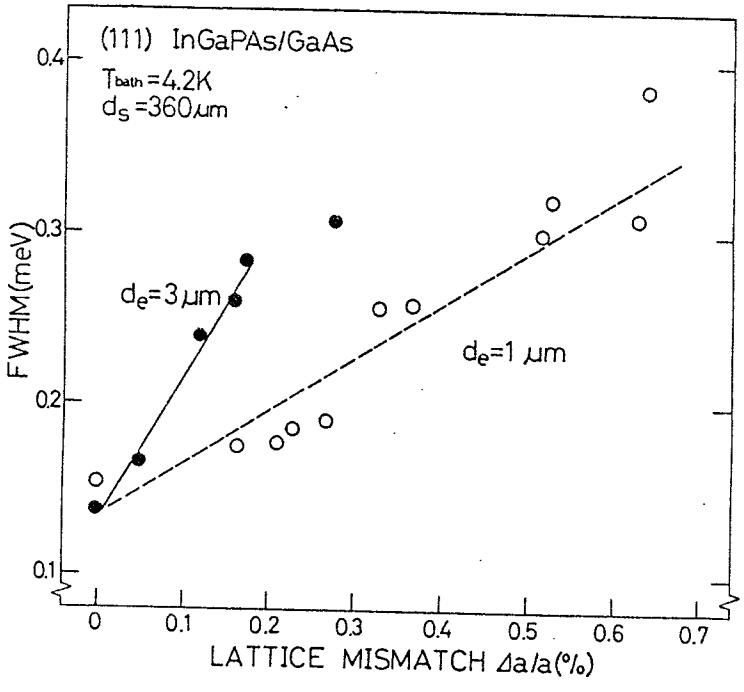

Fig. 5-8 FWHM of Cr-related PL line plotted as a function of lattice mismatch for (111)B InGaPAs/GaAs:Cr.

The increase in FWHM and the splitting of G-line, as shown in Figs. 5-4(a) and (b), are considered to be caused by the uniaxial stress component of the interface stress at InGaPAs/GaAs heterostructure. In Fig. 5-8, the FWHM of G-line is plotted as a function of $\Delta a/a$ for (111)B InGaPAs/GaAs:Cr, the results showing that the FWHM increases as $\Delta a/a$ increases and is larger for samples with d_e of 3 μm than those with d_e of 1 μm. The well-resolved G-line shown in the upper part of Fig. 5-4(b) for (111)B InGaPAs/GaAs:Cr with $\Delta a/a$ of 0.28% is in good agreement with the previously reported data for a GaAs:Cr wafer applied by uniaxial stress along [111] direction. Therefore, the increase in FWHM is considered to be caused by an unresolved splitting of G-line.

5-4-2. Estimation of interface stress

In Fig. 5-9, Cr-related PL spectra obtained from the interface and the rear-substrate-face of InGaPAs/GaAs:Cr heterostructures are shown for the (100) oriented substrate. These spectra correspond to the cases of large interface stress. As can be seen in the figure, both shift and splitting of the G-line were observed in the spectra from the interface. For (100) InGaPAs/GaAs:Cr heterostructure the values of d_e and d_s were 3 μm and 120 μm, respectively, and $\Delta a/a$ was 0.23%. The substrate was etched, from the thickness of 360 μm to 120 μm after the LPE growth. By this procedure, the splitting of G-line was clearly observed since the magnitude of interface stress, which is proportional to the thickness ratio d_e/d_s, becomes three times larger than the initial value. The PL lines denoted by G1 and G2 in Fig. 5-9 correspond to the G-line splitting due to the compressive uniaxial component of the interface stress, and the lineshape is in good agreement with the previously

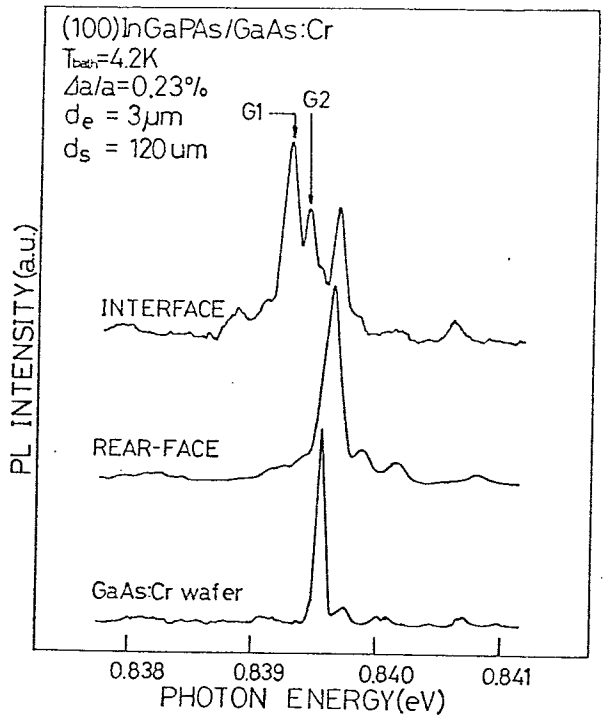

Fig. 5-9 Cr-related PL spectra from (100) InGaPAs/GaAs:Cr. Upper curve is for heterointerface and middle curve is for rear-substrate-face of InGaPAs/GaAs:Cr.

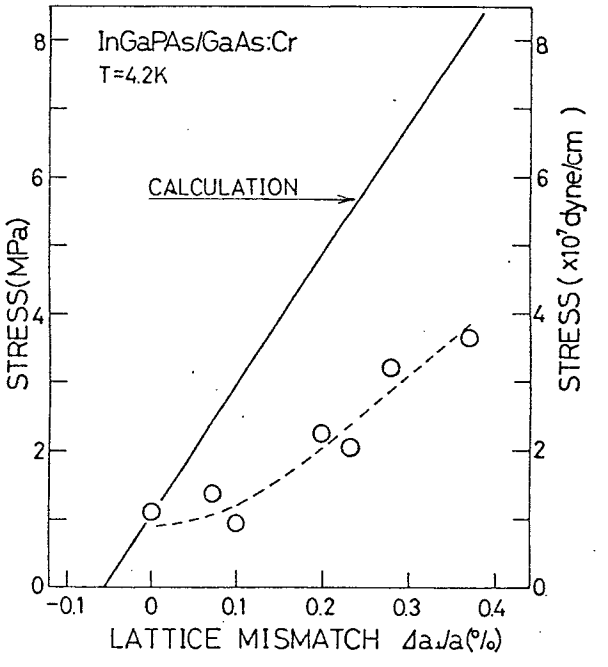

Fig. 5-10 Interface stress at (100) InGaPAs/GaAs heterostructure plotted as a function of lattice mismatch. Open circle and solid line denote the experimental and theoretical values, respectively.

reported PL lineshape for plastically bent GaAs:Cr samples.[8,9] If we compare the energy splitting between G1- and G2- lines with the stress coefficient of 4.1×10^{-2} meV/MPa[19], the interface stress for the spectrum in Fig. 5-9 is estimated to be 3.6 MPa. In this PL spectrum, the shift of the G-line is 0.18 meV, which is due to the tensile hydrostatic pressure component of the biaxial stress at the heterointerface. It has been found from the equation (5-1) that the magnitude of the hydrostatic pressure is equal to that of the uniaxial stress at the heterointerface. By using this relationship, the hydrostatic pressure coefficient of the peak shift in G-line is estimated to be -5.0×10^{-2} meV/MPa. One can estimate the magnitude of interface stress from the peak shift using this coefficient even if the splitting of the G-line is not observed. In Fig. 5-10, the interface stress at (100)InGaPAs/GaAs:Cr heterostructures estimated in such a manner is plotted as a function of lattice mismatch together with that calculated at 4.2K using equations (5-2)∿(5-4). It can be seen in the figure that the interface stress estimated from the PL spectra is a half as small as that calculated. This may be related to the relaxation of the heterointerface stress due to the formation of misfit dislocations[22] or a transition layer. The result shown in Fig. 5-10 agrees fairly well with the previous report by Olsen et al. that in the case of VPE grown (100)InGaP/GaAs, at least 30% of the elastic strain is found to be relaxed due to the introduction of misfit dislocation, which has been estimated from the analysis of the lattice constant and the band-gap energy.[23] The relaxation of the interface stress can be further supported by the following experimental results. In Fig. 5-5, the samples grown with ΔT of 15°C show a smaller peak shift of G-line

than those with ΔT of 5°C. The estimated interface stress of (100) InGaPAs/GaAs:Cr is smaller than that of the calculated value, while in (111)B InGaPAs/GaAs:Cr the estimated value agrees roughly with the calculated one. In plastically bent GaAs:Cr samples, it has been found that the relaxation of the residual stress occurs more easily for [001] orientation than other orientations of [111] and [110] orientations, leading to the appearance of the stress-relaxed G-line.[8,9)]

Furthermore, it is noted in Fig. 5-9 that G-line shifts to higher energy compared with the unperturbed peak energy for the spectrum obtained with the rear-substrate-face. This suggests that stress of 0.5 MPa with the opposite sign acts on the rear-substrate-face, indicating a stress distribution in the substrate. This result agrees qualitatively with the calculation of the stress distribution in the substrate using equations (5-2)-(5-4), this showing that there is a neutral point of stress inside the substrate.

5-5. Application to other heterostructures

In order to apply this interface stress characterization technique to other heterostructures, the interface stress at several heterostructures has been calculated and compared with the detection limit of this method. The interface stress at $In_{1-x}Ga_xP_{1-y}As_y$/GaAs:Cr, $Al_xGa_{1-x}As$/GaAs:Cr and ZnS_xSe_{1-x}/GaAs:Cr has been calculated using equations (5-2)∿(5-4) with d_e/d_s of 0.01, and the result is shown in Fig. 5-11. The detection limit of this characterization technique has been estimated to be 0.4 MPa from the hydrostatic pressure coefficient

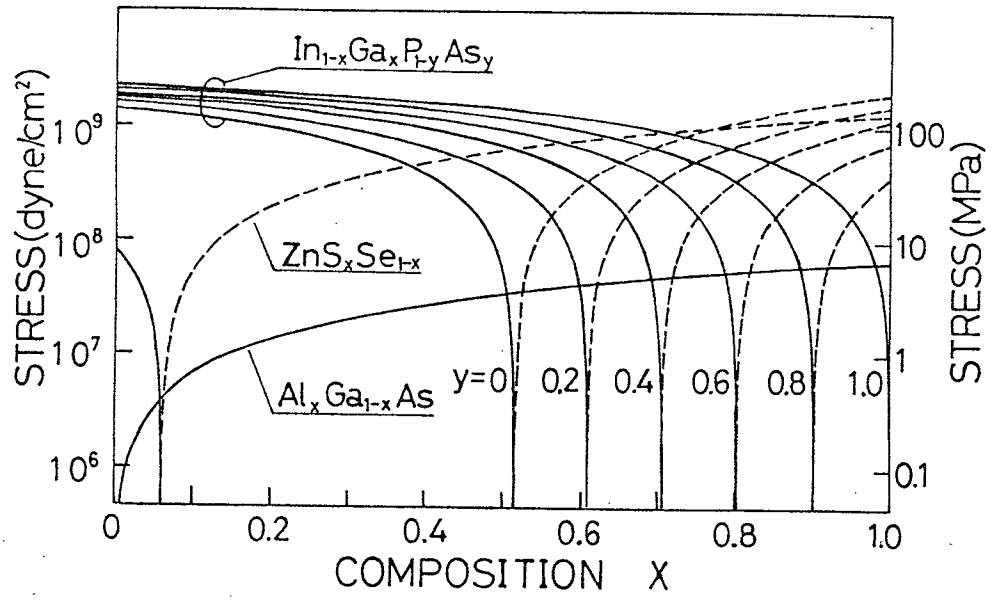

Fig. 5-11 Calculated interface stress plotted as a function of alloy composition for $In_{1-x}Ga_xP_{1-y}As_y$, $Al_xGa_{1-x}As$/GaAs and ZnS_xSe_{1-x}/GaAs heterostructures.

(-5×10^{-2} meV/MPa), the resolution (5×10^{-2} meV) and wavelength reproducibility (2×10^{-2} meV) of the measurement system used in the present study. It can be seen in Fig. 5-11 that the measurement of the interface stress is possible for these heterostructures except for the very small composition range near the lattice matching condition.

In Fig. 5-12, the Cr-related PL spectra from the heterointerface of (100)$Al_xGa_{1-x}As$/GaAs:Cr (x=0.35 and 0.70) are shown together with that from GaAs:Cr wafer. The AlGaAs layers with the thickness of 3 μm were grown by LPE at 800°C on (100)GaAs:Cr wafer. As can be seen in the figure, the G-line slightly shifts to lower energy as x increases. This negative shift indicates the existence of the tensile hydrostatic pressure component in the biaxial stress at the interface region of the

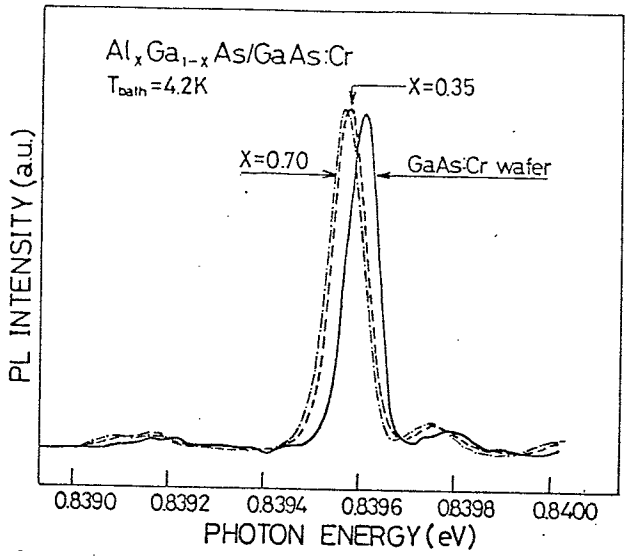

Fig. 5-12 Cr-related PL spectra of GaAs from (100)$Al_xGa_{1-x}As$/GaAs:Cr heterostructure.

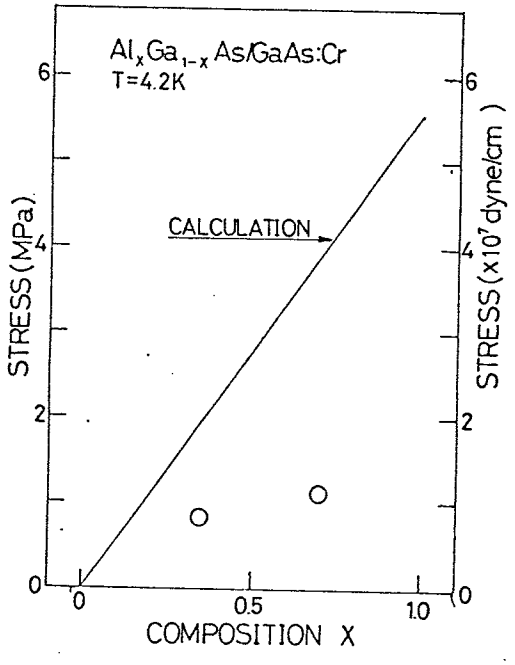

Fig. 5-13 Interface stress at $Al_xGa_{1-x}As$/GaAs heterostructure plotted as a function of alloy composition x. Open circle and solid line denote experimental and theoretical values, respectively.

GaAs substrate, in good agreement that expected from the lattice constant. In Fig. 5-13, the magnitude of the interface stress estimated from the peak shift is plotted as a function of the Al composition x together with that calculated. The interface stress estimated from the peak shift of the G-line is smaller than that calculated. The relaxation of interface stress may occur similar to the case of InGaPAs/GaAs.

Figure 5-14 shows the Cr-related PL spectra from the heterointerface of (100) and (111) ZnSe/GaAs:Cr heterostructure with the epitaxial layer thickness of 7.7 μm. The ZnSe/GaAs:Cr heterostructure has been prepared by the OMVPE method in Kyoto university, and the details of the crystal growth have been described in Ref. 24. It can be seen in Fig. 5-14 that the peak energy of the G-line slightly shifts to higher energy and its half-width becomes larger compared with that in the GaAs:Cr wafer. The peak shift to higher energy indicates that the GaAs substrate suffers the compressive hydrostatic pressure at the heterointerface. The splitting of the G-line is observed in the (111)ZnSe/GaAs:Cr and the line-shape is in good agreement with that observed in the plastically bent GaAs:Cr wafer with tensile stress along [111] bending axis. Therefore, the uniaxial stress acting on the interface region of ZnSe/GaAs:Cr substrate is tensile. The unstrained lattice constant of ZnSe is larger than that of GaAs by 0.26%. If the ZnSe OMVPE layer grows coherently on GaAs substrate, the tensile biaxial stress composed of both tensile hydrostatic pressure and compressive uniaxial stress is expected as in the case of InGaPAs/GaAs and AlGaAs/GaAs. However, the experimentally obtained sign of the interface stress is opposite to that expected from the coherent growth, that is,

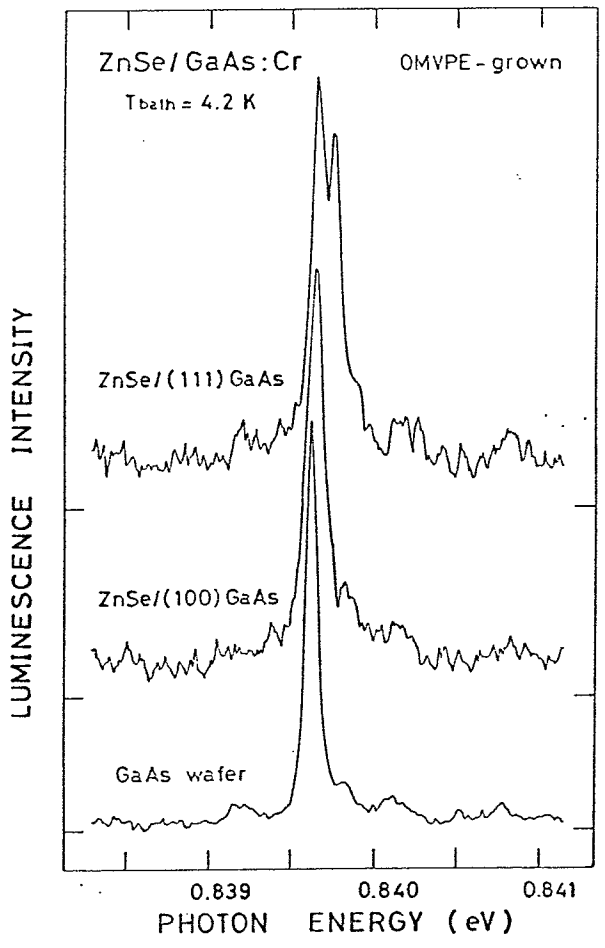

Fig. 5-14 Cr-related PL spectra of GaAs from ZnSe/GaAs:Cr heterostructure.

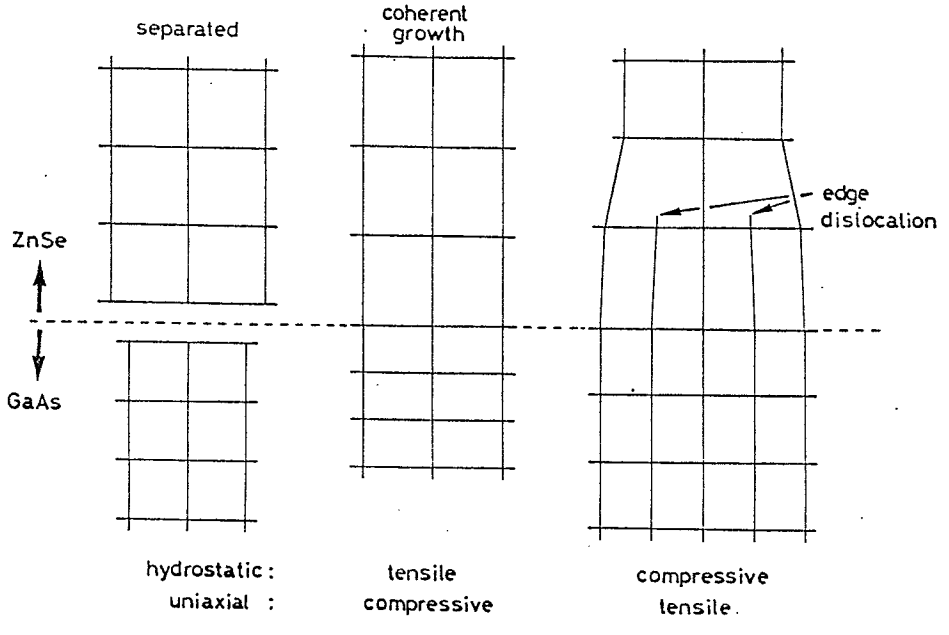

Fig. 5-15 A model for interface stress at ZnSe/GaAs heterostructure.

an anomalous stress is existing in the heterostructure of ZnSe/GaAs. In order to explain this anomalous interface stress, the author proposed a model for lattice distortion at the interface region of the ZnSe epitaxial layer, and the lattice model is schematically shown in the right side of Fig. 5-15, and the distortion of the lattice is compared with the case of the ideal coherent growth. It is considered that a large number of misfit dislocations of edge dislocation type have been introduced into the near-heterointerface region of the ZnSe epitaxial layer due to the large lattice mismatch between ZnSe and GaAs during the OMVPE growth of ZnSe on GaAs substrate. Since the thickness of the ZnSe OMVPE layer of 7.7 μm far exceeds the calculated critical thickness of ∿0.07 μm,[22] the misfit dislocation generation is the most preferable. In fact, it has been reported that the lattice constant of a strained ZnSe layer becomes smaller than that of bulk ZnSe when the epitaxial layer thickness exceeds 0.15 μm by the precise lattice parameter measurement using the double crystal x-ray diffraction method.[25,26] Also, the lattice distortion model recently presented based on x-ray and low-temperature reflectance measurements is consistent with the model present in this work.[27]

5-6. Summary

A new characterization technique for the interface stress at heterostructure has been proposed and applied to InGaPAs/GaAs heterostructure using the Cr-related PL line at 0.839 eV which is very sensitive to stress.

First, the effect of biaxial stress on the energy level of the Cr^{2+} ion in GaAs has been examined based on the crystal field schema. The Cr-related PL line at 0.839 eV from InGaPAs/GaAs:Cr has been examined in terms of the crystal orientation, lattice mismatch, epitaxial layer and substrate thickness. As a result, the shift and splitting of the Cr-related PL line have been observed at InGaPAs/GaAs heterointerface. These changes in the Cr-related PL spectra have been found to be due to the tensile hydrostatic pressure and the compressive uniaxial pressure component of the biaxial stress existing at the heterointerface. The sign of the stress is in good agreement with that expected from the coherent growth. The photon energy of the Cr-related PL line strongly depends on the thickness ratio of epitaxial layer and substrate, showing the stress distribution in the thickness direction of the substrate. The magnitude of the interface stress has been estimated from the peak shift of the Cr-related PL line and the result has been compared with that calculated. It has been found that the interface stress increases with lattice mismatch though some part of the stress is relaxed due to the formation of misfit dislocations.

The application of this interface stress characterization technique to other heterosuructures has been examined. The interface stress at

InGaPAs/GaAs, AlGaAs/GaAs and ZnSSe/GaAs has been calculated and compared with the detection limit in this technique of 0.4 MPa, and the usefulness of this technique has been predicted. Practically, this method has been applied to technologically important AlGaAs/GaAs and ZnSe/GaAs heterostructures. The small interface stress in AlGaAs/GaAs has been successfully characterized. Furthermore, an anomalous interface stress has been found in the ZnSe/GaAs heterostructure, and the result has been interpreted using the lattice distortion model with the formation of edge dislocations, which is consistent with recently reported x-ray and reflectance data.

REFERENCES

1) G. A. Rozgonyi and M. B. Panish: Appl. Phys. Lett. 23 (1973) 533.

2) H. Kressel and J. K. Butler, Semiconductor Lasers and Heterojunction LEDs, (Academic Press, New York, 1977).

3) G. H. Olsen, C. J. Nuese and R. T. Smith: J. Appl. Phys. 49, (1978) 5523.

4) S. N. G. Chu, A. T. Macrander, K. E. Strege and W. D. Johnston,Jr, J. Appl. Phys. 57 (1985) 249.

5) K. Yamazaki, M. Yamada, K. Yamamoto and K. Abe: Jpn. J. Appl. Phys. 23 (1984) 681.

6) K. Kakimoto and T. Katoda: Appl. Phys. Lett. 40 (1982) 826.

7) A. K. Sood, E. Anastassakis and M. Cardona: Phys. Stat. Sol. (b) 129 (1985) 505.

8) Y. Fujiwara, T. Nishino and Y. Hamakawa: Appl. Phys. A, 41 (1986) 115.

9) Y. Fujiwara, A. Kojima, T. Nishino, Y. Hamakawa, K. Yasutake, M. Umeno, and H. Kawabe, Ext. Abst. 16th Conf. Solid State Devices and Mater., Kobe, 1984 (Japan Business Center for Academic Societies, Tokyo, 1984) p. 177.

10) S. Shirakata, Y. Fujiwara, M. Kondo, T. Nishino and Y. Hamakawa: Ext. Abst. 16th Conf. Solid State Devices and Mater.,Tokyo, 1985 (Japan Business Center for Academic Societies, Tokyo, 1985) p. 205.

11) S. Shirakata, Y. Fujiwara, M. Kondo, T. Nishino and Y. Hamakawa: J. Electronic Materials 15 (1986) 323.

12) S. Shirakata, M. Kondo, A. Tsushi, T. Nishino,Y. Hamakawa and T. Kariya: Jpn. J. Appl. Phys. 24 (1985) 524.

13) M. Kondo, S. Shirakata, A. Tsushi, T. Nishino and Y. Hamakawa: Jpn. J. Appl. Phys. 24 (1985) 806.

14) Y. Fujiwara, S. Shirakata, T. Nishino, Y. Hamakawa and S. Fujita: Jpn. J. Appl. Phys. 25 (1086) 1628.

15) M. D. Sturge, Phys. Rev. 127 (1962) 768.

16) R. H. Bube, Semiconductors and Semimetals, ed. R. K. Willardson and A. C. Beer (Academic Press, New York & London, 1967) Vol. 3, Ch. 11, p. 475.

17) S. Sugano, Y. Tanabe and H. Kamimura: Multiplet of Transition-Metal Ion in Crystals (Academic Press, New York & London, 1070).

18) E. M. Onel'yanovskii and V. I. Fistul': Transition Metal Impurities in Semiconductors (Adam Hilger Ltd, Bristol, 1983).

19) J. Barrau, F. Voillot, M. Brousseau, J. C. Brabant and G. Poiblaud: J. Phys. C 14 (1981) 3447.

21) F. K. Reinhart and R. A. Logan: J. Appl. Phys. 44 (1973) 3171.

22) J. W. Matthews, A. E. Blakeslee and S. Mader: Thin Solid Films 33 (1976) 253.

23) G. H. Olsenm C. J. Nusse and R.T. Smith: J. Appl. Phys. 49 (1978) 5523.

24) S. Fujita, Y. Matsuda and A. Sasaki: Jpn. J. Appl. Phys. 23 (1984) 1360.

25) H. Mitsuhashi, I. Mitsui, M. Mizuta and H. Kukimoto: Jpn. J. Appl. Phys. 24 (1985) L578.

26) A. Kamata, K. Hirahara, M. Kawachi and T. Beppu: Ext. Abst. 17th Conf. Solid State Devices and Mater., Tokyo, 1985 (Japan Business Center for Academic Societies, Tokyo, 1985) p.233.

27) T. Yao, Y. Okada, S. Mitsui and K. Ishikawa: to be published in Jpn. J. Appl. Phys.

6. LOCAL STRUCTURES OF InGaP AND GaAsP ALLOYS

6-1. Introduction

The reliability and stability of semiconductor devices using III-V semiconducting alloys strongly depend on the stability of the semiconducting alloys used. For devices such as semiconductor laser diodes operating under high photon and current densities, and also for superlattice containing high strain field, the stability of alloy semiconductors under the device operating condition is a serious problem, because their atomic structure under the operating condition is not necessarily thermodynamically stable. Therefore, this problem should be solved based on the understanding of the microscopic structure of the alloy semiconductors. So far, much attention has been paid to the local structure of III-V semiconducting alloys. Recent extended x-ray absorption fine structure studies[1-3] and the calculation of the bond-length based on the valence force field theory[4] showed that the bond-length in III-V semiconducting alloys has bimodal distribution which is much different from that had been predicted by the virtual crystal approximation. It is well known that III-V semiconducting alloys contain inherent structural defects as disordering, ordering and clustering, and the theoretical approaches based on thermodynamics[5-7] and bond theory[8,9] have been presented. However, the local structure of III-V semiconducting alloys has not yet been made clear. Recently, Samuelsen et al. have reported that PL spectra related to Cu impurity in GaAsP alloy reflect the local atomic environment around the Cu center.[10] Also studies on Cr-related PL

spectra in In-doped GaAs showed the appearance of new PL lines due to presence of the In impurities around the Cr center.[11,12] These reports showed that the 3d-TM impurity can be used as a probe to study local structures in III-V semiconducting alloy. This is based on the fact that 3d-TM impurities occupy the cation site and the wave-functions of d-electrons are localized. Since PL due to TM impurities is caused by transitions between the crystal field split d-levels, it is expected that the PL spectra are largerly affected by the presence of structural defects in III-V semiconducting alloys as has been described in Chapter 4. Very few have been reported on the TM-related optical spectra in III-V semiconducting alloys. They are restricted to Cr impurity in AlGaAs[13,14] and GaAsP[15] alloys, and intended to study the charge state of Cr impurity in such alloys. The purpose of this Chapter is to study the local structure of III-V semiconducting alloys through the TM-related PL spectra. In this Chapter, measurements on TM (V, Cr, Co and Ni)-related PL spectra have been carried out on bulk-grown $In_{1-x}Ga_xP$ alloys which are free from substrate effects. Especially, Co-related PL spectra in InGaP and GaAsP alloys have been systematically measured with the alloy composition $0.70<x<1$ for InGaP and $0.65<x<1.0$ for GaAsP.[16] The change in the Co-related PL spectra with composition is compared between InGaP and GaAsP, the former belonging to the III-III-V type alloy and the latter belonging to the III-V-V type alloy. The Co-related PL spectra in InGaP and GaAsP are discussed with relation to the local atomic arrangement around the Co luminescent center.

6-2. Experimental procedure

6-2-1. Sample preparation

The samples studied here were bulk-grown InGaP crystals as have been described in Chapter 2 and thick VPE GaAsP layers. The GaAsP samples were VPE grown epitaxial layers with thickness of 30-50 μm grown on (100) oriented GaP substrate. The GaAsP VPE layers were undoped n-type with room temperature carrier concentration of 10^{16} cm^{-3}.

The doping of transition metal impurities into InGaP and GaAsP was carried out by a solid diffusion in a sealed quartz tube at 1100°C. The diffusion time was 24 h for InGaP bulk samples. For the Co-doping of GaAsP VPE layer, the diffusion time was varied from 15 min to 24 h, and mainly the diffusion time of 1 h was used for PL measurements, because the Co impurity has a large diffusion constant and the PL spectra due to the Co impurity in GaP substrate have been observed in samples with long-time diffusion. After the diffusion, the surface of samples was mechanically polished and several microns of the surface layer was removed in order to eliminate the effect of thermal damage during the diffusion.

6-2-2. Measurement system

All PL measurements were performed at 4.2K. Samples were photo-excited by an Ar^+-laser, and the PL was analyzed by SPEX 1704 monochromator equipped with a 3 μm brazed grating and phase sensitively detected using a cooled PbS (77K) photodetector with a chopping frequency of 40 Hz. The wavelength of the exciting light was

514.5 nm for InGaP and 457.9 nm for GaAsP VPE layer. For time-resolved PL measurements, the exciting laser beam was chopped by an acousto-optical modulator and detected by a box-car integrator using a cooled InAs photodetector with the response time of 1 μs.

6-3. Transition metal related luminescence in InGaP

In Fig. 6-1, PL spectra related to Co, Ni, V and Cr impurities are shown for $In_{0.1}Ga_{0.9}P$ alloy together with those for GaP. As can be seen, all the TM-related PL spectra in GaP show characteristic sharp zero-phonon lines and their phonon replica, in good agreement with those previously reported,[17-20] and the details have been presented in Chapter 4. The TM-related PL spectra in $In_{0.1}Ga_{0.9}P$ are, however, quite different from those in GaP, that is, they are dominated by very broad PL bands without any zero-phonon line. It is noted here that broad PL bands spread in the lower energy regions than the corresponding zero-phonon PL lines in GaP. Among these four TM impurities, there is a difference in the PL spectra of GaP and $In_{0.1}Ga_{0.9}P$. For the Cr impurity, strong phonon coupling and hence strong phonon replica is observed in GaP, and the Cr-related PL spectrum in $In_{0.1}Ga_{0.9}P$ also show similar broad PL bands with disappearance of the zero-phonon line. The line shape of the broad PL band observed in $In_{0.1}Ga_{0.9}P$:Cr is not so much different from that of the phonon side band in GaP:Cr except for a small peak shift to low-energy by 27 meV and the increase in the half-width. These features are similar to the result previously reported for $GaAs_{0.1}P_{0.9}$:Cr[15]. In the case of Co and V impurities which show weak

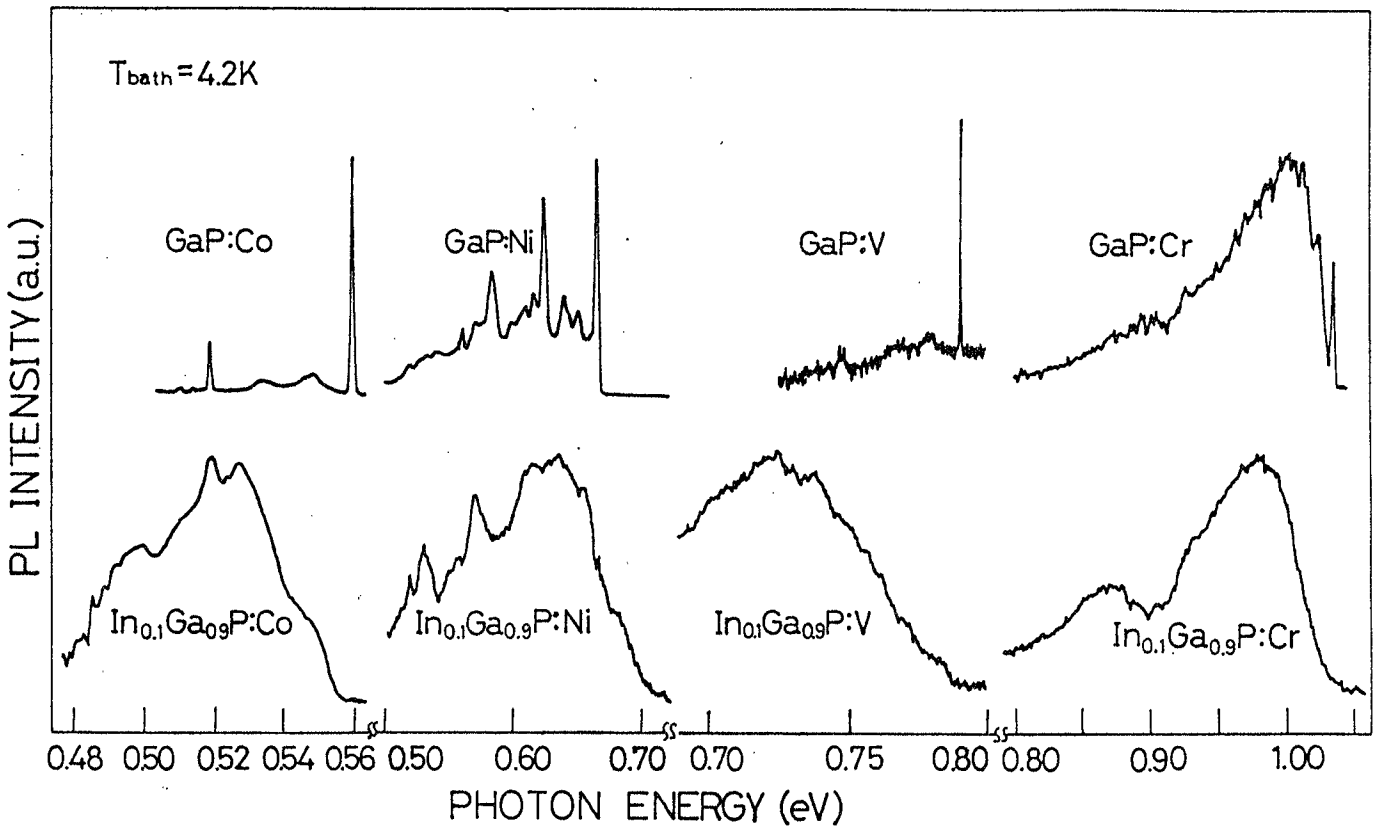

Fig. 6-1 PL spectra related to Co, Ni, V and Cr impurities in GaP and $In_{0.1}Ga_{0.9}P$.

phonon coupling in GaP, it can be seen that the line shapes of broad PL bands in $In_{0.1}Ga_{0.9}P$ are much different from the phonon replicas observed in GaP though the observed broad PL bands show some weak structures. Furthermore, these broad PL bands in $In_{0.1}Ga_{0.9}P$ extend down to the energy region where no PL signal is observed in GaP. In Ni impurity, the broad PL band extends even to the higher energy side than that of the zero-phonon line in GaP unlike other three TM impurities. Such large difference in the TM-related PL spectra in $In_{0.1}Ga_{0.9}P$ from those in GaP seems to suggest that a very different perturbation acts on TM luminescent centers in these alloy materials.

6-4. Co in InGaP and GaAsP

6-4-1. PL spectra

Figures 6-2 and 6-3 show Co-related PL spectra in InGaP and GaAsP, respectively. Composition x is $0.74 \leqq x \leqq 1$ and $0.65 \leqq x \leqq 1$ for InGaP and GaAsP, respectively. In both InGaP and GaAsP, Co-related PL spectra are broad and much different from that in GaP, and these composition dependences are represented by broadening and evolution of PL bands. In InGaP alloy, drastic changes in PL spectra are observed with composition x between 1 and 0.91. The sharp zero-phonon line at 0.559 eV observed in GaP shifts to lower energy and becomes broader as x decreases. The zero-phonon line is completely broadened and can not be resolved from the TA phonon replica with x of 0.96, and disappears completely with x smaller than 0.91. New PL bands peaked at 0.53, 0.515 and 0.49 eV appear. Relative intensities of these bands change systematically with alloy

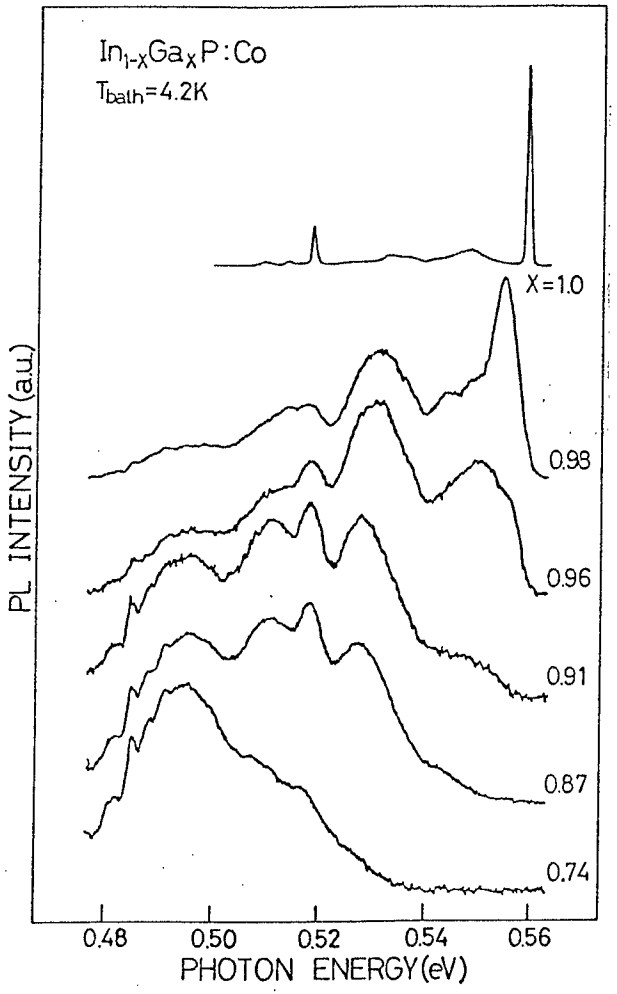

Fig. 6-2 Co-related PL spectra in $In_{1-x}Ga_xP$ alloys.

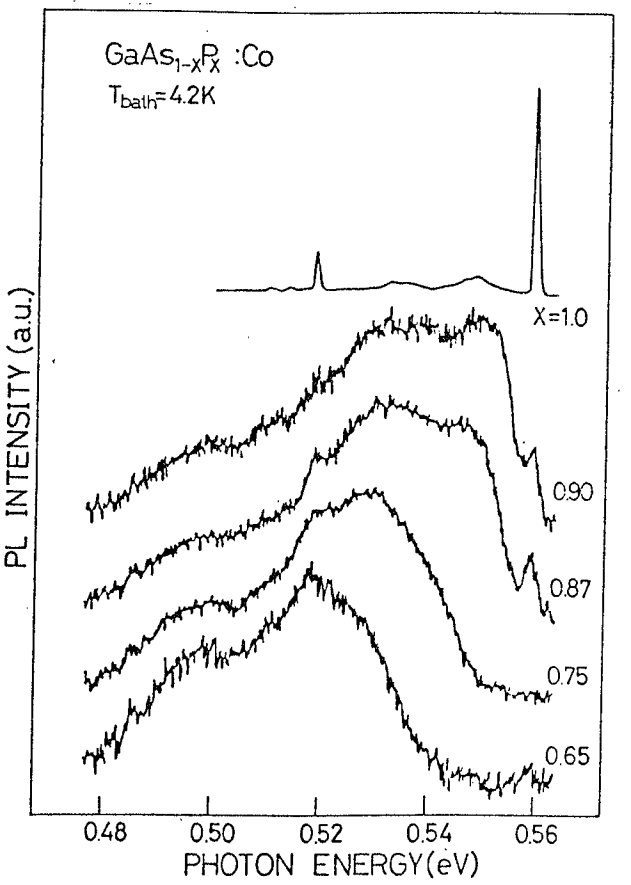

Fig. 6-3 Co-related PL spectra in $GaAs_{1-x}P_x$ alloys.

composition. The intensity of the 0.53 eV band increases as x decreases from 1 and becomes the maximum around x of 0.9. The PL band disappears with x of 0.74. The intensity of the 0.49 eV band increases monotonously as x increases, and with x of 0.74, the PL spectrum is dominated by this PL band. In the case of GaAsP alloy, the zero-phonon line has not been observed in the composition range studied. The weak PL peak observed at 0.559 eV in $GaAs_{0.10}P_{0.90}$ and $GaAs_{0.13}P_{0.87}$ is a Co-related PL from substrate GaP, this fact being clarified by the excitation wavelength dependence and the thermal diffusion time dependence of the Co impurity on PL spectra. The characteristic features of the Co-related PL spectra in GaAsP are as follows; (1) PL spectra are as a whole broader and structureless compared with those in InGaP, (2) the line shapes of PL bands between 0.53 and 0.55 eV resemble that of acoustic phonon replica observed in GaP when composition is close to GaP, (3) the evolution of broad PL bands in the lower energy region between 0.48 and 0.52 eV has been observed. It can be found from the facts above mentioned that the Co-related broad PL spectra observed in both InGaP and GaAsP are composed of several PL bands, and the changes in line shapes with composition are interpreted as changes in the relative intensity of them.

In order to verify that these broad PL spectra observed in InGaP and GaAsP alloys are due to transitions $^4T_2(F) \rightarrow {}^4A_2(F)$ of Co^{2+}, the same as that in GaP not due to other reasons such as thermal damage or defects, the time-resolved characteristics of these PL bands have been measured. The PL decay in both InGaP:Co and GaAsP:Co is composed of the fast decay component with time constants of 200-270 μs and the

weak slow decay component with time constants of 600-900 μs, and the results are shown in Fig. 6-4 and 6-5. The fast decay time for GaP:Co is 270 μs in good agreement with the previously reported result[21]. In InGaP alloys, the decay-time of the dominant fast decay component is 240∿260 μs comparable to that in GaP being 270 μs and almost independent of composition. The fast-decay time in GaAsP tends to decrease from 270 to ∿200 μs as x decreases from 1 to 0.65. The slow decay-time tends to decrease with decreasing x in both InGaP and GaAsP alloys. It is noted that both fast and slow decay times in InGaP and GaAsP are connected continuously with those in GaP. In order to study the decay characteristics of PL spectra, the exciting light-chopping frequency dependence of PL spectra has been measured. In Fig. 6-6, the chopping frequency dependence of Co-related PL spectra in $In_{0.10}Ga_{0.90}P$ is shown. The PL intensity decreases with increasing chopping frequency according to the luminescent life time, and line shapes of PL spectra do not change. This result shows that the decay-time is constant throughout the PL energy region. The similar result has been obtained for GaAsP. The fact that the decay times in InGaP and GaAsP do not change abruptly but connect smoothly with that in GaP may indicate that PL spectra observed in these alloys are due to the same origin as that in GaP.[17,22-24] Therefore, it is concluded that the PL bands are due to transitions from $^4T_2(F)$ to $^4A_2(F)$ of the Co^{2+} center.

6-4-2. Local atomic arrangements around Co luminescent center

The Co impurity occupying the cation site is tetrahedrally coordinated by four anions in its nearest neighbor site and also

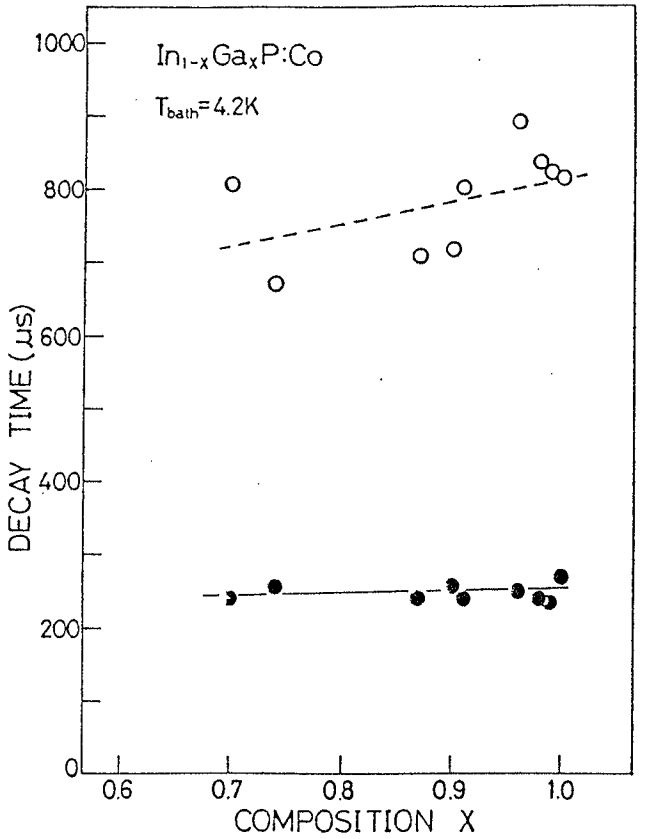

Fig. 6-4 Composition dependence of PL decay time in $In_{1-x}Ga_xP$. Closed and open circle plots denote decay time of fast and slow decay components, respectively.

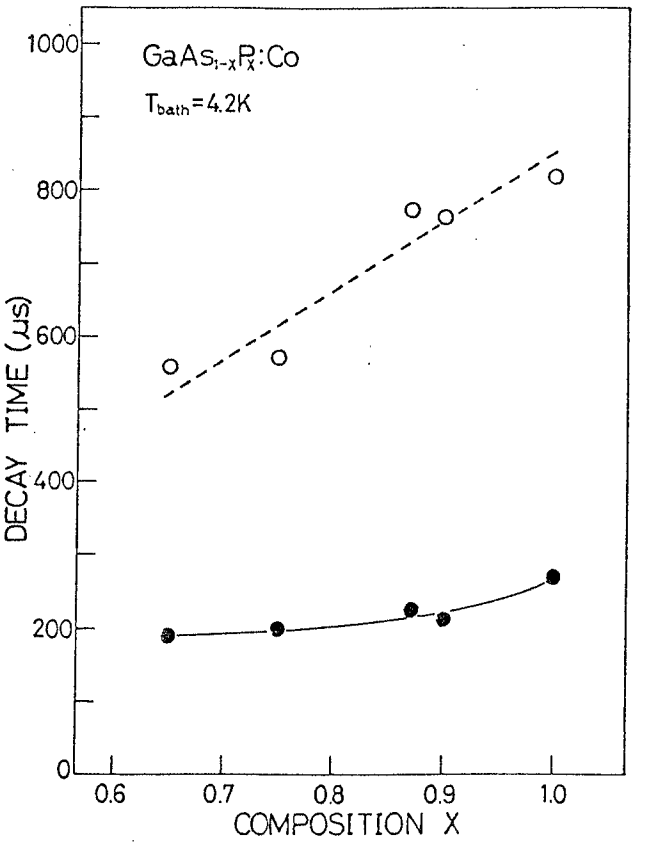

Fig. 6-5 Composition dependence of PL decay time in $GaAs_{1-x}P_x$. Closed and open circle plots denote decay time of fast and slow decay components, respectively.

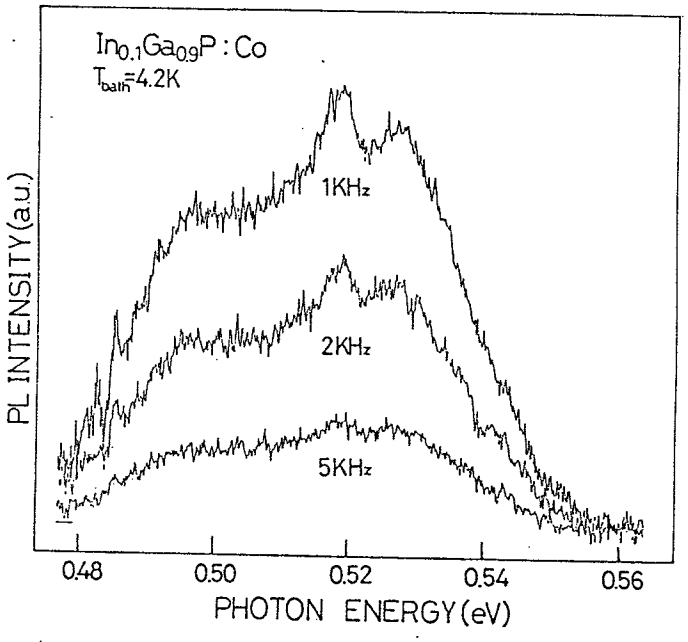

Fig. 6-6 Co-related PL spectra in $In_{0.10}Ga_{0.90}P$ taken with various chopping frequencies of the excitation light.

surrounded by twelve cations at the second-nearest neighbor sites. The local arrangement of atoms around the Co luminescent center in InGaP being the III-III-V type alloy is different from that in GaAsP being the III-V-V type alloy, in that the former shows the distribution of Ga and In atoms at the second-nearest neighbor sites of the Co atom while the latter shows the distribution of As and P atoms at the first-nearest neighbor site of it. This consideration gives InGaP thirteen local atomic arrangements, X_0, X_1,..., X_{12}, around the Co luminescent center if the symmetry of the arrangement is ignored, and gives GaAsP five local arrangements, X_0, X_1,..., X_4, where X_n denotes the luminescent center containing n In or As atoms in the shell within the second-nearest neighbor site of Co in InGaP and GaAsP, respectively. The schematic view of these local atomic arrangements around the Co luminescent center, for example, is shown in Fig. 6-7 for X_2 in InGaP and for X_1 in GaAsP. If the 3d wave-function of the excited $^4T_2(F)$ state and the ground $^4A_2(F)$ state of the Co^{2+} center is limited within the second-nearest neighbor sites, the Co luminescent center suffers the perturbation corresponding to the local atomic arrangements, which gives rise to different localized levels. This consideration is supported by the fact that the extention of 3d wave-function of a Co^{2+} ion has been estimated $\sim$0.5 A.[25] In fact, the Co-related PL spectra in both InGaP and GaAsP shown in Figs. 6-2 and 6-3 can be interpreted as the superposition of several PL bands, and their changes with composition can be interpreted as the systematic change in relative intensities of them. Provided that In and Ga atoms in InGaP and As and P atoms in GaAsP distribute completely randomly, the probability, $P(X_n)$, that a

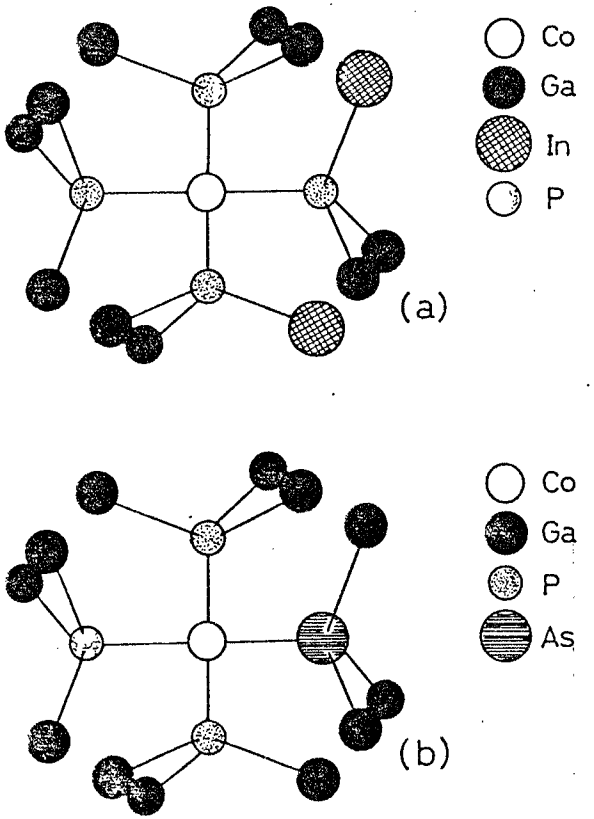

Fig. 6-7 Schematic representation of atomic arrangement around Co luminescent center for InGaP (a) and GaAsP (b). Atoms within shell including the second-nearest neighbor site from Co atom are shown.

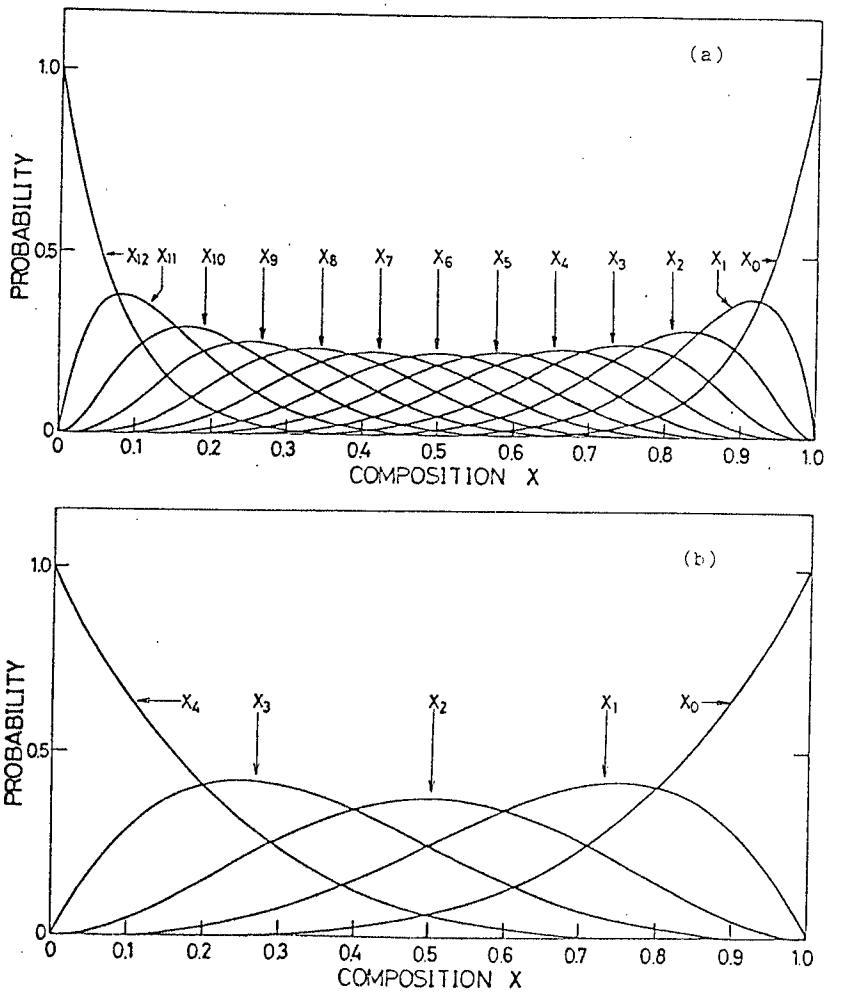

Fig. 6-8 Calculated probability that Co center forms X_n arrangement for $In_{1-x}Ga_xP$ (a) and $GaAs_{1-x}P_x$ (b).

Co center forms the local atomic arrangement, X_n, is calculated by a binomial distribution, $\binom{N}{n}x^{N-n}(1-x)^n$, where N and n are the number of site and the number of the same type atoms, In or As, occupying the site, respectively. In the case of InGaP, N is 12 and n is 0, 1, ..., 12, where n is the number of In atoms occupying the second-nearest neighbor sites of a Co center, and in the case of GaAsP alloy, N is 4 and n is 0, 1, ...,4, where n is the number of As atoms occupying the first-nearest neighbor site of a Co center. The binomial distribution of the local atomic arrangement for InGaP and GaAsP is shown in Fig. 6-8. As can be seen in the figure, the dominant local arrangements are X_0, X_1, X_2, and X_3 for InGaP and X_0, X_1, and X_2 for GaAsP in the composition range studied.

6-4-3. PL bands due to local atomic arrangement of Co center

By comparing PL spectra in InGaP and GaAsP with the binomial distribution, the assignment of PL bands corresponding to the local atomic arrangement has been done. Prior to the assignment, the Co-related PL spectra in Figs. 6-2 and 6-3 have been decomposed into Gaussian bands as shown in Fig. 6-9. The decomposition has been carried out using a non-linear least-square fitting method with the number of peaks as an input parameter. The number of peaks has been determined by the composition dependence of PL spectra with aids of the second and third derivative of PL spectra. The assignment of decomposed peaks has been done by comparing their intensities with the calculated probabilities shown in Fig. 6-8. Results of the assignment are summarized in Table 6-1. In this Table, the numbered peaks correspond to peaks shown in Fig. 6-9.

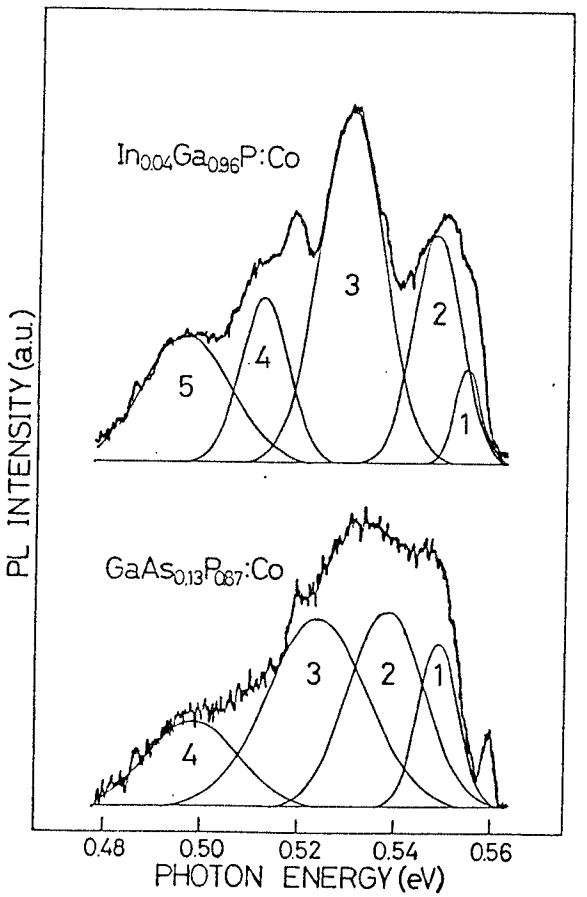

Fig. 6-9 Best fitting of Gaussian bands for Co-related PL spectra in $In_{0.04}Ga_{0.96}P$ and $GaAs_{0.13}P_{0.87}$.

Table 6-1 Assignment of Co-related PL peak in InGaP and GaAsP alloys. The peak number corresponds that in Fig. 6-9. The peak energy is for $In_{0.04}Ga_{0.96}P$:Co and $GaAs_{0.13}P_{0.87}$.

alloy	peak number	peak energy (eV)	assignment
InGaP	1	0.553	X_0 (zero-phonon line)
	2	0.548	X_0 (TA phonon replica)
	3	0.530	X_1
	4	0.512	X_2
	5	0.496	$X_3+X_4+....$
GaAsP	1	0.549	X_0 (TA phonon replica)
	2	0.538	X_0 (LA phonon replica)
	3	0.523	X_1
	4	0.498	$X_2+X_3+X_4$

It is also important to verify the assignment based on the transition energy of the Co center between $^4T_2(F)$ and $^4A_2(F)$ levels corresponding to the crystal field splitting, Δ. In Figs. 6-10 and 6-11, the shift of photon energies of the decomposed PL peaks from the zero-phonon energy in GaP is plotted against the number of In and As atoms occupying the second-nearest neighbor and the nearest neighbor site of the Co center for InGaP and GaAsP alloys, respectively, based on the assignment in Table 1. In these figures, error-bars indicate the FWHM of PL bands. As can be seen in these figures, the negative shift of the transition energy increases as the number of In and As atoms increases in the shell. In order to estimate the transition energy corresponding to these local atomic arrangements of the Co center, the local lattice constant around the Co center is assumed to be determined by the shell within the second-nearest neighbor of the Co center. We have defined an effective local lattice constant, a^*, for InGaP as; $a^*=\{(12-n)/12\}a_{GaP}+(n/12)a_{InP}$, and for GaAsP as; $a^*=\{(4-n)/4\}a_{GaP}+(n/4)a_{GaAs}$, where n is the number of In and As atom included in the shell considered for InGaP and GaAsP, respectively. According to the crystal field theory,[26] the crystal field parameter, Δ, corresponding to the transition energy for the transition $^4T_2(^4F)\rightarrow{}^4A_2(^4F)$ varies as a^{-5}, where a is the lattice constant. Therefore, Δ values corresponding to local atomic arrangements of the Co center have been estimated in a manner that Δ varies in proportional to a^{*-5}. The Δ value for n=0 is taken that for GaP. In Figs. 6-10 and 6-11, calculated Δ values are plotted and compared with PL energies experimentally obtained. As can be seen in the figure, the higher energy position of PL bands agrees fairly well with the

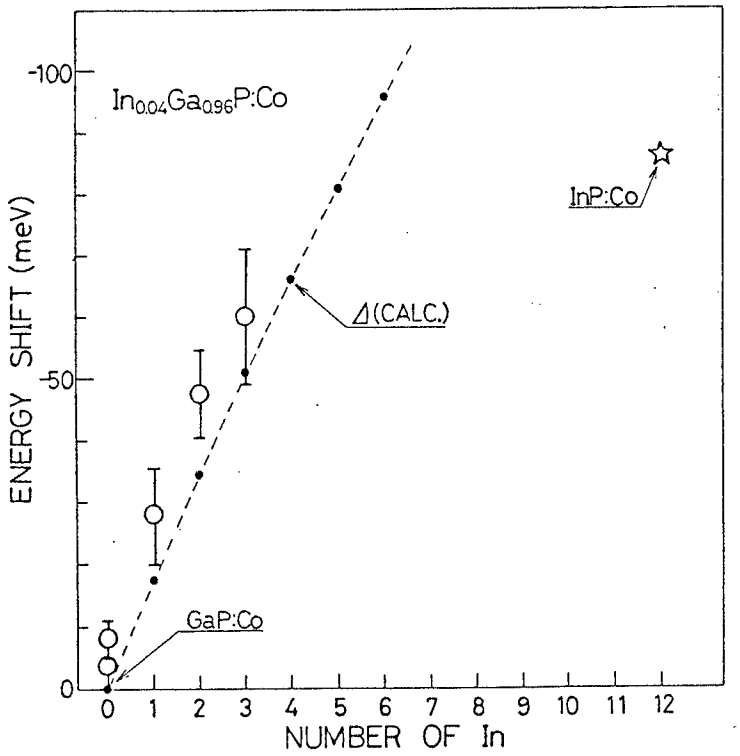

Fig. 6-10 Energy difference of PL bands from the energy of the zero-phonon line in GaP:Co plotted against the number of In atom included in the local atomic arrangement of the Co center for $In_{0.04}Ga_{0.96}P$. Open circles and dots denote experimental values and calculated values, respectively.

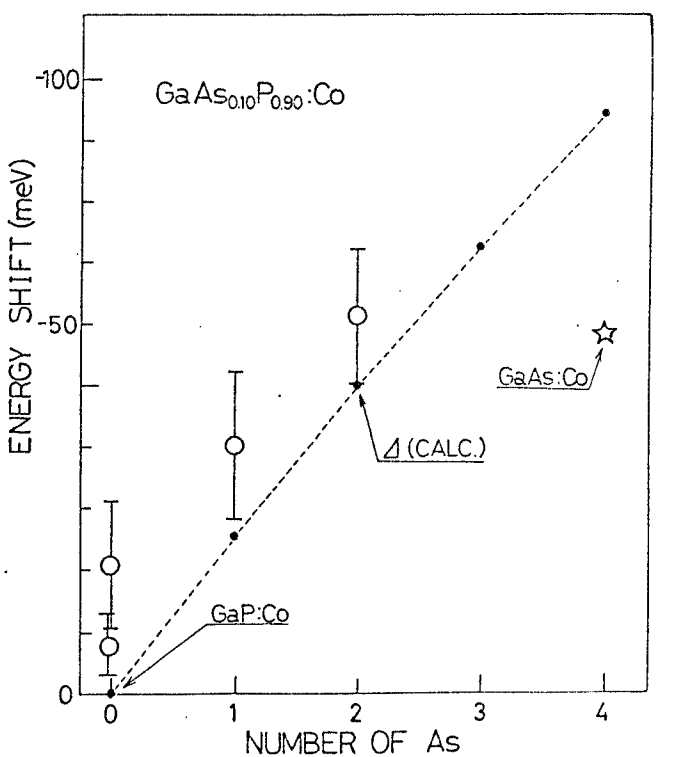

Fig. 6-11 Energy difference of PL bands from the energy of the zero-phonon line in GaP:Co plotted against the number of As atom included in the local atomic arrangement of the Co center for $GaAs_{0.10}P_{0.90}$. Open circles and dots denote experimental values and calculated values, respectively.

calculated Δ value for both InGaP and GaAsP. This fact suggests that the lattice constant around the Co impurity is determined by atoms in the shell within the second-nearest neighbor site.

Let us discuss the intensity of the decomposed PL bands. If we assume that transition probabilities are all the same for transitions corresponding to these local atomic arrangements, the ratio of the integrated intensity of each PL band to that of the whole PL band is considered to represent the number of Co luminescent centers having the corresponding local atomic arrangement. And therefore, the composition dependence of the PL intensity ratio is expected to resemble that of the probability shown in Fig. 6-8. In Figs. 6-12 and 6-13, the PL intensity ratio of PL bands corresponding to main local atomic arrangements is plotted as a function of composition together with the probability calculated by the binomial distribution. In the case of InGaP, a correction in the integrated intensity of each PL band has been done, because the PL band 3 is in the same energy region of the LA phonon replica of X_0, and that the PL band due to X_1 may be over estimated when x is close to 1. The correction has been done for PL bands corresponding to X_0 and X_1, assuming that the PL intensity ratios of LA phonon replica, TA phonon replica and the zero-phonon line are the same as that in GaP, being 33%:25%:22%. As can be seen in Figs. 6-12 and 6-13, the composition dependence of the PL intensity ratio agrees well with that of the binomial distribution for both InGaP and GaAsP. This fact confirms the assignment of the decomposed PL bands indicated in Table 1.

However, there remains a question why the zero-phonon line is so broadened in InGaP and even disappears in GaAsP, and the PL peaks

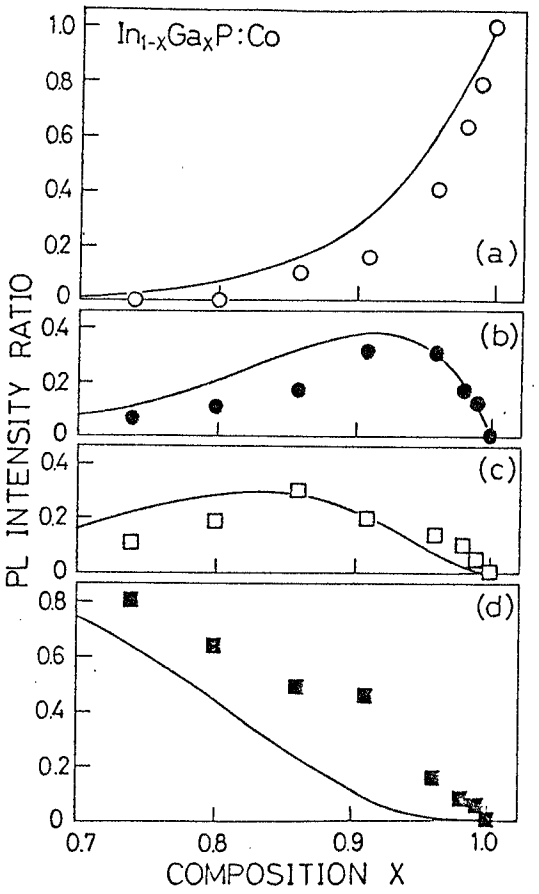

Fig. 6-12 Ratio of integrated intensity of PL bands related to atomic arrangements X_0 (a), X_1 (b), X_2 (c), and $X_3+X_4+\ldots$ (d) with respect to that of whole PL band plotted against composition for $In_{1-x}Ga_xP$. Solid lines show calculated values.

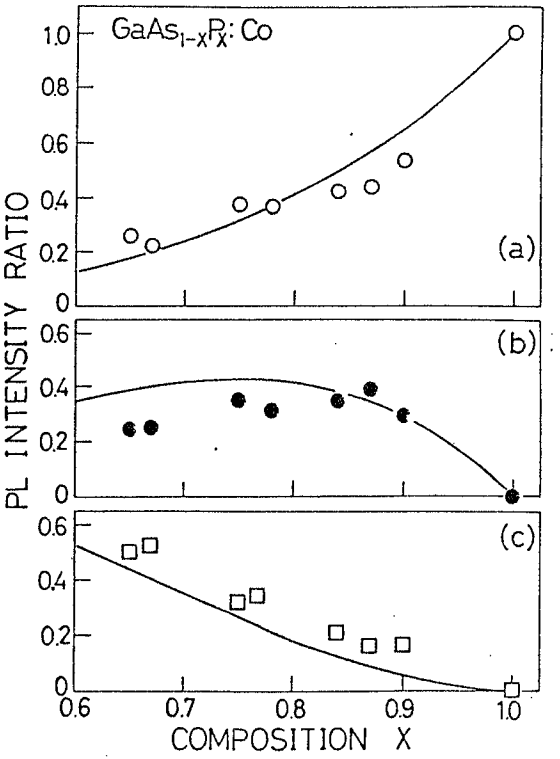

Fig. 6-13 Ratio of integrated intensity of PL bands related to atomic arrangements X_0 (a), X_1 (b) and $X_2+X_3+X_4$ (c) with respect to that of whole PL band plotted against composition for $GaAs_{1-x}P_x$. Solid lines show calculated values.

related to the local atomic arrangement of the Co center are so broad. If the perturbation acting on the Co luminescent center is limited within the shell containing the second-nearest neighbor atoms, the interpretation of the broadening of these PL bands is rather difficult. Even if the Co luminescent centers forming the local atomic arrangement discussed above have reduced symmetry lower than T_d, sharp zero-phonon lines corresponding to the reduced symmetry of the center should appear. Two reasons are considered for this broadening. One reason is that the local atomic arrangement around the Co center contains point defects such as vacancy, which further reduce the symmetry of the center and there is the possibility that more than one vacancy exist in the shell including the second-nearest neighbor sites of the Co center. Another reason is that the Co center suffers the perturbation from disordering occurring farther than the second-nearest neighbor site. Considering that the 3d wave-function of the Co^{2+} ion is strongly localized and the extension of it is $\sim$0.5 A, the perturbation from such distant atoms is considered to be effect of strain field caused by the difference in the bond lengths between In-P and Ga-P for InGaP and that between Ga-As and Ga-P for GaAsP. This perturbation comes from the fourth-nearest neighbors for InGaP and the third-nearest neighbors for GaAsP. From the rough estimation, the <111> strain of 2.5% [27] produced by an In atom occupying the forth-nearest neighbor site of the Co center in InGaP propagates to the nearest neighbor P atom, and the P atom at the nearest neighbor site is forced to deviate from the original position toward <100> direction by the reduction factor of $0.36\beta/\alpha$ being 0.086, where α and β are the bond stretching and bond bending force constants,

respectively. In the case of GaAsP, the <111> strain of 1.2% [27] produced by an As atom occupying the third-nearest neighbor site propagates to the site of the Co atom, and the Co atom is forced to deviate toward the <100> direction by the same reduction factor as in InGaP. Values of α and β are 44.8 and 10.7 N/m [4], respectively, for Ga-P bond and therefore the Co center suffers the strain field one order smaller than that in fourth and third nearest neighbors of the Co center. The strain that perturbs the Co center is <100> strain of 0.21 and 0.10%, corresponding to stress of 220 and 100 MPa for InGaP and GaAsP, respectively. The amount of splitting of the energy level estimated by the <100> uniaxial stress coefficient in GaP:Co, 0.036 meV/MPa[23], is 3.0 and 1.4 meV for InGaP and GaAsP, respectively. Therefore, the random distribution of different atoms in the third and fourth nearest neighbor sites from the Co center produces further complicated strain field at the site of the Co center, and such strain field is considered to make these PL band so broad.

6-5. Summary

3d-transition metal (V, Cr, Co and Ni)-related PL spectra have been measured for $In_{0.1}Ga_{0.9}P$ alloy. Broad PL bands without the zero-phonon lines have been observed for all transition metal impurities in InGaP alloys, the results suggesting a very strong perturbation acting on the transition metal luminescent center.

The Co-related PL spectra in InGaP and GaAsP alloys have been systematically investigated. Broadening and evolution of PL bands have been observed for both InGaP and GaAsP when either InP or GaAs

compositions have been increased from GaP-rich one. It has been verified from time-resolved PL measurements that the observed PL spectra arise from the transition $^4T_2(^4F) \rightarrow {}^4A_2(^4F)$ of the Co^{2+} ion for both alloys. The observed Co-related PL spectra have been interpreted in connection with the local atomic structures of alloys in such a manner that the PL spectra are composed of PL bands at the transition energies being changed by the perturbation according to the local atomic environment of the Co luminescent center. The transition energies of the PL bands attributed to these atomic structures around the Co center have been interpreted by introducing an effective lattice constant around the Co center. The composition dependences of the PL intensity of these bands have been well explained by the probabilities that the Co center forms various local atomic arrangements. These results and discussion led us to the conclusion that the Co-related PL spectra are essentially associated with the distribution of In and Ga atoms at the second-nearest neighbor site of the Co center for InGaP and that of As and P atoms at the nearest neighbor site of the Co center for GaAsP. Furthermore, it is considered that strain field generated by difference in the bonding length at more distant sites can perturb the Co center, making PL spectra further broader.

REFERENCES

1) J. C. Mikkelesen, J. R. and J. B. Boyce: Phys. Rev. B 28 (1983)7130.

2) T. Sakai, T. Onda, R. Ito and N. Ogasawara: Jpn. J. Appl. Phys. 25 (1986) 231.

3) H. Ohyanagi, Y. Takeda, T. Matsushima, T. Ishiguro and A. Sasaki: 5th Symposium Record of Alloy Semiconductor Phyics and Electronics p.85.

4) A. B. Chen and A. Sher: Phys. Rev. B 32 (1985) 3695.

5) A. Balzarotti, N. Motta, A. Kisiel, M. Zimnal-Starnawska, M. T. Czyzyk and M. Podgorny: Phys. Rev. B 31 (1985) 7526.

6) A. Balzarotti, P. Letardi and N. Motta: Solid State Commun. 56 (1985) 471.

7) M. T. Czyzyk, M. Podgorny, A. Balzarotti, P. Letardi, N. Motta, A. Kisiel and M. Zimnal-Starnawska: Z. Phys. B 62 (1986) 153.

8) J. L. Martins and A. Zunger: Phys. Rev. B 30 (1984) 6217.

9) A. A. Mbaye and H. Mariette: J. Phys. C 17 (1984) 6663.

10) L. Samuelson, S. Nilsson, Z. -G. Wang and H. G. Grimmeiss: Phys. Rev. Lett. 53 (1984) 1501.

11) Y. Fujiwara, Y. Kita, Y. Tonami, T. Nishino and Y. Hamakawa: Jpn. J. Appl. Phys. 25 (1986) L232.

12) Y. Fujiwara, Y. Kita, Y. Tonami, T. Nishino and Y. Hamakawa: Appl. Phys. Lett. 48 (1986) 161.

13) B. Deveaud, B. Lambert, H.L'haridon and G. Picoli: J. Luminescence 24/25 (1981) 273.

14) K. Kocot and G. L. Pearson: Solid State Comm. 25 (1978) 113.

15) Y. Fujiwara, A. Kojima, T. Nishino and Y. Hamakawa: Jpn. J. Appl. Phys. 23 (1984) L4.

16) S. Shirakata, T. Nishino, Y. Hamakawa, T. Kato and T. Ishida: to be published in Jpn. J. Appl. Phys. Lett. 26, No. 2 (1987).

17) J. Weber, H. Ennen, U. Kaufmann and J. Schneider: Phys. Rev. B 21 (1980) 2394.

18) P. J. Dean, A. M. White, B. Hamilton, A. R. Peaker and R. M. Gibb: J. Phys. D 10 (1977) 2545.

19) U. Kaufmann, H. Ennen, J. Schneider, R. Worner, J. Weber and F. Kohl: Phys. Rev. B 25 (1982)5598.

20) U. Kaufmann and W. H. Koschel: Phys. Rev. B17 (1978) 2081.

21) C. Benjeddou, A. Nouailhat and G. Guillot: Abst. 5th. "Lund" Int. Conf. Deep-Level Impurities in Semicond. (1985) p.4.

22) A. P. Radlinski and J. M. Baranowski: J. Luminescence 24&25 (1981) 237.

23) W. Hayes, J. F. Ryan, C. L. West and P. J. Dean: J. Phys. C: Solid State Phys. 13 (1980) L149.

24) S. G. Bishop, P. J. Dean, P. Porteous and D. J. Robbins: J. Phys. C: Solid State Phys. 13 (1980) 1131.

25) J. F. Griffth: The Theory of Transition-Metal Ions (Cambridge University Press, London, 1961) p.102.

26) S. Sugano, Y. Tanabe and H. Kamimura: Multiplet of Transition Metal Ions in Crystals (Academic Press, New York & London, 1970).

27) C. K. Shih, W. E. Spicer, W. A. Harrison and Arden Sher: Phys. Rev. B 31 (1985) 1139.

7. CONCLUSIONS

The conclusions obtained in this thesis work on the preparation and characterization of InGaPAs alloys are summarized as follows;

1) The liquid phase epitaxial (LPE) growth of InGaPAs alloys on GaAs substrate has been studied. The two-phase melt method with excess GaP has been developed and examined in terms of the growth conditions such as growth temperature, initial supercooling (ΔT) and growth time. It has been found that the accurate setting of ΔT is possible independent of liquid composition, and the growth occurs by the diffusion limited process. The liquid compositions, and relationship between liquid and solid compositions have been made clear.

2) The effect of immiscibility on the LPE growth of $In_{1-x}Ga_xP_{0.7}As_{0.3}$ has been studied by both the two-phase melt (TPM) and the conventional supercooling (CS) methods. Mirror-like LPE layers in the large lattice mismatch ($\Delta a/a$) range, $-0.24\% < \Delta a/a < 0.30\%$, have been grown by the TPM method, while in the CS method, the growth range is limited and the surface morphology changes drastically depending on $\Delta a/a$, the results indicating that the growth in the immiscibility region is very sensitive to ΔT. The optimum ΔT has been found to be $3 \sim 5°C$.

3) The LPE growth was possible in the whole immiscibility composition region. However, the LPE growth with longer growth time than 20 s was unsuccessful and thick LPE layers have not be grown.

These results show that the LPE growth occurs by aid of the elastic energy from the substrate.

4) $In_{1-x}Ga_xP_{0.96}As_{0.04}$ LPE layers have been characterized by near-band edge photoluminescence (PL) and the electroreflectance (ER) measurements. The band-gap energies obtained by near-band edge PL spectra are slightly smaller than that obtained by ER measurements. The best crystal quality of LPE layer was obtained under the lattice-matching condition at the growth temperature corresponding to the room-temperature lattice mismatch of 0.2%.

5) ER spectra have been measured in $In_{1-x}Ga_xP_{0.7}As_{0.3}$ LPE layers grown in the immiscibility region. It has been found from the estimated broadening parameter that the crystal quality of LPE layer grown inside the immiscibility region is very sensitive to ΔT, depending on the LPE growth method.

6) The half-width of the near-band edge PL line in InGaPAs LPE layers becomes extraordinarily large in the immiscibility region, however sharp ER spectra in such samples have shown that the variation of composition due to spinodal decomposition is small. Furthermore in such a region, a strong broad PL band has been observed at $\sim$200 meV below the near-band edge PL line which becomes the weakest with $\Delta a/a$ of -0.05% being different from the lattice-matching condition at the growth temperature. This result shows that defects are introduced in the LPE layer when immiscibility is not stabilized by the strain energy due to lattice mismatch.

7) A new characterization technique for the interface stress at InGaPAs/GaAs heterostructure using a Cr-related PL line at 0.839 eV has been demonstrated. This PL line has been investigated as a function of lattice mismatch, crystal orientation, epitaxial layer thickness and substrate thickness. The analysis of the peak shift and splitting of the Cr-related PL line has shown that the tensile hydrostatic pressure and the compressive uniaxial stress co-exist in the interface region of the GaAs:Cr substrate. The stress has been estimated from the peak shift, and compared with that calculated. The result shows that the relaxation of the interface stress occurs more easily for (100) oriented samples than (111) oriented ones. The stress detection limit has been estimated to be 0.4 MPa.

8) This characterization technique has been successfully applied to the interface stress at LPE AlGaAs/GaAs and OMVPE ZnSe/GaAs heterostructures. It has been found that the peak shift of the Cr-related PL line observed at the AlGaAs/GaAs:Cr heterointerface is in good agreement with that expected from the lattice mismatch. While in the interface of ZnSe/GaAs:Cr, there exist the compressive hydrostatic pressure and the tensile uniaxial stress, which are not in agreement with that expected from the lattice constant, indicating an anomaly at the ZnSe/GaAs heterointerface. A model for lattice distortion in ZnSe epitaxial layer has been proposed.

9) The 3d transition metal (V, Cr, Co and Ni)-related PL spectra have been measured for InGaP bulk alloys. Broad PL bands without zero-phonon lines have been observed for all the transition metal

impurities in InGaP alloys, and this is quite different from that observed in binary compound. The results show a very strong perturbation acting on the transition metal luminescent center.

10) Co-related PL spectra in InGaP and GaAsP alloys have been measured as a function of alloy composition. It has been found that the Co-related PL spectra become broader as the composition is changed from GaP to InP-rich InGaP or GaAs-rich GaAsP. Time-resolved PL measurements have shown that these broad PL bands are due to the intracenter transition $^4T_2(^4F) \rightarrow {}^4A_2(^4F)$ of the isolated Co^{2+} center. The Co-related luminescence has been analyzed in connection with the local arrangements of atoms around the Co center, and has been found to be the superposition of several PL bands arising from the different atomic arrangements of the Co luminescent center. This result reflects also the difference in disordering between InGaP and GaAsP, i. e. III-III-V and III-V-V type alloy.

11) From the analysis of peak energies of these Co-related PL bands, it has been found that the local lattice constants of InGaP and GaAsP are determined by atoms in the shell within the second-nearest neighbor site. The probability that a Co center forms a local atomic arrangement has been estimated from the integrated intensity ratio of each PL band, which is in good agreement with that calculated by the binomial distribution for both InGaP and GaAsP. Broadenings of the PL bands are considered to be due to the strain field from the third- or fourth- nearest neighbor site of the Co center. From these results, it has been demonstrated that the local structure of III-V alloy

semiconductors can be effectively characterized by these transition meltal-related PL spectra.

VITA

Sho SHIRAKATA was born in Matsuyama, Ehime, Japan on February 16, 1959. He graduated from Matsuyama Higashi Senior High School, Ehime in March 1977 and entered Science University of Tokyo, Shinjyuku, Tokyo in April 1977. He graduated from Science University of Tokyo in March 1981 and entered the Graduate School of Osaka University, Suita, Osaka. He received his Master of Engineering degree in Electronic Engineering in March 1983 from Osaka University. He is a member of the Japan Society of Applied Physics.